

Regulation of Progression through Unperturbed Mitosis and in the Presence of Environmental Stress

Dissertation

zur Erlangung des Grades eines
Doktors der Naturwissenschaften

-Dr. rer. nat.-

der Fakultät für Biologie, Chemie und Geowissenschaften
der Universität Bayreuth

vorgelegt von

Rahul Pandey

2006

Die vorliegende Arbeit wurde in der Zeit von Juli 2002 bis November 2006 an der Universität Bayreuth am Lehrstuhl für Genetik unter der Betreuung von Prof. Dr. Christian F. Lehner angefertigt.

Vollständiger Abdruck der von der Fakultät für Biologie, Chemie und Geowissenschaften der Universität Bayreuth genehmigten Dissertation zur Erlangung des akademischen Grades eines Doktors der Naturwissenschaften (Dr. rer. nat.).

Promotionsgesuch eingereicht am: 15.11.2006

Erstgutachter: Prof. Dr. Christian F. Lehner

Zweitgutachter: Prof. Dr. Benedikt Westermann

Tag der mündlichen Prüfung: 12.01.2007

Acknowledgements

This thesis was carried out in the group of Prof. Dr. Christian F. Lehner at the Department of Genetics, University of Bayreuth.

I thank Christian Lehner not only for his excellent supervision during my graduation but also for my overall scientific training. Since the very start he has been a persistent and responsible academic teacher. All the way through my graduate studies, he has been extremely helpful and motivating.

In addition, I am grateful to the members of the laboratory for their co-operation, helpful discussions and providing a pleasant working environment. In particular, I am thankful to Stefan Heidmann, Sebastian Heeger, Ralf Schittenhelm, Brigitte Jaunich, Ivana Viktorinová, Friederike Althoff and Sonal Nagarkar for easily integrating me into the group.

Moreover, I am thankful to Ulrike Großkinsky and André Koch for their contribution to studies concerning anoxia and hypothermia, respectively. They have been instrumental in some of the important findings.

In all, I am grateful to everybody for making my stay in Germany a nice experience.

I am especially grateful to my parents, uncle and aunt for their motivation, perseverance and support.

Table of Contents

1	Zusammenfassung -----	1
2	Summary -----	3
3	Introduction -----	4
4	Aims of the Thesis -----	11
5	Detailed Summary and Discussion of the Results -----	12
5.1	The <i>Drosophila</i> Separase complex does not promote exit from mitosis --	12
5.2	The Separase complex is not needed for cytokinesis and centrosome duplication -----	15
5.3	The Separase complex is required for epithelial integrity -----	18
5.4	Acute Anoxia has rapid effects on mitotic spindle morphology-----	19
5.5	Kinetochores proteins re-localize in response to anoxia -----	23
5.6	The mitotic spindle checkpoint is activated by anoxia -----	24
5.7	Anoxia effects on mitosis are mimicked by metabolic inhibitors -----	26
5.8	The early syncytial cycles are the most cold-sensitive stages of <i>Drosophila</i> embryogenesis -----	26
5.9	The mitotic spindle checkpoint is important for cold survival -----	28
6	References -----	31
7	Appendix -----	37
	Part A	
	Contribution to Part A	
	Part B	
	Contribution to Part B	
	Part C	
	Contribution to Part C	
	Erklärung	

1 Zusammenfassung

Während der Mitose wird das replizierte Genom auf zwei Tochterzellen verteilt. Eine sorgfältige Regulation der verschiedenen mitotischen Prozesse ist von grösster Wichtigkeit für die fehlerfreie Verteilung und Weitergabe des Genoms. In der Evolution sind Überwachungsmechanismen entstanden, wie zum Beispiel der sogenannte Spindel-Kontrollpunkt, die Fehler während der Mitose weitgehend verhindern. Die molekularen Mechanismen dieser mitotischen Regulationsprozesse werden in der Bäckerhefe *Saccharomyces cerevisiae* besonders gut verstanden. Inwieweit diese Ergebnisse auch auf andere Eukaryoten übertragen werden können, ist jedoch noch nicht endgültig geklärt. In einem ersten Teil wurde daher die funktionelle Charakterisierung von Separase in *Drosophila melanogaster* weitergeführt. Dieser Protease wurden in der Bäckerhefe verschiedene Funktionen zugeschrieben. Die essentielle Bedeutung der Separase für die Trennung der Schwesterchromatiden am Übergang von der Meta- in die Anaphase ist in diversen Eukaryoten eindeutig gezeigt worden. In der Bäckerhefe wirkt Separase jedoch auch in einem regulatorischen Netzwerk (FEAR), das den Austritt aus der Mitose beschleunigt. Meine Untersuchungen ergaben keine Hinweise auf eine FEAR-artige Separase-Funktion in *D. melanogaster*. Da Centrosomen, die in tierischen Zellen die Pole mitotischer Teilungsspindeln ausbilden, strukturell völlig verschieden sind von den funktionell äquivalenten Spindelpolkörpern der Hefe, wurde auch die Bedeutung von Separase bei der Centrosomen-Verdoppelung studiert. Es ergaben sich keine Hinweise auf eine wichtige Rolle. Im zweiten Teil wurde die Bedeutung von Überwachungsmechanismen (insbesondere des Spindel-Kontrollpunktes) beim Ablauf von Mitosen unter Umweltstress (Anoxie und Hypothermie) untersucht. Bis anhin sind Interaktionen zwischen mitotischer Regulation und Umweltstress erstaunlicherweise kaum studiert worden. Sauerstoff-Deprivation verursacht jedoch zumindest in Invertebraten einen reversiblen mitotischen Arrest. Es konnte gezeigt werden, dass Sauerstoffentzug schnelle Veränderungen in Spindeln und Kinetochoren erwirkt und somit vermutlich auch die beobachtete Aktivierung des Spindelkontrollpunktes. Außerdem erwiesen sich die Konsequenzen von Anoxie auf mitotische Prozesse als nicht unterscheidbar von Effekten von Inhibitoren der

oxidativen Phosphorylierung. Der mitotische Arrest infolge von Anoxie wird daher vermutlich durch ein Absinken der ATP-Konzentration verursacht. Interessanterweise konnte gezeigt werden, dass der Spindelkontrollpunkt auch für das Überleben von Hypothermie wichtig ist, und die frühen syncytialen Stadien, in denen besonders schnelle mitotische Zyklen ablaufen, erwiesen sich als die kälteempfindlichsten der gesamten Embryonalentwicklung

2 Summary

During mitosis, the replicated genome is distributed onto two daughter cells. Perfect regulation of progression through mitosis is essential for an error-free segregation and propagation of the genome. Surveillance pathways like the mitotic spindle checkpoint have evolved to prevent mitotic defects effectively. The molecular basis of these regulatory mechanisms is particularly well understood in budding yeast. It is not entirely clear to what extent these findings are valid for other eukaryotes as well. Therefore, in a first part, I have addressed the function of *Drosophila* Separase, a protease which has been implicated in several regulatory processes in budding yeast. Although an essential role of this protease for sister chromatid separation has been demonstrated in a wide range of eukaryotes, its involvement in additional processes still remains controversial. In budding yeast, separase promotes rapid exit from mitosis in a dedicated regulatory network known as FEAR. In *Drosophila*, a FEAR-like role could not be confirmed. Similarly, an essential involvement in the duplication of centrosomes, which form the poles of mitotic spindles in metazoan cells and are highly divergent from the functionally equivalent fungal spindle pole bodies, could not be demonstrated. In a second part I have analyzed the importance of surveillance mechanisms (in particular the mitotic spindle checkpoint) for progression through mitosis in the presence of environmental stress like anoxia and hypothermia. So far, the interaction of environmental stress with mitotic regulation has been largely neglected. However, oxygen deprivation leads to a rapid and reversible mitotic arrest. Here, anoxia is shown to have rapid effects on spindle and kinetochore function which are proposed to cause the observed efficient activation of the mitotic spindle checkpoint. Moreover, the consequences of anoxia were found to be very similar to those caused by inhibitors of oxidative phosphorylation. This suggests that the reduction in ATP levels is responsible for metaphase arrest in anoxia. Interestingly, the mitotic spindle checkpoint was also found to be important for survival in hypothermia, and the early syncytial stages which are characterized by an extremely rapid progression through mitotic cycles, were found to be the most cold-sensitive stages of *Drosophila* embryogenesis.

3 Introduction

After replication of DNA during interphase, the genetic information needs to be distributed equally onto two daughter cells. This central phenomenon is conserved in all cells (see Nasmyth, 2002). In eukaryotes the distribution of the genetic material happens during anaphase, when the sister chromatids get segregated from each other (Fig. 1).

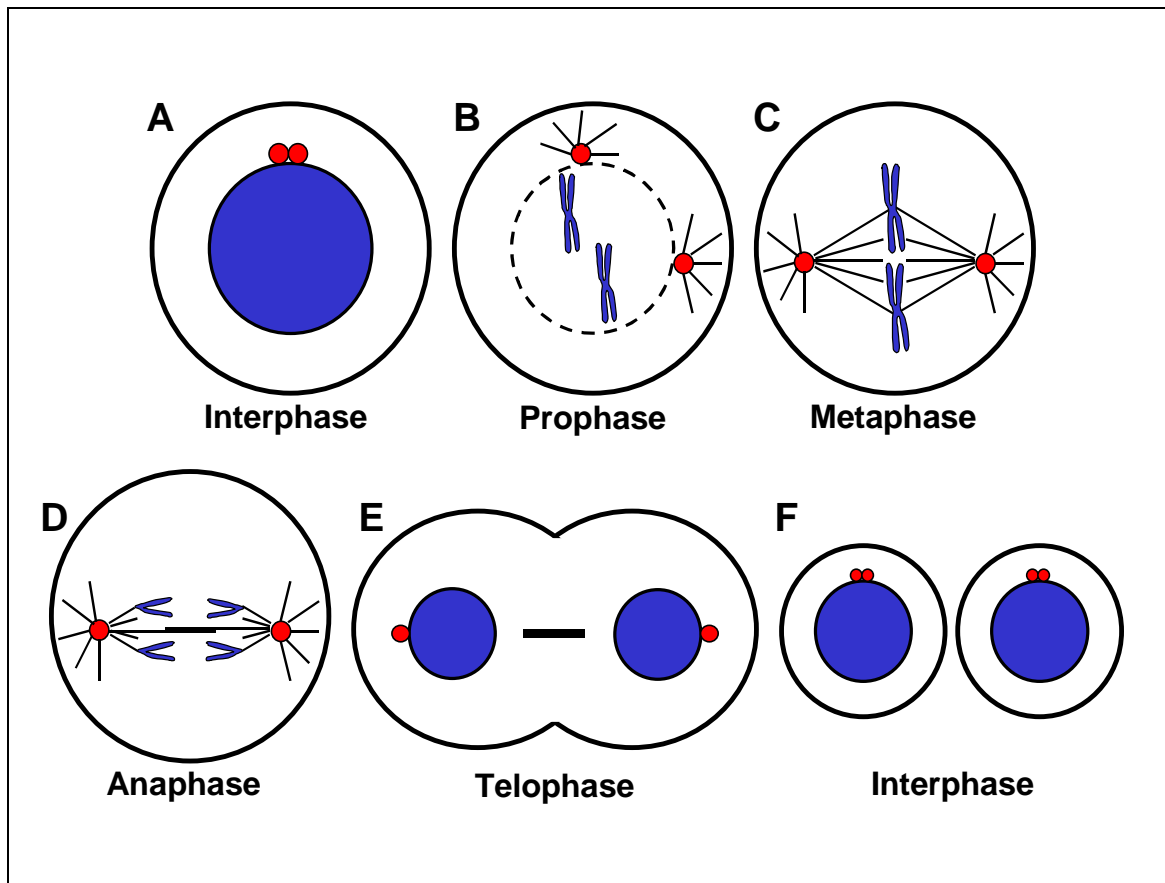


Figure 1: Schematic representation of various phases of the cell cycle. (A) Interphase. DNA is replicated and is decondensed. The two centrosomes (red) are together at the intact nuclear envelope (inner circle). **(B)** Prophase. The nuclear envelope breaks down (broken circle). The centrosomes start to move away from each other. Astral microtubules (black lines) begin to emanate from the centrosomes. Chromosomes (blue) are shown within the cell. **(C)** Metaphase. The chromosomes (blue) are integrated into a metaphase plate. The centrosomes (red) are at the opposite poles of the mitotic spindle (black lines). **(D)** Anaphase. The separated sister chromatids are segregated by the mitotic spindle to the poles. **(E)** Telophase. The chromatin starts to decondense and the mitotic spindle regresses. At the center of the cell, the midbody is formed from the microtubules and cytokinesis is initiated with the constriction of the cell membrane. **(F)** The completion of cytokinesis is followed by interphase. Here, in addition to DNA replication, centrosome duplication occurs. **(A-F)** DNA (blue), microtubules (black lines) and centrosomes (filled red circles) are shown.

Metaphase to anaphase transition and proper exit from mitosis need to be monitored and regulated extremely carefully. Cohesin complex, consisting of Scc1/Mcd1, Scc3, Smc1 and Smc3 (Michaelis et al., 1997; Toth et al., 1999), is responsible for keeping the sister chromatids together until the metaphase to

anaphase transition. In *Saccharomyces cerevisiae*, sister chromatid separation occurs as a result of proteolytic cleavage of Scc1 subunit of cohesin (Uhlmann et al., 1999). However, in higher eukaryotes, the dissolution of cohesion takes place in two steps. During prophase, cohesin complex dissociation occurs independent of Scc1 cleavage, along the chromosomal arms, by Polo-like kinase/Cdc5 activity (Sumara et al., 2002). Thus, the cohesion is left only in the centromeric region. Then in the second step and at the metaphase to anaphase transition, centromeric cohesion is resolved in a Scc1 cleavage-dependent manner (Waizenegger et al., 2000). Scc1 cleavage is achieved by the activation of a protease called separase (Uhlmann et al., 1999). Separases are known to be evolutionarily conserved, however, only in the C-terminal domain where the catalytically active protease center is located. In *Drosophila melanogaster* (Jäger et al., 2001), it forms a trimeric complex consisting of the securin, Pimples (PIM), Three-rows (THR) and Separase (SSE). During evolution, the separase in *D. melanogaster* got split into THR and SSE. THR corresponds to the N-terminal regulatory domain of separase in other organisms (Jäger et al., 2001; Jäger et al., 2004), while SSE is the C-terminal catalytic domain. PIM is a regulatory subunit which keeps separase in an inactive state. It though also provides a positive function of unknown nature as it is also required for separase activity (Stratmann and Lehner, 1996). PIM is ubiquitinated by APC/C (Anaphase Promoting Complex/Cyclosome) at the metaphase to anaphase transition and thus degraded by the proteasome. This activates separase which then cleaves off the Scc1 subunit of cohesin complex.

In addition, separase is known to provide non-catalytic functions in *S. cerevisiae*. It is required for spindle stability during exit from mitosis and catalytically dead versions of separase have been shown to provide these functions (Sullivan and Uhlmann, 2003). *S. cerevisiae* separase, ESP1 (Extra Spindle Poles 1) is a component of the FEAR (Cdc14 early anaphase release) network which in turn promotes proper and timely exit from mitosis both temporally and spatially by controlling Cdc14 release from the nucleolus (D'Amours and Amon, 2004). In all the organisms examined so far, exit from mitosis and cytokinesis requires inactivation of mitotic kinase, a cyclin-dependent kinase (Cdk) complexed with B type cyclins. This inactivation of Cdk is achieved by the release of Cdc14 phosphatase into the cytoplasm (Visintin et al., 1998). FEAR is an important regulatory mechanism which when perturbed leads to defects in exit

from mitosis, spindle stability, nuclear positioning and ribosomal DNA segregation (D'Amours and Amon, 2004). Lack of separase results in FEAR abolition indicating that in *S. cerevisiae*, separase has roles to play in FEAR pathway. Here, separase has an additional substrate called Slk19 (Fig. 2).

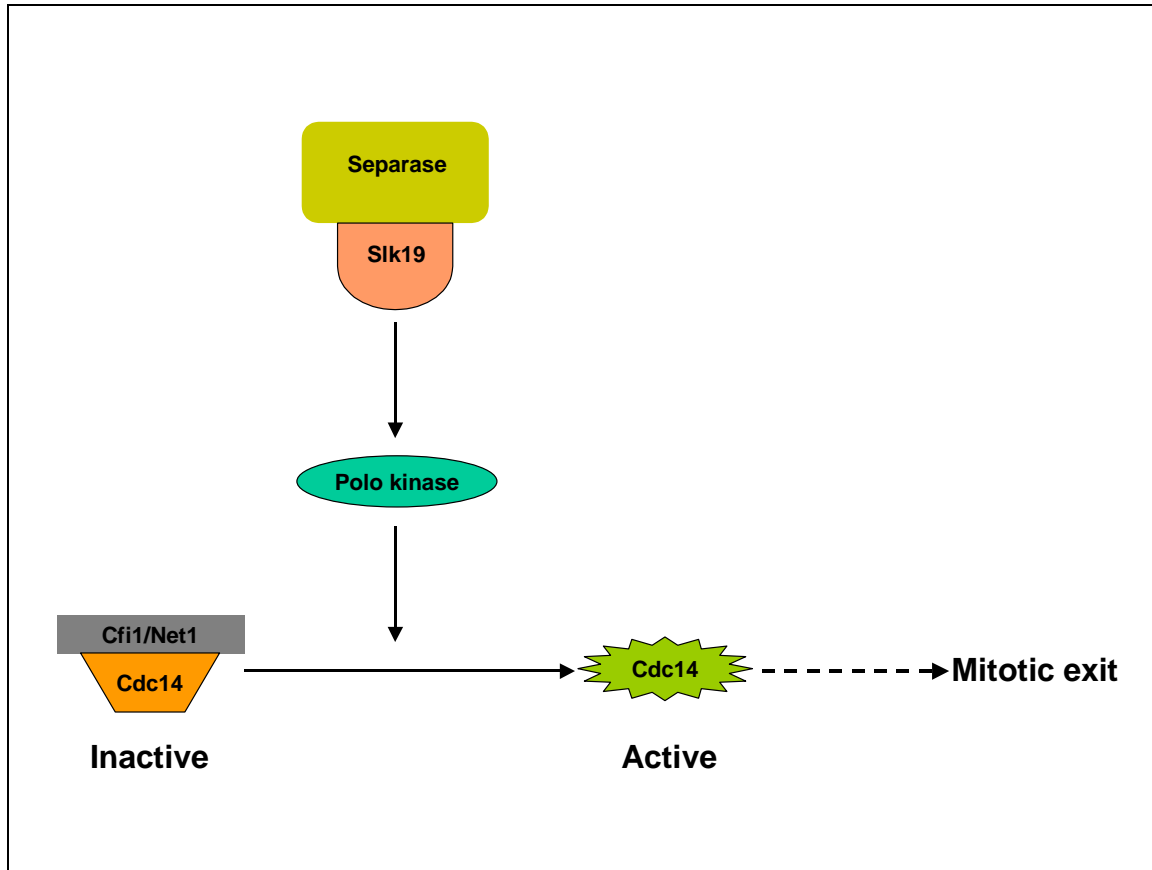


Figure 2: Simplified depiction of separase role in FEAR pathway. Separase together with its substrate Slk19 and polo kinase Cdc5 brings about Cdc14 release from the nucleolus, where its activity is kept in check by the inhibitor, Cfi1/Net1. Another protein Spo12 (not shown) functions in Cdc14 release. The release of Cdc14 from its nucleolar inhibitor is required for eventual inactivation of cyclin B and mitotic exit. (Modified from: D'Amours and Amon, 2004)

Similar as well as additional roles of separase in the model organism *D. melanogaster* remain an interesting hypothesis. Support to such a hypothesis comes from the studies showing non-cleavable THR expressing flies to be sterile at 18°C but not at 25°C (Herzig et al., 2002). The embryos having non-cleavable THR were shown to have defects during cellularization, a process where separase had not been implicated so far. Furthermore, separase involvement in centrosome cycle has been analysed in various organisms, but the issue is still controversial. Therefore, in this work, separase role has been evaluated in mitotic as well as non-mitotic processes in *D. melanogaster*.

Entry into anaphase is allowed if the cell satisfies the mitotic spindle checkpoint, an evolutionarily conserved surveillance mechanism that guarantees not only bi-orientation of all the chromosomes during metaphase, but also the correct anaphase initiation timing (Meraldi et al., 2004).

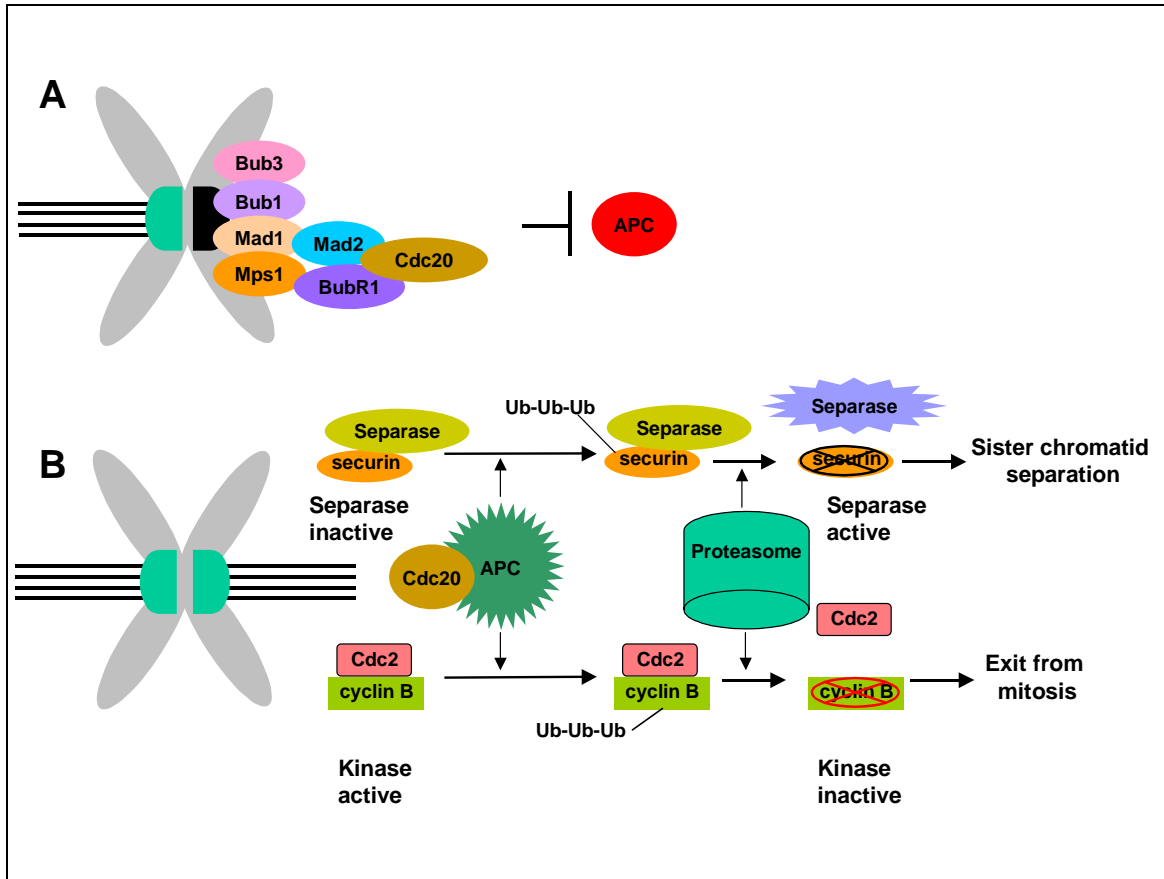


Figure 3: The mitotic spindle checkpoint.

(A) Schematic representation of the activated mitotic spindle checkpoint. Checkpoint proteins accumulate at the unattached kinetochore (black) of the chromosome (gray). This accumulation promotes inhibition of Cdc20 by Mad2 and BubR1. Since APC activation requires its binding to Cdc20, inhibiting Cdc20 inactivates APC. (B) Silenced mitotic spindle checkpoint and its consequences. When the kinetochore gets attached (green) to the spindle fibers (black lines), the checkpoint proteins disassemble and Cdc20 is set free to allow APC activation. APC ubiquitin ligase leads to ubiquitination of securin and cyclin B, which are then degraded by the proteasome. Securin degradation results in sister chromatid separation by activation of separase. Degradation of cyclin B renders Cdc2 kinase inactive eventually leading to exit from mitosis. Chromosome is shown in gray. Not all the proteins involved in mitotic spindle checkpoint are shown here. (Modified from: Karess, 2005).

The mitotic spindle checkpoint prevents anaphase by blocking the Cdc20-dependent activation of the APC/C that targets cyclin B and securin for degradation (Sironi et al., 2001; Musacchio and Hardwick, 2002). The checkpoint monitors and ensures that every single kinetochore, which is a multiprotein complex that is assembled at the centromere during mitosis, has acquired the perfect bipolar orientation before the cell goes into anaphase (Fig. 3). The sensitivity of this mechanism is highlighted by the ability of even a single

unoccupied or tension lacking kinetochore to trigger the mitotic spindle checkpoint (Rieder et al., 1994). This checkpoint is active since the start of mitosis and is silenced at the metaphase to anaphase transition. Some of the components of the mitotic spindle checkpoint originally identified in *S. cerevisiae* are Mps1, Mad1, Mad2, Mad3/BubR1, Bub1 and Bub3. With time homologues of many of these have been deciphered in other organisms as well. Ongoing research is revealing additional players involved in this signaling cascade. Previous studies in both vertebrates and invertebrates found that a defective mitotic spindle checkpoint invariably leads to aneuploidy and lethality (Basu et al., 1999; Dobles et al., 2000; Kalitsis et al., 2000). In *S. cerevisiae*, the checkpoint mutants do not get affected under unperturbed conditions. In contrast, it is often assumed that the metazoan checkpoint, in addition to being a surveillance system, performs an essential mitotic function in every division, presumably reflecting the increased complexity of metazoan mitosis.

Mps1 is believed to occupy an upstream position in the signalling cascade as its overexpression alone is sufficient to activate the checkpoint in *S. cerevisiae* (Hardwick et al., 1996). Most of the understanding concerning the checkpoint regulation has been provided by induction of metaphase arrest using spindle poisons, such as benomyl, nocodazole and colchicine (Li and Murray, 1991). There are reports demonstrating metaphase arrest induction upon oxygen deprivation in *D. melanogaster* (DiGregorio et al., 2001). Moreover, it has been shown in *Caenorhabditis elegans* and *D. melanogaster* that this arrest in metaphase is dependent on the presence of functional mitotic spindle checkpoint. In *C. elegans*, *san-1* (Mad3 homologue) and *mdf-2* (Mad2 homologue) mutants have been shown to not arrest in response to anoxia (operationally defined as <0.001 kPa O₂) (Nystul et al., 2003). Similarly, in *D. melanogaster*, *Mps1* mutant embryos were shown to not arrest in metaphase upon oxygen deprivation (Fischer et al., 2004). However, the mechanism that leads to metaphase arrest in anoxia is not yet understood. In principle, anoxia might trigger metaphase arrest by interfering with the mitotic spindle and consequential activation of the mitotic spindle checkpoint. Alternatively, anoxia might activate the checkpoint independent of its effects on the mitotic spindle and thereby trigger the metaphase arrest. These two possibilities have been evaluated in *D. melanogaster* in the presented studies.

Like oxygen supply, adequate temperature is very important for proper growth and development of most of the organisms. Most of the terrestrial organisms are poikilotherms and are often confronted with extensive temperature variations. Detailed studies have been carried out in bacteria describing the importance of membrane fluidity, translation and metabolism in the context of cold responses (Weber and Marahiel, 2003). However understanding of effects of hypothermia on higher eukaryotes is still very limited. It is conceivable that there are at least two types of responses to temperature lowering: shock response and acclimatization response. The extent of the shock response would be expected to correlate with the magnitude and the temporal rate of the temperature change. Contrary to this, the acclimatization response should be governed primarily by the absolute temperature. Furthermore, the shock response would be predominantly transient except for shifts to extreme low temperatures. On the other hand, the acclimatization response will be largely permanent for the time of the incubation at the low temperature.

The optimum temperature for the development of *D. melanogaster* is 25°C and the rate of development is known to get lowered by a factor of 2.25 at 18°C. Although population genetics studies in response to cold in *D. melanogaster* have been carried out (Hoffmann et al., 2003), detailed investigations at the cellular and/or molecular level are yet to be reported. *D. melanogaster* females preferentially lay their eggs at dusk, which can be followed by relatively dramatic drops in the ambient temperature during the night. The embryonic development is likely to be affected by these temperature changes. Therefore, addressing the effects of temperature lowering on the embryos of *D. melanogaster* would enhance our understanding of another physiological stress response. In addition, detailed knowledge of the components involved in sensing and reacting to cold is a prerequisite to understanding the involved molecular mechanisms. Finally, such studies would allow us to compare the cold response in bacteria and *D. melanogaster*. Such a comparison would be expected to provide an insight into the extent of evolutionary conservation of the cold response. Since in vitro studies have reported that microtubules are sensitive to temperature lowering (Brinkley and Cartwright, 1975; Rieder, 1981), it would be interesting to investigate the progression through the cell cycle with particular emphasis on mitosis as presumably spindle microtubule instability would result in defects in mitosis. In this

work, a detailed analysis of the embryonic development in *D. melanogaster* has, therefore, been carried out in response to hypothermia.

4 Aims of the Thesis

I focussed on studying pathways that monitor the metaphase to anaphase transition and exit from mitosis. There is increasing evidence claiming the importance of FEAR (Cdc14 early anaphase release) including separase for exit from mitosis in *S. cerevisiae* (see D'Amours and Amon, 2004). However, its involvement and roles in higher eukaryotes is not yet established. Similarly, separase requirement for centrosome cycle is controversial. I investigated these issues in *D. melanogaster* (Part A).

For metaphase to anaphase transition to occur, the signalling cascade, mitotic spindle checkpoint needs to be silenced. This checkpoint is required to arrest the cells in metaphase during unfavorable conditions such as spindle poisoning (Li and Murray, 1991) and anoxia (Nystul et al., 2003; Fischer et al., 2004). While, there are insights into the mechanisms triggering the arrest in response to spindle poisons, such as nocodazole, thorough analysis and characterization of metaphase arrest in anoxia is still lacking. Therefore, I have carried out a detailed study to characterize the metaphase arrest in response to anoxia (Part B).

Microtubules are known to be a sensitive target of temperature lowering (Brinkley and Cartwright, 1975; Rieder, 1981). Requirement of fully functional spindle microtubules for the metaphase to anaphase transition, therefore, would question the progression through cell cycle at low temperatures. Therefore, I have characterized the effects of temperature lowering on embryogenesis in *D. melanogaster*, with particular emphasis on progression through cell cycle (Part C).

5 Detailed Summary and Description of the Results

5.1 The *Drosophila* Separase complex does not promote exit from mitosis

Initial embryonic development in *pim*¹ as well as *thr*¹ homozygotes proceeds in a normal manner as long as the respective maternal *pim*⁺ or *thr*⁺ contribution to the egg provided by the heterozygous mothers is sufficient. However, mitosis 15 onwards, this maternal contribution is not enough for successful divisions. Hence, sister chromatid separation does not occur during mitosis 15, not only in *pim*¹ but also in *thr*¹ mutant embryos (Stratmann and Lehner, 1996; D'Andrea et al., 1993). *pim*¹ or *thr*¹ mutants are called separase complex mutants. In vivo imaging was employed to investigate the dynamics of progression through mitosis 15 in separase complex mutants in *D. melanogaster*. For this purpose, *pim*¹ and *thr*¹ mutants (Stratmann and Lehner, 1996; D'Andrea et al., 1993) expressing red fluorescent histone H2Av and *G147*, which carries a gene trap insertion in *CG31363*, resulting in expression of a microtubule-binding GFP fusion protein (Morin et al., 2001) were analysed. As has been reported earlier with fixed *pim*¹ and *thr*¹ embryos (Stratmann and Lehner, 1996; D'Andrea et al., 1993), the first mitotic defects were detected at the metaphase to anaphase transition. Sister chromatids were found to not separate in *pim*¹ (Part A, Fig. 1) and *thr*¹ (data not shown) mutants. Still, the dynamic re-organization of the mitotic spindle that is observed in wild-type anaphase and telophase clearly occurred in *pim*¹ (Part A, Fig. 1) and *thr*¹ (data not shown) mutants. In contrast to the findings in *S. cerevisiae* (Stegmeier et al., 2002; Sullivan and Uhlmann, 2003), such spindle behavior in *pim*¹ and *thr*¹ mutants during exit from mitosis 15 suggested absence of separase activity to not have a prominent effect on microtubule stability. In *S. cerevisiae*, separase, ESP1 is known to significantly accelerate the exit from mitosis. To address the scenario in *D. melanogaster*, the chromosome decondensation and spindle disassembly in *pim*¹ and *thr*¹ mutants was compared with *pim*⁺ and *thr*⁺ siblings. Unlike in *S. cerevisiae*, only a minor delay was observed during exit from mitosis 15 in *pim*¹ (Part A, Fig. 1) and *thr*¹ mutants (Part A, Table1 and data not shown). In addition, in vivo imaging using transgenic strains expressing red fluorescent histone H2Av together with *Spider*, which carries gene trap insertion in *gilgamesh*, resulting in expression of a green

fluorescent protein marking the cell cortex (Morin et al., 2001) confirmed that progression through mitosis 15 occurs with normal kinetics in *pim¹* and *thr¹* mutants except for the slight but significant delay during exit from mitosis (Part A, Table 1). Instead of about 80 minutes in *S. cerevisiae*, mitosis 15 was found to last 10-11 minutes in *D. melanogaster* (Part A, Fig. 1 and Table 1). These studies revealed an extension by at most a minute in the separase complex mutants in *D. melanogaster*, which is much less than about 30 minutes delay during exit from mitosis resulting in mutations in *S. cerevisiae* separase gene, *ESP1* (Stegmeier et al., 2002; Sullivan and Uhlmann, 2003). Hence, only very slight delay could be confirmed in separase complex mutants in *D. melanogaster*.

Since PIM and THR have been shown to get degraded during mitosis (Leismann and Lehner, 2003; Herzig et al., 2002; Stratmann and Lehner, 1996), any residual maternal contribution, which might still be present during mitosis 15, is expected to be further reduced during mitosis 16. Therefore, the mitotic exit analyses were extended to mitosis 16 in *pim¹* and *thr¹* mutant embryos. Unlike FEAR-defective *S. cerevisiae*, where delays have been observed during exit from mitosis, an extensive delay was observed in metaphase of mitosis 16, in *pim¹* (Part A, Fig. 2) and *thr¹* mutants (Part A, Table1 and data not shown) both by in vivo imaging and in fixed embryos (Part A, Fig. 3), where the mitotic index was dramatically increased. In contrast to mitosis 15, average duration of mitosis 16 in *pim¹* and *thr¹* mutants was found to be at least four times longer than in *pim⁺* and *thr⁺* siblings (Part A, Table1). This difference might reflect the maternal *pim⁺* or *thr⁺* contribution exhaustion dynamics. Alternatively, the unusual diplochromosomes, present during mitosis 16 in *pim¹* and *thr¹* mutants due to the sister chromatid separation failure during the preceding mitosis 15 (Stratmann and Lehner, 1996; D'Andrea et al., 1993), might activate the mitotic spindle checkpoint because of difficulties in aligning these abnormal chromosomes in a bipolar fashion into the mitotic spindle. The established fact that cyclin B degradation is blocked by the mitotic spindle checkpoint (Minshull et al., 1989; Whitfield et al., 1990; Minshull et al., 1994) and the belief that separase functions only after cyclin B and securin degradation were exploited to decipher the cause of prolonged mitosis 16 in separase complex mutants. *pim¹* and *thr¹* mutant embryos were fixed at the stage of mitosis 16 followed by immunolabeling with anti-cyclin B antibodies. The great majority of mitotic cells were found to have enriched levels of cyclin B (Part A, Fig.

3). Moreover, in vivo imaging confirmed that the delay occurred during metaphase, clearly before the onset of anaphase (Part A, Fig. 2). In addition, embryos with mutations in both *pim* and *double-parked* (*dup*) gene were analysed. *dup* encodes the *Cdt1* homolog in *D. melanogaster* and is required for DNA replication (Whittaker et al., 2000). Since, *dup^{a1}* mutants have been shown to not replicate the DNA during cycle 16 (Garner et al., 2001; Whittaker et al., 2000), *pim¹ dup^{a1}* double mutants were generated by meiotic recombination and number of mitotic cells present during mitosis 16 in *pim¹* and *dup^{a1}* single and *pim¹ dup^{a1}* double mutants were compared. In comparison to sibling control embryos, the increment in number of mitotic cells was observed in *pim¹* mutants as well as in *dup^{a1}* mutants (Part A, Fig. 3). The enhanced mitotic index in *dup^{a1}* mutants has been shown to result due to the single chromatid chromosomes, since their stable alignment in a bipolar fashion into the mitotic spindle cannot be achieved (Parry et al., 2003; Whittaker et al., 2000). Hence, the chromosome congression into a metaphase plate does not occur during mitosis 16 in *dup^{a1}* mutants (Part A, Fig. 3) (Parry et al., 2003). Also, since the chromosomes lack tension within the centromeric region, the spindle checkpoint stays active (Garner et al., 2001; Whittaker et al., 2000). In *pim¹dup^{a1}* double mutants, unsuccessful sister chromatid separation followed by failure of S-phase during cycle 16 would be expected to restore normal chromosomes in mitosis 16. Indeed, unlike *pim¹* and *dup^{a1}* single mutants, increase in mitotic cell number was not found in the *pim¹dup^{a1}* double mutants (Part A, Fig. 3). Moreover, in the double mutants, chromosomes were able to congress into a metaphase plate (Part A, Fig. 3). These findings indicated that the extensive delay during mitosis 16 in the *pim¹* single mutants is largely a consequence of the abnormal diplochromosomes. In vivo imaging experiments with *pim¹dup^{a1}* mutant embryos expressing red fluorescent histone H2Av and a green fluorescent protein marking the cell cortex confirmed the above mentioned conclusion (Part A, Table 1 and data not shown). It should be pointed out that the delay during metaphase 16 in *pim¹* mutants was not completely reversed in *pim¹dup^{a1}* double mutants. This residual delay might well be a reflection of adaptation effects, resulting due to incomplete inhibition of progression through the preceding S phase 16 (Garner et al., 2001).

Thus, in the presented studies with separase complex mutants in *D. melanogaster* no FEAR pathway analogue could be detected. In addition, no

difference has been revealed so far between *pim*¹ and *thr*¹ during their phenotypic characterization, neither in fixed samples (Stratmann and Lehner, 1996; D'Andrea et al., 1993) nor in vivo (Part A, Table 1). So far, the effect of separase on the kinetics of exit from mitosis has not been addressed in vertebrate systems. Furthermore, in *C. elegans*, reduction of separase to levels resulting in inhibition of sister chromatid separation has been reported to not significantly delay exit from mitosis in controlled osmotic conditions (Siomos et al., 2001).

Mutations in *S. cerevisiae* ESP1, that abolish protease activity and prevent sister chromatid separation, have been shown to not necessarily eliminate activity in the FEAR pathway (Sullivan and Uhlmann, 2003). Thus, one could point out that the presence of separase in *pim*¹ and *thr*¹ mutants could provide functions of the FEAR network. However, studies in *S. cerevisiae* showed that even slight truncations in the N-terminal region of separase abolish its FEAR activity (data not shown), thereby making it highly unlikely for *D. melanogaster* separase to be active without its partner, THR. In addition, ablation of *Cdc14* by RNA interference experiments in cultured *Drosophila* cells did not show any discernible phenotype (data not shown).

In all, these studies could not detect a FEAR pathway upto cycle 16 during embryogenesis of *D. melanogaster*. It is worth pointing out that it is not excluded that even during cycle 16 there is some maternal contribution left in *pim*¹ and *thr*¹ mutant embryos which is sufficient to provide FEAR functions. Moreover, extensively prolonged metaphase during mitosis 16 was found to be a consequence of the activation of mitotic spindle checkpoint due the alignment problems of abnormal diplochromosomes into the mitotic spindle.

5.2 The Separase complex is not needed for cytokinesis and centrosome duplication

In the previously reported phenotypic characterizations, mitosis 15 in *pim*¹ and *thr*¹ mutant embryos was analysed after fixation (D'Andrea et al., 1993; Stratmann and Lehner, 1996). These studies found that in the fixed *pim*¹ and *thr*¹ mutant embryos, cleavage furrows were often pinching the undivided chromosomes during exit from mitosis 15. However, the nuclear density in the epidermis during interphase 16 was found to be 1.6-fold lower in mutant embryos

than in sibling control embryos (D'Andrea et al., 1993; Stratmann and Lehner, 1996), thereby suggesting the cleavage furrows to have failed to cut completely through the chromosomes during mitosis 15. Hence, it was believed that the cleavage furrows eventually retracted in the majority of the cells during exit from mitosis 15 in *pim*¹ and *thr*¹ mutants. Such a cytokinesis failure during mitosis 15 followed by duplication of centrosomes during cycle 16, would result in tetrapolar mitotic spindles during mitosis 16 in most *pim*¹ or *thr*¹ mutant cells. When analysed, apparently bipolar mitotic spindles and normal metaphase plates were seen during mitosis 16 in *pim*¹ and *thr*¹ mutants (Part A, Fig. 3 and data not shown). Immunolabeling with anti- γ -tubulin antibodies revealed that most of the epidermal cells in *pim*¹ and *thr*¹ mutants during mitosis 16 contain only two and not four centrosomes (Part A, Fig. 4 and Table 2). In contrast, *pebble* (*pbl*) mutant embryos showed an increase in centrosome number from two to four during the cycle following a cytokinesis failure (Part A, Fig. 4 and Table 2). *pbl* has been shown to encode a Rho-GEF required for cytokinesis (Hime and Saint, 1992; Lehner, 1992; Prokopenko et al., 1999). Since the centrosome number increase from two to four in the following cell cycle was observed in *pbl* mutant embryos but not in *pim*¹ and *thr*¹ mutant embryos, it was interesting to test the possibility that separase complex in *D. melanogaster* is required for centrosome duplication. The centrosome numbers were then evaluated in *pim*¹, *pbl* double mutant embryos and were found to increase with every cycle (Part A, Fig. 4). Moreover, centrosome duplication was found to be not affected by depletion of *pim* in RNA interference experiments with cultured *Drosophila* cells (data not shown). This, in addition to the observations mentioned above indicates that separase complex is not involved in centrosome duplication.

In *S. cerevisiae*, the separase, *ESP1* (Extra Spindle Poles 1) mutants were first identified because they accumulate extra spindle pole bodies (Baum et al., 1988), the equivalent of centrosomes in higher eukaryotes. Thus, separase in *S. cerevisiae* is not required for the duplication of spindle pole bodies. Similarly, *Schizosaccharomyces pombe* separase, *cut1* has been shown to be not required for duplication of the spindle pole bodies (Uzawa et al., 1990). It is important to point out that spindle pole body in yeast is structurally very different from centrosomes in animal cells and so the situation in animal cells could be different from yeast. On these lines, RNA interference studies in *C. elegans* have shown

that separase is not involved in centrosome duplication (Siomos et al., 2001). However, studies in *Xenopus laevis* have suggested that separase is required for centriole disengagement (Tsou and Stearns, 2006). It is worth pointing out that in the studies presented here, centrosome and not centriole separation was analysed (Part A, Fig. 4). Also, Tsou and Stearns have not directly tested the role of separase by depletion from extract or cells. Their findings are based on experiments involving non-degradable versions of cyclin B and securin. Hence the evidence is indirect and it is not excluded that the two different approaches they adopted block an additional activity and not just separase. So there are conflicting reports concerning involvement of separase in centrosome cycle. On the one hand, in *X. laevis*, it is playing a role in the centrosome cycle, while on the other hand, in *S. cerevisiae*, *S. pombe*, *C. elegans* and *D. melanogaster*, it is not.

Alternatively, no increase in centrosome number in *pim*¹ and *thr*¹ mutant embryos could be explained if cytokinesis during mitosis 15 in these mutants was successful. To test this possibility, cytokinesis during mitosis 15 in *pim*¹ and *thr*¹ mutants was analysed by vivo imaging with transgenic embryos expressing red fluorescent histone H2Av together with *Spider*. Time-lapse imaging demonstrated successful completion of cytokinesis during mitosis 15 in almost all the epidermal cells in both *pim*¹ (Part A, Fig. 5) and *thr*¹ mutants (data not shown). In comparison to the sibling controls, the dynamics of cytokinesis was found to be only slightly slower in the mutants (Part A, Fig. 5 and Table 1), thereby indicating that the undivided chromosomes are not a significant obstacle for cytokinesis. The aberrant cytokinesis was found to result in two nucleate cells or a nucleate cell and a cytoplasm with comparable frequency. The two nucleate cells that resulted often contained unequal amounts of chromatin.

Consistent with these findings in *D. melanogaster*, cleavage furrows in *S. pombe* have been shown to cut readily through the chromosomes (Uzawa et al., 1990). However, contrary to these, studies in cultured human cells demonstrated eventual regression of the cleavage furrow after expression of mutant Scc1 versions, which are resistant to processing by separase (Hauf et al., 2001). Thus, the undivided equatorial mass of chromosomes affects completion of cytokinesis to a variable extent in different cell types.

5.3 The Separase complex is required for epithelial integrity

Successful completion of cytokinesis in *pim*¹ and *thr*¹ mutants during mitosis 15 was surprising because these mutants showed significantly lower cell and nuclear densities within the superficial epidermal layer during cycle 16. According to the predictions based on detailed analysis of cytokinesis during mitosis 15, cell density in *pim*¹ and *thr*¹ mutants before mitosis 16 should be comparable to *pim*⁺ or *thr*⁺ sibling embryos. The nuclear density, on the other hand, would be expected to be 25% (see Part A) lower in the mutants, compared to the siblings. Interestingly, upon evaluation the cell and nuclear densities were found to be significantly lower than the predicted ones. When quantified, 38% lower nuclear density was found in *pim*¹ mutant embryos compared to *pim*⁺ siblings before mitosis 16. The density of nucleated cells in *thr*¹ mutant embryos before mitosis 16 was also found to be reduced to an extent comparable to *pim*¹ mutant embryos.

This reduced nuclear density might well result due to apoptosis of aneuploid cells generated by the aberrant cytokinesis that occurs even though the sister chromosomes do not separate during cycle 15 in *pim*¹ and *thr*¹ mutants. With TUNEL (Terminal deoxynucleotidyl Transferase Biotin-dUTP Nick End Labeling) assay, which detects nucleate apoptotic cells, the rate of apoptosis between separase complex mutants and siblings was compared before and after progression through mitosis 16. No difference in apoptosis between *pim*¹ and *pim*⁺ sibling embryos was detectable before mitosis 16 (Part A, Fig. 6). Thus, apoptosis was found to be not responsible for the lower nuclear density before mitosis 16 in separase complex mutants.

To understand the basis of further reduced density of nucleated cells, the appropriately staged embryos were labeled for DNA and the cell cortex protein α -spectrin. This double labeling further confirmed the suspicion that after mitosis 15 the epithelium in *pim*¹ (Part A, Fig. 7) and *thr*¹ (data not shown) mutants develops an abnormal pseudostratified appearance. As expected, it was easily possible to obtain single confocal sections through the nucleus of every epidermal cell before mitosis 16 in *pim*⁺ (Part A, Fig. 7) and *thr*⁺ (data not shown) sibling embryos. In striking contrast, confocal sections from similarly staged *pim*¹ (Part A, Fig. 7) and *thr*¹ (data not shown) mutant embryos were never found to include all the nuclei of the nucleated epidermal cells present in other planes. These

observations confirmed the pseudostratification of the normally columnar epithelium in separate complex mutants.

This very interesting and novel aspect of the studies presented here demonstrates separate involvement in maintenance of epithelial integrity. In *pim*¹ and *thr*¹ mutants, the regular epithelial organization which is maintained in the epidermis throughout the three postblastoderm division cycles, 14-16, is lost after mitosis 15. Abnormal pseudostratified appearance of the epidermis was found to develop rapidly and much before apoptotic responses. Hence, impairment of separate complex function might have effects on the cytoskeleton and thereby on epithelial organization. Since it has been shown in *S. cerevisiae* that separate regulates microtubule stability (Stegmeier et al., 2002; Sullivan and Uhlmann, 2003), a similar role of the separate complex in *D. melanogaster* could be a favorable possibility. In addition, amounts of chromatin in *pim*¹ and *thr*¹ mutant cells was found to be quite variable after mitosis 15. They contained either no nuclei or nuclei of variable sizes. Since the nucleus might function as a mechanical element within the cells, its variability might contribute to the epithelial integrity loss in the mutants. Also, even though cleavage furrows were found to be able to cut through the undivided chromatin mass and the formation of central spindles and midbodies was clearly detectable, these structures would most likely be not entirely normal and therefore might not be fully functional. As a consequence, establishment of effective junctional contacts between the newly formed daughter cells would suffer. Moreover, cells round up on the apical side during entry into mitosis, this might generate a force resulting in displacement of some of the cells that have already divided, towards the basal side.

The presented phenotypic analyses in the embryos of *D. melanogaster* emphasize that a loss of separate function can have consequences on the maintenance of epithelial integrity. Such aspects would be expected to be difficult to study and detect with cultured cells.

5.4 Acute Anoxia has rapid effects on mitotic spindle morphology

The metaphase to anaphase transition has been shown to be blocked by oxygen deprivation (Foe and Alberts, 1985; DiGregorio et al., 2001). Mitotic spindle checkpoint has been reported to be required for this block (Nystul et al.,

2003; Fischer et al., 2004), however, the mechanisms involved are not yet understood.

Since spindle defects can result in metaphase arrest, it was intriguing to analyse spindle morphology in anoxia. The embryogenesis in *D. melanogaster* starts with 13 rapid syncytial cycles occurring in a common cytoplasm (Foe and Alberts, 1983). These rapid cycles lack gap phases and proceed without cytokinesis upto the cellularization event which leads to the formation of the cellular blastoderm (Foe and Alberts, 1983). The syncytial stages allow studying cell cycle progression of thousands of nuclei undergoing synchronous divisions. Therefore, for analysing effects of anoxia, syncytial embryos were incubated in degassed buffer followed by fixation and immunolabeling with anti- α -tubulin antibodies. The experiments revealed spindle defects within two minutes. The spindles after anoxic incubation were found to be narrower and slightly longer than the normoxic ones (Part B, Fig. 1). In addition, the connection to the centrosomes was severely diminished and sometimes abolished. After prolonged anoxia for 20 minutes, in many cases the spindles were either detectable only at the equatorial plane (Part B, Fig. 1) or not visible at all (data not shown). The centrosomes were often not detectable. However, when the spindles were analysed in vivo in response to anoxia (induced by N₂ or Ar) using *w¹¹¹⁸*; *P{GAL4::VP16-nos.UTR}MVD1*, *P{UASp-GFPS65C- α Tub84B}3* transgene that loads GFP-labeled α -tubulin 84B maternally into eggs (Grieder et al., 2000), much less severe affects were found. These spindles never looked as abnormal as the ones upon fixation, not even after 20 minutes of anoxia. The narrowing down of the spindles was, however, clearly detectable also during in vivo experiments (Part B, Fig. 1). These observations highlight that spindles suffer as a result of fixation. In fact, it has been shown earlier that spindles after fixation never look like the ones in vivo. These earlier studies report that all the features of the spindles in vivo are never revealed in the studies with fixed samples, irrespective of the type of fixation used (Kellogg et al., 1988). In another earlier study, spindle morphology defects in anoxia have been described (Sciambi et al., 2005). However, in this report the precise information about duration of anoxic incubation has not been provided. The anoxic incubation timings have been dealt with, in a much more careful manner in the studies presented here (Part B, Fig. 1). In vivo analyses also allowed the tracking of spindles after re-aeration. Interestingly, upon re-aeration,

the intercentrosomal distance decreased and was found to be comparable to prophase length (Part B, Fig. 1). Also, the centrosomal asters were strongly rebuilt, thus implying that after re-aeration and before entry into anaphase, there occurs an extensive re-organization of the spindle structure.

These abnormalities associated with the spindles were also found in *Mps1*¹ mutant embryos (embryos derived from females with *Mps1*¹ germ line clones) (Part B, Fig. 2) which have been shown to lack the functional mitotic spindle checkpoint and hence not arrest in response to anoxia (Fischer et al., 2004). This observation suggests that the abnormal spindle morphology in anoxia is not a consequence of spindle checkpoint activation. Moreover, in vivo imaging with *Mps1*¹ mutant embryos expressing the green fluorescent centromere protein Cenp-A/Cid and red fluorescent histone H2Av (Heeger et al., 2005) demonstrated that the congression into metaphase plate in anoxia in *Mps1*¹ mutants was severely hampered and as a consequence the following anaphase was found to be catastrophic with lagging chromosomes and anaphase bridges (Part B, Fig. 2). These observations are in agreement with the reported studies of anoxic *Mps1*¹ mutant embryos after fixation (Fischer et al., 2004). In addition, *Mad2* mutants in *D. melanogaster* were also found to not arrest in response to anoxia (data not shown). These findings support the claim that the mitotic spindle checkpoint is required for metaphase arrest in response to anoxia (Nystul et al., 2003).

When the spindle morphology is abnormal, kinetochore attachment to the spindle fibers would also be expected to get impaired. Since metaphase, and not prophase centromeres are under tension, the distance between sister centromeres during prophase is less than the distance during metaphase. The extent of attachment abnormalities was then analysed by measuring the sister centromere distances in prophase and evaluating the increase in normoxic and anoxic metaphase respectively, in the syncytial embryos that were fixed and stained with anti-Cid and anti- α -tubulin antibodies. Comparable to the observations in cultured *Drosophila* cells and cellularized embryos (Logarinho et al., 2004; Goshima et al., 2005; Heeger et al., 2005), bipolar orientation of the chromosomes in normoxic syncytial embryos was found to be associated with an increase in the average sister centromere distance, from 0.42 μm in prophase to 0.71 μm in metaphase (Part B, Fig 2). In anoxic metaphase, however, the average distance between the

sister centromeres was 0.63 μm . One sees that the increase in average sister centromere distance from prophase to metaphase was found to be 70% in normoxic conditions. In contrast, only 50% increase was observed in the average sister centromere distance from prophase to anoxic metaphase (Part B, Fig 2). Thus, tension generated by the mitotic spindle appears to be reduced in anoxia. These defects in kinetochore attachment leading to reduced tension, in combination with the spindle damage, might be enough to trigger the spindle checkpoint in response to anoxia. However, an increased stiffness of the anoxic metaphase chromosomes might also contribute to lower sister centromere distance in anoxic metaphases. In addition to the reduction in inter sister centromere distances, the double labeling also demonstrated that the anoxic spindles were largely composed of kinetochore fibers (Part B, Fig 2), which are known to be the most stable spindle fibers (McIntosh, 2002). In vivo imaging with strains expressing red fluorescent histone H2Av and green fluorescent Cid/CenpA never indicated any apparent difference between the normoxic and anoxic metaphases (data not shown). In addition, chromosome congression defects were never detectable in checkpoint competent embryos during anoxia. Since metaphase to anaphase transition is blocked in response to anoxia in checkpoint competent embryos, unambiguous determination of chromosome congression in these could not be achieved.

Since anoxia rapidly resulted in reduced astral and spindle fibers as well as centrosome detachment, it was intriguing to look at the behavior of centrosomal components in response to anoxia. Centrosomal components, Aurora A, γ -tubulin, Centrosomin (Cnn) and D-TACC (*Drosophila*-Transforming Acidic Coiled Coil) were evaluated in further detail. To study the anoxic effects on Aurora A, γ -tubulin and Cnn, w^1 syncytial embryos fixed after anoxic incubation were immunolabeled with respective antibodies. Aurora A kinase has been shown to play a crucial role in centrosome maturation (Giet et al., 2002; Barros et al., 2005; Kinoshita et al., 2005). Its localization was, however, found to be affected subtly in anoxia (Part B, Fig. 3). It is possible that Aurora A localization to the centrosomes is not affected unlike its activity in anoxia. Aurora A kinase has been shown to phosphorylate D-TACC during centrosome maturation (Giet et al., 2002; Barros et al., 2005). To test the kinase activity of Aurora A, syncytial embryos fixed after anoxic incubation,

followed by immunostaining with antibodies against p-TACC (Barros et al., 2005) were evaluated. Impairment of Aurora A activity was not detectable in these experiments (data not shown). While analysing syncytial embryos expressing green fluorescent D-TACC, fixed after anoxic incubation, D-TACC localization to the centrosomes was found to be clearly affected. In contrast to normoxic controls, upon anoxia, it formed asterisk like structures at the centrosomes (Part B, Fig. 3). By in vivo imaging, the transgenic D-TACC-GFP syncytial embryos, the speed of D-TACC re-localization was determined. It took about eight minutes for the change in D-TACC localization to get apparent, thereby, indicating that these changes occurred when the embryos were already in the metaphase arrest (data not shown). Time lapse imaging also allowed evaluation of D-TACC behavior upon re-aeration. It returned to normal appearance and the asterisk-like structures disappeared upon re-aeration and before entry into anaphase (data not shown). Moreover, major re-organization of the centrosomal asters was observed, soon after re-aeration (data not shown). Like Aurora A, γ -tubulin was affected in a subtle fashion in response to anoxia (Part B, Fig. 3). Cnn flares that represent transport to and from the centrosome primarily on dynamic astral microtubules during metaphase as well as interphase (Megraw et al., 2002) were not detectable in anoxia (Part B, Fig. 3), thus indicating that the transport of material along the astral microtubules might be hampered in anoxia. To analyse the transport along the spindle microtubules, motor proteins, Kin-8/KLP67A and dynein localization behavior upon exposure to anoxia was studied by immunolabeling anoxic *w*¹ syncytial embryos with anti-KLP67A and anti-dynein light intermediate chain antibodies respectively. KLP67A, which co-localizes with the spindles in normoxia, was significantly diminished in response to anoxia and concentrated only at the equatorial plane (Part B, Fig. 4). In contrast, dynein intermediate chain migrated from the equatorial plane to the spindle fibers around the kinetochores in anoxia (Part B, Fig. 4). Moreover, in vivo imaging of the syncytial embryos expressing green fluorescent dynein intermediate chain demonstrated its particle movement along the spindles in anoxia (data not shown). Thus, motor activity is clearly present during anoxia, at least initially.

5.5 Kinetochores proteins re-localize in response to anoxia

The reduced tension experienced at the kinetochores in response to anoxia might be a consequence of inappropriate behavior of certain kinetochore proteins. In an effort to characterize the effects of anoxia on the centromere/kinetochore architecture, behavior of some of the inner and outer kinetochore proteins was studied. Syncytial embryos from *w*¹ flies stained with anti-Cid (Jäger et al., 2005) and anti-Cenp-C (Heeger et al., 2005) antibodies after anoxic incubation and fixation were used for studying the behavior of Cid/Cenp-A and Cenp-C, respectively. Constitutive centromere protein, Cid/CenpA was found to be not affected in anoxia (Part B, Fig. 2). In contrast, CenpC, another constitutive centromere protein, was dramatically re-distributed in response to anoxia (Part B, Fig. 5). It accumulated strongly at the centrosomes and along the spindles, in addition to the equatorial plane (Part B, Fig. 5). Immunolabeling with two different anti-Cenp-C antibodies showed similarly altered behavior in anoxia. Also, in vivo imaging experiments with strains expressing yellow fluorescent Cenp-C (Heeger et al., 2005) (data not shown) were in accord with the analysis in fixed samples. Moreover, since Ndc-80 complex proteins have been shown to be necessary to sustain tension during interactions with spindle microtubules (Cheeseman et al., 2004), it was interesting to check their behavior in response to anoxia. For deciphering the reaction of Ndc-80 complex in anoxia, syncytial embryos from transgenic flies expressing green fluorescent Nuf2, a component of the Ndc-80 complex, were analysed after anoxic incubation and fixation. Nuf2, in anoxia, was found to be very similar to Cenp-C (Part B, Fig. 5). Re-organization of a constitutive centromere protein as well as an outer kinetochore protein likely indicates that the kinetochore architecture is not completely intact in anoxia. Further experiments, however, would be needed to investigate the precise nature of kinetochore architecture perturbation in response to anoxia.

5.6 The mitotic spindle checkpoint is activated by anoxia

Since spindle checkpoint is required for metaphase arrest in response to anoxia, it is of interest to know the behavior of checkpoint components in anoxia. The effect of anoxia on the mitotic spindle checkpoint machinery was studied not only by in vivo imaging but also after fixation, using strains expressing various green fluorescent checkpoint components. Proteins functioning in the mitotic spindle checkpoint were found to be rapidly re-distributed in response to anoxia

(Part B, Fig 6). Amongst the players analysed, Mps1 and BubR1 were found to be re-localizing most dramatically. Under normoxic conditions, green fluorescent Mps1 has been shown to be weakly present at centrosomes, spindle and kinetochores (Fischer et al., 2004). Upon anoxia, however, within a few minutes it accumulated at the equatorial plane during the metaphase arrest (Part B, Fig 6). In addition, in about 5% embryos, it formed conspicuous filaments and aggregates at or around the centrosomes. These conspicuous aggregates and structures were also seen at the surface of pre-blastoderm embryos and unfertilized eggs in about 80% of the cases (Part B, Fig 6). Green fluorescent BubR1 was affected similarly by anoxia. Double labeling clearly demonstrated co-localization of Mps1 and BubR1 in response to anoxia, even at the filamentous structures (Part B, Fig. 6). Another spindle checkpoint component, Bub3 was also found to aggregate at the equatorial region in anoxia. The filamentous structures and aggregates were, however, not seen in this case.

RZZ (Rod ZW-10 Zwilch) (Karess, 2005) and Mad2 have also been shown to be a part of the spindle checkpoint. Their response to anoxia was also evaluated by analysing strains expressing green fluorescent Rod and Mad2 (data not shown). They were found to accumulate at the spindle and equatorial plane (Part B, Fig. 6). In addition, particle movement in anoxic conditions was observed during in vivo experiments with transgenic embryos expressing green fluorescent dynein, Rod (data not shown) and Mps1 (Part B, Fig. 6), respectively, thereby favoring that the motor activity is still present in anoxia. Consistent with the existing models, claiming Fzy/Cdc20 inhibition by Mad2 and BubR1 during spindle checkpoint activation, Fzy was found to be enriched at the spindles in anoxia.

Interestingly, certain checkpoint components were also re-distributed in anoxic interphase. During normoxic interphase, Mps1 is weakly detectable at the centrosomes (Fischer et al., 2004). At anoxic interphase, however, it formed distinct spots closely associated with the interphase centrosomes, hinting its localization at the centrioles (Part B, Fig 6). BubR1 was found to be like Mps1, also during oxygen deprived interphase (data not shown). Moreover, Bub3, which is not detectable at the centrosomes during normoxic conditions, was found to be at the centrosomes (data not shown) during the anoxic interphase. Altered Mps1, BubR1 and Bub3 localization suggests that spindle checkpoint is triggered not only in mitosis but also in interphase. Mps1 electrophoretic mobility was analysed

during interphase in response to anoxia, since spindle checkpoint activation is known to be associated with its shift. This experiment using anti-Mps1 antibodies revealed no shift in Mps1 electrophoretic mobility in anoxic interphase, although it was detectable during normoxic and anoxic metaphases (Part B, Fig. 7).

5.7 Anoxia effects on mitosis are mimicked by metabolic inhibitors

Effects of anoxia were compared with that of metabolic inhibitors as both lead to decrease in ATP levels (DiGregorio et al., 2001). For poisoning metabolism, syncytial embryos expressing green fluorescent Mps1 were incubated in medium containing potassium cyanide. Metabolic inhibition also arrested the embryos in metaphase as well as interphase (Part B, Fig. 8). In addition, Mps1 accumulation in metaphase as well as interphase and spindle morphology defects observed after treatment with cyanide were very similar to the effects of anoxia (Part B, Fig. 8). Like anoxia, oxidative inhibition also resulted in rapid reduction of aster microtubules. It should be pointed out that after treatment with cyanide and 2-deoxyglucose, enhancement of aster microtubules has been observed in mitotic mammalian cells in culture (Wadsworth and Salmon, 1988). Since these conditions inhibit not only oxidative phosphorylation but also glycolysis, a further decline in ATP levels is expected, which in turn might result in increased aster microtubules. These findings indicate that proper chromosome attachment to the mitotic spindle is more sensitive to reduction in ATP levels than the post-metaphase processes.

5.8 The early syncytial cycles are the most cold-sensitive stages of *Drosophila* embryogenesis

Amongst environmental stress types, other than anoxia, hypothermia is often experienced by most of the organisms. Therefore, cold sensitivity of various processes and stages during embryogenesis was studied. To identify the embryonic stages that are most sensitive to low temperatures, collections from *w*¹ flies were made spanning various stages of embryogenesis. Incubation of these stages at 9°C for 12 hours followed by recovery for 30 hours and larval hatch rate evaluation revealed that syncytial stages of embryogenesis are most cold-sensitive (Part C, Fig. 1). Interestingly, after cellularization the embryos were much more resistant to cold. This difference might be a consequence of the fact

that syncytial embryos consist of nuclei in a common cytoplasm, while the cellularized stages have nuclei surrounded with cell membranes, which are likely to confer further resistance in combatting environmental stress. In addition, the survival of syncytial embryos was evaluated after a 12 hour exposure to temperatures ranging from 8 to 12°C, followed by 30 hours recovery at 25°C. Less than 20% embryos could survive the cold exposure to temperatures below 10°C. However, about 80% embryos were able to survive exposure to 12°C (Part C, Fig. 2). The embryonic development of *D. melanogaster* is known to occur even at 12°C. However, the males raised at this temperature have been shown to be completely sterile (Chakir et al., 2002). Using immunofluorescence, the embryos exposed to low temperatures were analysed to provide an insight into the abnormalities associated with syncytial embryonic development. At 9°C, mitoses appeared to get affected resulting in unequal nuclear spacing after short incubations and defective cellularization after extended exposure (Part C, Fig. 3). It is worth pointing out that rapid cooling is almost never experienced in the wild. However, gradual cooling is often experienced during the night. Therefore, the effects of physiological gradual cooling and rapid cooling were compared. Contrary to the expectations, extent of nuclear irregularities were found to be similar after gradual physiological cooling and rapid cooling (Part C, Fig. 4). Such a phenotype is conceivable upon temperature lowering because spindles were found to be not entirely normal after temperature decline to 9°C (Part C, Fig. 5). To get the temporal information concerning spindle stability at low temperatures, syncytial embryos expressing red fluorescent Histone H2Av and green fluorescent *G147* (Part A, Fig 1) were used. This allowed simultaneous analysis of chromatin and spindle behavior at 4°C. Spindles were found to depolymerize within minutes at 4°C (Part C, Fig. 5). Normal cell cycle progression through the syncytial cycles was found to require temperatures above 10°C (Part C, Fig. 2). In contrast to 9°C, defects in progression through the syncytial cycles and cellularization were not detectable at 12°C (Part C, Fig. 3). However, severe defects were observed in gastrulation (Part C, Fig. 7) indicating that processes other than mitoses are also sensitive to low temperatures. Such a defect might be a result of cold induced membrane plasticity, as has been reported in bacteria (Weber and Marahiel, 2003). Moreover, the interference of low temperature with expression of certain genes might result in defective gastrulation. There is at least one report showing

that gastrulation defects can occur due to other types of environmental stresses as well, hypoxia being one such example (DiGregorio et al., 2001). Since both hypoxia and hypothermia result in lowered ATP levels, gastrulation problems are likely to be a reflection of reduced ATP levels.

5.9 Mitotic spindle checkpoint is important for cold survival

In order to understand the mechanisms adopted by the organisms to withstand cold, precise information about the candidate genes involved is important. Therefore, a deficiency screen was devised based on interference of cold exposure with embryogenesis. The screen was aimed at identification of chromosomal regions important for conferring cold survival during embryonic development. Eventually such chromosomal regions are expected to reveal genes involved in pathways that sense and react to cold. Conditions were chosen allowing the development in 50% of the syncytial embryos derived from w^1 females. Using these conditions, a screen was carried out with syncytial embryos derived from females lacking one copy of molecularly defined chromosomal regions. Unfortunately, the reproducibility of larval hatch rates with eggs derived from control w^1 females was found to be relatively low (Part C, Fig. 6). Hence, an initial screening round was done analysing two successive collections from each deficiency stock. 0-0.5 hour syncytial embryos from the deficiency stocks belonging to the Exelixis deficiency kit (Parks et al., 2004; Thibault et al., 2004) were incubated at 11°C for 12 hours followed by recovery at 25°C for 30 hours and evaluation of survivors by counting hatched and unhatched eggs. To evaluate the unperturbed larval hatch rates, half of the egg collection was incubated at 25°C for 30 hours followed by counts of hatched and unhatched eggs. Vast majority of the deficiency stocks had a ratio of 0.5 between larval hatch rates after exposure to 11 and 25°C (Part C, Fig. 6). A total of 12 deficiency stocks were found to have similar larval hatch rates after the two treatments, indicating these to be cold resistant. 11 out of the selected 44 deficiency stocks were reproducibly found to be associated with especially pronounced cold sensitivity. These stocks reproducibly yielded a ratio value two standard deviations below the overall average ratio. In addition, these deficiencies were associated with a healthy egg laying rate (~60 eggs in 30 minutes from ~200 females) (Part C, Table 1). 9 of the 11 deficiencies were on the second chromosome and the remaining 2 were on the third

chromosome. The females often lay variable number of unfertilized and overaged eggs in a collection. Moreover, females lacking chromosomal regions usually lay more overaged and unfertilized eggs. Unfertilized eggs would not be supposed to cause a problem but overaged eggs would be expected to have a significant impact on the computed larval hatch rates, as they are cold resistant (Part C, Fig. 1). This fact might thus affect the findings of the deficiency screen, since the quality of the collections was not monitored there. However, control larval hatch rate analysis was always performed and only those cases were selected where the ratio of the two treatments was significantly below the average value. Since always the ratios were compared, the possibility of false positives due to the overaged eggs can be ruled out. The 12 cold resistant deficiency stocks, however, could in principle be explained by majority of the eggs in the collection being overaged ones. This still remains a possibility and should be resolved by cytological analysis. An additional aspect is that of contribution of balancers to cold sensitivity. The deficiency stocks tested for especially pronounced cold sensitivity carried a balancer and it is not excluded that the enhancement in cold sensitivity is conferred by the balancer and not the chromosomal deficiency. It is less likely to be the case, since the deficient chromosome and not the balancer varied from one deficiency stock to another and if the cold sensitivity was to be a consequence of balancer effects, then most of the deficiencies would be associated with enhanced cold sensitivity. It should be explored whether the severe cold sensitivity in the above mentioned 11 deficiencies is a synthetic effect of the balancer together with these specific deficiencies. Even though there are some open questions, the studies presented here provide an initial step towards discovering the components of an almost unexplored environmental stress response.

In addition, some potential candidate genes were tested for cold sensitivity. Since mitotic defects were frequent and spindle microtubule depolymerization has been reported and observed upon exposure to low temperatures, mitotic spindle checkpoint is likely to have a contribution in sensing and responding to cold. To test this possibility, *Mps1*¹ mutant syncytial embryos (Fischer et al. 2004) were analyzed for the enhanced cold sensitivity in a manner analogous to the above mentioned deficiency screen. These were found to have a ratio value that was clearly two standard deviations below the average ratio. Although, formally it is not excluded that the enhanced cold sensitivity is a consequence of a role of Mps1

independent of spindle checkpoint, it is likely that the role of Mps1 kinase in the mitotic spindle checkpoint is important for the survival of embryos in response to cold. Further establishment of the checkpoint involvement in cold survival would require analyses of cold sensitivity in the absence of additional spindle checkpoint components. Finally, contribution of DNA damage checkpoint to cold survival was also tested. The syncytial embryos lacking the protein kinase *chk2/loki* (Masorouha et al., 2003) which is involved in sensing DNA damage, were found to be as cold-sensitive as the control embryos. This suggests that DNA damage checkpoint may not be conferring cold resistance in *D. melanogaster*.

These findings provide suggestions for Mps1 and spindle checkpoint involvement in cold response, a novel role that has never been implicated in any earlier study.

6 References

- Barros, T. P., K. Kinoshita, A. A. Hyman and J.W. Raff. 2005. Aurora A activates D-TACC-Msps complexes exclusively at centrosomes to stabilize centrosomal microtubules. *J Cell Biol* **170**: 1039-46.
- Basu, J., H. Bousbaa, E. Logarinho, Z. Li, B. C. Williams, C. Lopes, C. E. Sunkel and M.L. Goldberg. 1999. Mutations in the essential spindle checkpoint gene *bub1* cause chromosome missegregation and fail to block apoptosis in *Drosophila*. *J Cell Biol* **146**: 13-28.
- Baum, P., C. Yip, L. Goetsch and B. Byers. 1988. A yeast gene essential for regulation of spindle pole duplication. *Mol Cell Biol* **8**: 5386-97.
- Brinkley, B.R. and J. Cartwright, Jr. 1975. Cold-labile and cold-stable microtubules in the mitotic spindle of mammalian cells. *Ann N Y Acad Sci* **253**: 428-439.
- Chakir, M., A. Chafik, B. Moreteau, P. Gibert and J.R. David. 2002. Male sterility thermal thresholds in *Drosophila*: *D. simulans* appears more cold-adapted than its sibling *D. melanogaster*. *Genetica* **114**: 195-205.
- Cheeseman, I. M., S. Niessen, S. Anderson, F. Hyndman, J. R. 3rd. Yates, K. Oegema and A. Desai. 2004. A conserved protein network controls assembly of the outer kinetochore and its ability to sustain tension. *Genes Dev* **18**: 2255-68.
- D'Amours, D. and A. Amon. 2004. At the interface between signaling and executing anaphase-Cdc14 and the FEAR network. *Genes Dev* **18**: 2581-95.
- D'Andrea, R.J., R. Stratmann, C.F. Lehner, U.P. John and R. Saint. 1993. The *three rows* gene of *Drosophila melanogaster* encodes a novel protein that is required for chromosome disjunction during mitosis. *Mol Biol Cell* **4**: 1161-1174.
- DiGregorio, P.J., J.A. Ubersax and P.H. O'Farrell. 2001. Hypoxia and nitric oxide induce a rapid, reversible cell cycle arrest of the *Drosophila* syncytial divisions. *J Biol Chem* **276**: 1930-7.
- Dobles, M., V. Liberal, M. L. Scott, R. Benezra and P.K. Sorger. 2000. Chromosome missegregation and apoptosis in mice lacking the mitotic checkpoint protein Mad2. *Cell* **101**: 635-45.
- Fischer, M.G., S. Heeger, U. Häcker and C.F. Lehner. 2004. The mitotic arrest in response to hypoxia and of polar bodies during early embryogenesis requires *Drosophila* Mps1. *Curr Biol* **14**: 2019-24.
- Foe, V.E. and B.M. Alberts. 1983. Studies of nuclear and cytoplasmic behaviour

- during the five mitotic cycles that precede gastrulation in *Drosophila* embryogenesis. *J Cell Sci* **61**: 31-70.
- Foe, V. E., and B.M. Alberts. 1985. Reversible chromosome condensation induced in *Drosophila* embryos by anoxia: visualization of interphase nuclear organization. *J Cell Biol* **100**: 1623-36.
- Garner, M., S. van Kreeveld and T.T. Su. 2001. mei-41 and bub1 block mitosis at two distinct steps in response to incomplete DNA replication in *Drosophila* embryos. *Curr Biol* **11**: 1595-1599.
- Giet, R., D. McLean, S. Descamps, M. J. Lee, R. W. Raff, C. Prigent and D.M. Glover . 2002. *Drosophila* Aurora A kinase is required to localize D-TACC to centrosomes and to regulate astral microtubules. *J Cell Biol* **156**: 437-51.
- Goshima, G., R. Wollman, N. Stuurman, J. M. Scholey and R.D. Vale. 2005. Length control of the metaphase spindle. *Curr Biol* **15**: 1979-88.
- Grieder, N.C., M. de Cuevas and A.C. Spradling. 2000. The fusome organizes the microtubule network during oocyte differentiation in *Drosophila*. *Development* **127**: 4253-64.
- Hajeri, V. A., J. Trejo, P.A. Padilla. 2005. Characterization of sub-nuclear changes in *Caenorhabditis elegans* embryos exposed to brief, intermediate and long-term anoxia to analyze anoxia-induced cell cycle arrest. *BMC Cell Biol* **6**: 47.
- Hardwick, K.G., E. Weiss, F.C. Luca, M. Winey and A.W. Murray. 1996. Activation of the budding yeast spindle assembly checkpoint without mitotic spindle disruption. *Science* **273**: 953-6.
- Hauf, S., I. C. Waizenegger and J.M. Peters. 2001. Cohesin cleavage by separase required for anaphase and cytokinesis in human cells. *Science* **293**: 1320-1323.
- Heeger, S., O. Leismann, R. Schittenhelm, O. Schraidt, S. Heidmann and C.F. Lehner. 2005. Genetic interactions of separase regulatory subunits reveal the diverged *Drosophila* Cenp-C homolog. *Genes Dev* **19**: 2041-53.
- Herzig, A., C. F. Lehner and S. Heidmann. 2002. Proteolytic cleavage of the THR subunit during anaphase limits *Drosophila* separase function. *Genes Dev* **16**: 2443-54.
- Hime, G. and R. Saint. 1992. Zygotic expression of the *pebble* locus is required during the postblastoderm mitoses of *Drosophila*. *Development* **114**: 165-171.
- Hoffmann, A. A., M. Scott, L. Partridge and R. Hallas. 2003. Overwintering in

- Drosophila melanogaster*: outdoor field cage experiments on clinal and laboratory selected populations help to elucidate traits under selection. *J Evol Biol* **16**: 614-23.
- Jäger, H., A. Herzig, C. F. Lehner and S. Heidmann. 2001. *Drosophila* separase is required for sister chromatid separation and binds to PIM and THR. *Genes Dev* **15**: 2572-84.
- Jäger, H., B. Herzig, A. Herzig, H. Sticht, C. F. Lehner and S. Heidmann. 2004. Structure predictions and interaction studies indicate homology of separase N-terminal regulatory domains and *Drosophila* THR. *Cell Cycle* **3**: 182-8.
- Jäger, H., M. Rauch, and S. Heidmann. 2005. The *Drosophila melanogaster* condensin subunit Cap-G interacts with the centromere-specific histone H3 variant CID. *Chromosoma* **113**:350-361.
- Kalitsis, P., E. Earle, K. J. Fowler and K.H. Choo. 2000. *Bub3* gene disruption in mice reveals essential mitotic spindle checkpoint function during early embryogenesis. *Genes Dev* **14**: 2277-82.
- Karess, R. 2005. Rod-Zw10-Zwilch: a key player in the spindle checkpoint. *Trends Cell Biol* **15**: 386-92.
- Kellogg, D. R., T. J. Mitchison, and B. M. Alberts. 1988. Behaviour of microtubules and actin filaments in living *Drosophila* embryos. *Development* **103**: 675-86.
- Kinoshita, K., T. L. Noetzel, L. Pelletier, K. Mechtler, D. N. Drechsel, A. Schwager, M. Lee, J. W. Raff and A.A. Hyman. 2005. Aurora A phosphorylation of TACC3/maskin is required for centrosome-dependent microtubule assembly in mitosis. *J Cell Biol* **170**: 1047-55.
- Lehner, C. F. 1992. The *pebble* gene is required for cytokinesis in *Drosophila*. *J. Cell Sci* **103**: 1021-1030.
- Leismann, O. and C.F. Lehner. 2003. *Drosophila* securin destruction involves a D-box and a KEN-box and promotes anaphase in parallel with Cyclin A degradation. *J Cell Sci* **116**: 2453-60.
- Li, R. and A.W. Murray. 1991. Feedback control of mitosis in budding yeast. *Cell* **66**: 519-31.
- Logarinho, E., H. Bousbaa, J. M. Dias, C. Lopes, I. Amorim, A. Antunes-Martins and C.E. Sunkel. 2004. Different spindle checkpoint proteins monitor microtubule attachment and tension at kinetochores in *Drosophila* cells. *J Cell Sci* **117**: 1757-71.
- Masrouha, N., L. Yang, S. Hijal, S. Laroche and B. Suter. 2003. The *Drosophila* *chk2* gene loki is essential for embryonic DNA double-strand-break checkpoints induced in S phase or G2. *Genetics* **163**: 973-982.

- McIntosh, J. R., E. L. Grishchuk and R.R. West. 2002. Chromosome-microtubule interactions during mitosis. *Annu Rev Cell Dev Biol* **18**: 193-219.
- Megraw, T.L., S. Kilaru, F. R. Turner and T.C. Kaufman. 2002. The centrosome is a dynamic structure that ejects PCM flares. *J Cell Sci* **115**: 4707-18.
- Meraldi, P., V.M. Draviam and P.K. Sorger. 2004. Timing and checkpoints in the regulation of mitotic progression. *Dev Cell* **7**: 45-60.
- Michaelis, C., R. Ciosk and K. Nasmyth. 1997. Cohesins: Chromosomal proteins that prevent premature separation of sister chromatids. *Cell* **91**: 35-45.
- Minshull, J., J. Pines, R. Golsteyn, N. Standart, S. Mackie, A. Colman, J. Blow, J.V. Ruderman, M. Wu and T. Hunt. 1989. The role of cyclin synthesis, modification and destruction in the control of cell division. *J Cell Sci* **12**: 77-97.
- Minshull, J., H. Sun, N.K. Tonks and A.W. Murray. 1994. A MAP kinase-dependent spindle assembly checkpoint in *Xenopus* egg extracts. *Cell* **79**: 475-486.
- Morin. X., R. Daneman, M. Zavortink and W. Chia. 2001. A protein trap strategy to detect GFP-tagged proteins expressed from their endogenous loci in *Drosophila*. *Proc Natl Acad Sci U S A* **98**: 15050-5.
- Musacchio, A and K.G. Hardwick. 2002. The spindle checkpoint: structural insights into dynamic signalling. *Nat Rev Mol Cell Biol* **3**: 731-41.
- Nasmyth, K. 2002. Segregating sister genomes: the molecular biology of chromosome separation. *Science* **297**: 559-65.
- Nystul, T.G., J.P. Goldmark, P.A. Padilla and M.B. Roth. 2003. Suspended animation in *C. elegans* requires the spindle checkpoint. *Science* **302**: 1038-41.
- Parry, D. H., G.R. Hickson and P.H. O'Farrell. 2003. Cyclin B destruction triggers changes in kinetochore behavior essential for successful anaphase. *Curr Biol* **13**: 647-653.
- Prokopenko, S. N., A. Brumby, L. O'Keefe, L. Prior, Y. He, R. Saint and H.J. Bellen. 1999. A putative exchange factor for Rho1 GTPase is required for initiation of cytokinesis in *Drosophila*. *Genes Dev* **13**: 2301-2314.
- Rieder, C. L. 1981. The structure of the cold-stable kinetochore fiber in metaphase PtK1 cells. *Chromosoma* **84**: 145-158.
- Rieder, C. L., A. Schultz, R. Cole and G. Sluder. 1994. Anaphase onset in vertebrate somatic cells is controlled by a checkpoint that monitors sister kinetochore attachment to the spindle. *J Cell Biol* **127**: 1301-10.
- Sciambi, C. J., D. J. Komma, H. N. Skold, K. Hirose, S.A. Endow. 2005. A

- bidirectional kinesin motor in live *Drosophila* embryos. *Traffic* **6**: 1036-46.
- Siomos, M. F., A. Badrinath, P. Pasierbek, D. Livingstone, J. White, M. Glotzer and K. Nasmyth. 2001. Separase is required for chromosome segregation during meiosis I in *Caenorhabditis elegans*. *Curr Biol* **11**: 1825-1835.
- Sironi, L., M. Melixetian, M. Faretta, E. Prosperin, K. Helin and A. Musacchio. 2001. Mad2 binding to Mad1 and Cdc20, rather than oligomerization, is required for the spindle checkpoint. *EMBO J* **20**: 6371-82.
- Stegmeier, F., R. Visintin and A. Amon. 2002. Separase, polo kinase, the kinetochore protein Slk19, and Spo12 function in a network that controls Cdc14 localization during early anaphase. *Cell* **108**: 207-20.
- Stratmann, R. and C.F. Lehner. 1996. Separation of sister chromatids in mitosis requires the *Drosophila pimples* product, a protein degraded after the metaphase anaphase transition. *Cell* **84**: 25-35.
- Sullivan, M. and F. Uhlmann. 2003. A non-proteolytic function of separase links the onset of anaphase to mitotic exit. *Nat Cell Biol* **5**: 249-54.
- Sullivan, M., C. Lehane and F. Uhlmann. 2001. Orchestrating anaphase and mitotic exit: separase cleavage and localization of Slk19. *Nat Cell Biol* **3**: 771- 777.
- Sumara, I., E. Vorlaufer, P.T. Stukenberg, O. Kelm, N. Redemann, E. A. Nigg and J.M. Peters. 2002. The dissociation of cohesin from chromosomes in prophase is regulated by Polo-like kinase. *Mol Cell* **9**: 515-25.
- Toth, A., R. Ciosk, F. Uhlmann, M. Galova, A. Schleiffer and K. Nasmyth. 1999. Yeast cohesin complex requires a conserved protein, Eco1p(Ctf7), to establish cohesion between sister chromatids during DNA replication. *Genes Dev* **13**: 320-33.
- Tsou, M. F. and T. Stearns. 2006. Mechanism limiting centrosome duplication to once per cell cycle. *Nature* **442**: 947-51.
- Uhlmann F., F. Lottspeich and K. Nasmyth. 1999. Sister-chromatid separation at anaphase onset is promoted by cleavage of the cohesin subunit Scc1. *Nature* **400**: 37-42.
- Uzawa, S., I. Samejima, T. Hirano, K. Tanaka, and M. Yanagida. 1990. The fission yeast cut1+ gene regulates spindle pole body duplication and has homology to the budding yeast esp1 gene. *Cell* **62**: 913-925.
- Visintin, R., K. Craig, E. S. Hwang, S. Prinz, M. Tyers and A. Amon. 1998. The phosphatase Cdc14 triggers mitotic exit by reversal of Cdk-dependent phosphorylation. *Mol Cell* **2**:709-18.
- Wadsworth, P., and E. D. Salmon. 1988. Spindle microtubule dynamics:

- modulation by metabolic inhibitors. *Cell Motil Cytoskeleton* **11**: 97-105.
- Waizenegger, I. C., S. Hauf, A. Meinke and J.M. Peters. 2000. Two distinct pathways remove mammalian cohesin from chromosome arms in prophase and from centromeres in anaphase. *Cell* **103**: 399-410.
- Weber, M. H. and M.A. Marahiel. 2003. Bacterial cold shock responses. *Sci Prog* **86**: 9-75.
- Whitfield, W. G. F., C. Gonzalez, G. Maldonado-Codina and D.M. Glover. 1990. The A- and B-type cyclins of *Drosophila* are accumulated and destroyed in temporally distinct events that define separable phases of the G2-M transition. *EMBO J* **9**: 2563-2572.
- Whittaker, A. J., I. Royzman and T.L. Orr-Weaver. 2000. *Drosophila* double parked: a conserved, essential replication protein that colocalizes with the origin recognition complex and links DNA replication with mitosis and the down-regulation of S phase transcripts. *Genes Dev* **14**: 1765-1776.

7 Appendix

Part A

Contribution to Part A

Part B

Contribution to Part B

Part C

Contribution to Part C

Erklärung

Part A

Epithelial re-organization and dynamics of progression through mitosis in *Drosophila* separase complex mutants.

Rahul Pandey, Stefan Heidmann and Christian F. Lehner

Journal of Cell Science 118, 733-742 (2005).

Contribution to Part A

The study was designed by the last author and myself. All the results of this part are from my work. *His2Av-mRFP* lines were provided by Stefan Heidmann.

The part was written by the last author with contributions by the other authors.

Epithelial re-organization and dynamics of progression through mitosis in *Drosophila* separase complex mutants

Rahul Pandey, Stefan Heidmann and Christian F. Lehner*

BZMB, Department of Genetics, University of Bayreuth, 95440 Bayreuth, Germany

*Author for correspondence (e-mail: chle@uni-bayreuth.de)

Accepted 24 November 2004

Journal of Cell Science 118, 733-742 Published by The Company of Biologists 2005
doi:10.1242/jcs.01663

Summary

Separase cleaves a subunit of the cohesin complex and thereby promotes sister chromatid separation during mitotic and meiotic divisions. *Drosophila* separase associates with regulatory subunits encoded by the *pimples* and *three rows* genes. Three rows and Pimples, the *Drosophila* securin, are required for sister chromatid separation during mitosis. Budding yeast separase provides other functions in addition to cohesin subunit cleavage, which are required for spindle organization and temporal regulation during exit from mitosis. Therefore, using time-lapse imaging in live embryos, we have carefully analyzed progression through mitosis in *pimples* and *three rows* mutants. We demonstrate that despite the total failure of sister chromatid separation, exit from mitosis, including a

complete cytokinesis, proceeds with only a minor temporal delay in the epidermal cells of these mutants. Interestingly, however, pronounced defects in the epithelial organization develop in the following interphase, indicating that the separase complex is not only important for genetic stability but also and perhaps indirectly for epithelial integrity.

Supplementary material available online at
<http://jcs.biologists.org/cgi/content/full/118/4/733/DC1>

Key words: Cytokinesis, Centrosome, Junctional dynamics, Mitotic exit network (MEN), Cdc fourteen early anaphase release (FEAR), Separase

Introduction

Separase is a thiol protease that cleaves α -kleisin subunits (Scc1/Mcd1/Rad21/Rec8 family members) of cohesin complexes and thereby contributes to sister chromatid separation during mitotic and meiotic divisions (Buonomo et al., 2000; Uhlmann et al., 1999; Uhlmann et al., 2000). Before anaphase onset, protease activity is inhibited by securin, a protein that binds to separase during interphase. However, at the metaphase-to-anaphase transition securin is degraded after ubiquitination by the anaphase-promoting complex/cyclosome (APC/C) (Ciosk et al., 1998; Cohen-Fix et al., 1996; Funabiki et al., 1996; Uhlmann et al., 2000; Zou et al., 1999).

Apart from α -kleisin cleavage, budding yeast separase has been shown to function in an additional pathway during exit from mitosis (Stegmeier et al., 2002; Tinker-Kulberg and Morgan, 1999). Interestingly, protease activity does not appear to be required in this FEAR (Cdc fourteen early anaphase release) pathway. Catalytically inactive separase versions are sufficient to trigger Cdc14 release from the nucleolus during early anaphase (Sullivan and Uhlmann, 2003). The released active Cdc14 phosphatase promotes exit from mitosis (Jaspersen et al., 1999; Shou et al., 1999; Stegmeier et al., 2002; Visintin et al., 1998). The inner centromere protein Sli15 is dephosphorylated by Cdc14, resulting in the transfer of Sli15-Ipl1(Aurora) kinase complexes from a centromeric chromosomal localization to the central spindle (Pereira and Schiebel, 2003). Slk19, another yeast protein, which transfers

to the central spindle during exit from mitosis, is also regulated by separase. Slk19 associates with separase following securin degradation. Slk19 and its cleavage by separase enhances the stability of anaphase spindles (Sullivan et al., 2001; Ross and Cohen-Fix, 2004). Moreover, Slk19 co-operates with separase in the early anaphase release of Cdc14. In addition to regulating spindle and mitotic exit dynamics, FEAR has recently been shown to promote sister chromatid separation in the nucleolus by stimulating the binding of condensin complexes to the rDNA region (D'Amours et al., 2004; Sullivan et al., 2004).

The FEAR pathway, however, does not appear to be absolutely essential. Completion of mitosis is only transiently delayed by about 30 minutes in separase mutants, but eventually cells exit from mitosis because Cdc14 release in budding yeast can also be triggered by an additional regulatory system, the mitotic exit network (MEN). In wild-type cells, MEN activation is controlled by the mitotic spindle position and it maintains Cdc14 activity after the initial release by FEAR (Bardin et al., 2000; Stegmeier et al., 2002).

It is not yet clear whether pathways comparable to budding yeast FEAR and MEN operate in higher eukaryotes that also express Cdc14 homologues. Some, but not all of the other pathway components can also be identified in higher eukaryotes, but it remains to be determined whether Cdc14 and the other apparent homologues provide the same function as in yeast. In particular, it is not known whether separase provides FEAR-like functions in higher eukaryotes. Cytokinesis and

exit from mitosis are not delayed after RNAi-mediated separase elimination in *C. elegans* (Siomos et al., 2001). In contrast, completion of cytokinesis appears to depend on separase function in human cells (Hauf et al., 2001; Waizenegger et al., 2000).

To elucidate the role of separase during completion of mitosis in further detail, we describe phenotypic analyses in *Drosophila*. During the evolution of *Drosophila*, the separase gene has apparently become two genes, *three rows* (*thr*) and *Separase* (*Sse*) which encode the N-terminal regulatory domain and the C-terminal protease domain, respectively (Jäger et al., 2001; Jäger et al., 2004). *Drosophila* securin is encoded by the *pimples* (*pim*) gene (Leismann et al., 2000; Stratmann and Lehner, 1996). SSE, THR and PIM form a trimeric complex during interphase. After degradation of PIM at the metaphase-to-anaphase transition, SSE promotes sister chromatid separation and also cleaves the associated THR subunit, a process that contributes to timely SSE inactivation (Herzig et al., 2002). We have previously shown that a loss of PIM, THR or SSE function results in a failure of sister chromatid separation during mitosis (D'Andrea et al., 1993; Jäger et al., 2001; Stratmann and Lehner, 1996). In addition, non-cleavable THR versions were shown to interfere with cellularization (Herzig et al., 2002), which corresponds to a modified form of cytokinesis converting the syncytial into the cellularized blastoderm during interphase of cycle 14.

Here, we describe time-lapse analyses of progression through mitosis in live *pim* and *thr* mutant embryos. These analyses indicate that *Drosophila* separase is primarily required for sister chromatid separation. Cytokinesis and exit from mitosis appear to be surprisingly normal in the mutants. Cleavage furrows do not revert because of the non-separated chromatin mass present in these mutants. Interestingly, however, we find that the epithelial organization is severely affected in these mutants.

Materials and Methods

Fly stocks

Fly stocks with the mutant alleles *pim*¹, *thr*¹, *dup*^{al}, *pbl*⁷⁰ and *pbl*^{11D} have been described previously (Lehner, 1992; Stratmann and Lehner, 1996; Whittaker et al., 2000). A *pim*¹ *dup*^{al} double mutant chromosome was obtained by meiotic recombination. The *pim*¹ *pbl* double mutant embryos were obtained by crossing males heterozygous for *pim*¹ and *pbl*⁷⁰ with females heterozygous for *pim*¹ and *pbl*^{11D}. We used blue balancer chromosomes, which allowed the distinction of homozygous mutant from sibling progeny derived from heterozygous parents by anti-β-galactosidase labeling. *G147* carries a gene trap insertion in *CG31363*, resulting in expression of a microtubule-binding GFP fusion protein (Morin et al., 2001). *Spider* carries a gene trap insertion in *gilgamesh*, resulting in expression of a GFP fusion protein marking the cell cortex (Morin et al., 2001). The *His2AvD-mRFP* transgene driving expression of histone H2AvD fused to mRFP1 (Campbell et al., 2002) was constructed analogously to the *His2AvD-GFP* transgene (Clarkson and Saint, 1999) and will be described in detail elsewhere. A *His2AvD-mRFP* insertion on chromosome III was recombined meiotically with either the *G147* or the *Spider* gene trap insertion and crossed into the *pim*¹, *thr*¹ or *pim*¹ *dup*^{al} mutant background.

In vivo imaging

Eggs were collected on apple juice agar plates and aged to the desired

stages. Embryos were dechorionated, aligned and immobilized on coverslips according to standard procedures. After covering embryos with halocarbon oil, confocal laser scanning microscopy on an inverted Leica DM IRBE microscope equipped with a TCS SP1 system was used for time-lapse imaging of GFP and mRFP1 fluorescence signals at 22–24°C in a temperature-controlled room. Light damage was prevented by minimizing the laser intensity and opening the pinhole. Frames were acquired at intervals of 10 or 30 seconds. Representative examples of time-lapse movies are provided as supplementary material.

Immunolabeling

Embryos aged to the desired developmental stages were fixed according to standard procedures. For immunofluorescent staining we used mouse anti-γ-tubulin GTU-88 (Sigma) at 1:500, rabbit anti-Bazooka (kindly provided by E. Knust, University of Düsseldorf, Germany) at 1:600, rabbit anti-phospho-histone H3 (Upstate) at 1:800, mouse anti-α-spectrin 9A (Dubreuil et al., 1987) at 1:50, rabbit anti-cyclin B (Jacobs et al., 1998) at 1:2000 and mouse (Promega) and rabbit (Cappel) anti-β-galactosidase at 1:250 and 1:1000, respectively. In addition, secondary goat antibodies conjugated to Alexa488 (Molecular Probes), Cy3 or Cy5 (Jackson Immuno Research Laboratories) were applied. DNA was labeled with either Hoechst 33258 (1 μg/ml) or propidium iodide (1 μg/ml) for confocal microscopy. Terminal transferase dUTP nicked-end labeling (TUNEL) assays of apoptotic cells was performed essentially as described previously (Wang et al., 1999). For comparisons of the density of nucleated cells and of the numbers of mitotic cells, we analyzed three and ten pairs of fixed mutant and sibling wild-type embryos, respectively, which were carefully matched with regard to developmental stage and orientation. Fields of identical size from identical regions of the epidermal cell layer were imaged with a 63× objective and used for the determination of cell and nuclear counts.

Results

Mitosis 16 but not mitosis 15 is severely prolonged in *pim* mutants

The *Drosophila* securin PIM not only functions as an inhibitor of SSE, it also provides a positive function which is absolutely required for sister chromatid separation during mitosis (Stratmann and Lehner, 1996). Nevertheless, initial development of embryos homozygous for *pim*¹ is normal as long as the maternal *pim*⁺ contribution to the egg provided by the heterozygous mothers is sufficient. However, starting with mitosis 15, this maternal contribution is no longer sufficient for successful divisions. Sister chromatids are therefore not separated during mitosis 15 in *pim*¹ mutants (Stratmann and Lehner, 1996). The mutation present in *pim*¹ affects a splice junction (Stratmann and Lehner, 1996) and we have failed to detect protein products expressed from this allele in immunoblotting experiments (data not shown). To complement our previous characterization of fixed embryos by live analyses, we collected eggs from a *pim*¹/CyO stock carrying two transgenes that result in expression of a red fluorescent histone H2AvD variant (*His2AvD-mRFP*) and a green fluorescent microtubule binding protein. Progression through mitosis 15 in both *pim*¹ and *pim*⁺ sibling embryos was followed by time-lapse imaging of live embryos. Representative movies from these and the following analyses are available as supplementary material.

As expected from the previous findings with fixed *pim*

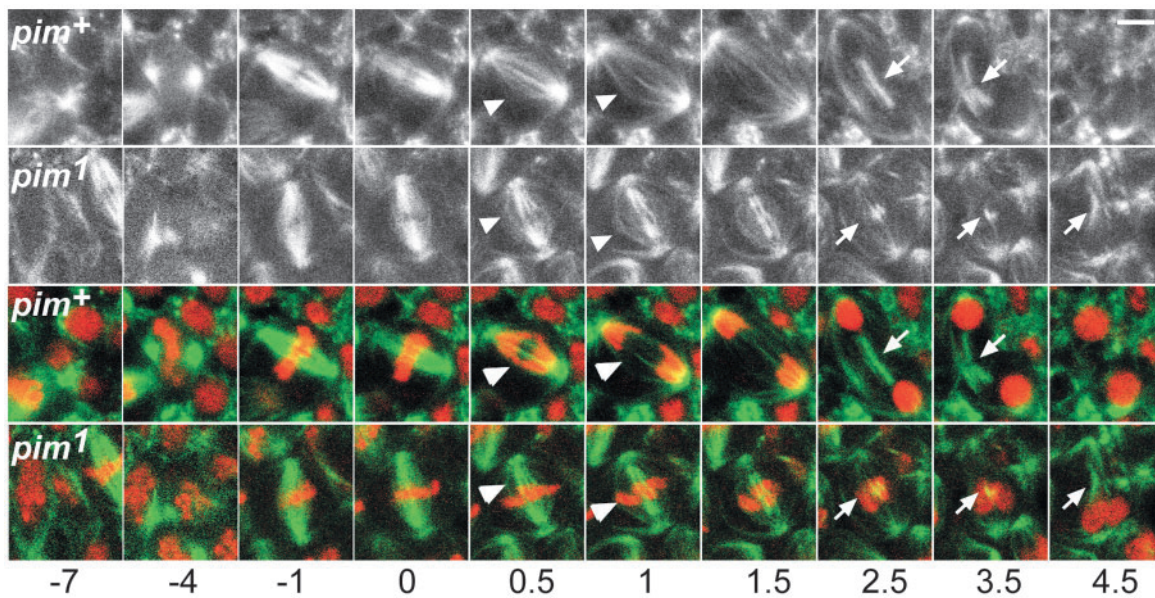


Fig. 1. Exit from mitosis 15 after failure of sister chromatid separation in *pim* mutant embryos. Time-lapse in vivo imaging was used for the analysis of progression through the fifteenth round of mitosis during *Drosophila* embryogenesis in *pim*¹ mutant (*pim*¹) and *pim*⁺ (*pim*⁺) sibling embryos expressing red fluorescent histone H2AvD-mRFP and a green fluorescent microtubule-binding protein. Selected frames showing microtubule distribution (top) or merged color images (bottom) are shown. Numbers below the frames indicate the time in minutes relative to the last metaphase frame, which was set to zero. The appearance of prominent inter-polar microtubules characteristic of anaphase is indicated by arrowheads. Central spindle and midbody during telophase are indicated by arrows. Bar in upper right frame, 5 μ m.

embryos, the first mitotic defects became apparent at the metaphase-to-anaphase transition (Fig. 1). Sister chromatids did not separate in *pim*¹ mutants. However, the dynamic reorganization of the mitotic spindle that accompanies wild-type anaphase and telophase clearly occurred in *pim*¹ mutants. The observed spindle behavior in *pim*¹ mutants during exit from mitosis suggested that absence of separase activity does not have a prominent effect on microtubule stability, in contrast to the findings in budding yeast.

Since budding yeast separase accelerates the exit from mitosis significantly, we compared the speed of chromosome

decondensation and spindle disassembly in *pim*¹ and *pim*⁺ sibling embryos. These comparisons revealed only a minor delay during exit from mitosis in *pim*¹ mutants (Fig. 1). The time from anaphase onset until the end of mitosis was determined as 4.8 minutes in *pim*¹ mutant cells ($n=10$), a value that was only 1.2-fold higher than in the *pim*⁺ sibling embryos ($n=7$). In vivo imaging using *His2AvD-mRFP* in combination with a GFP fusion protein marking the cell cortex confirmed that progression through mitosis 15 occurs at normal speed in *pim*¹ mutants except for the surprisingly minor delay during exit from mitosis (Table 1).

Table 1. Dynamics of progression through mitosis in *pim* and *thr* mutants

Genotype*	Stage [†]	n^{\ddagger}	Duration (minutes \pm s.d.)			
			Total [§]	Prophase and metaphase	Meta/ana until onset cytokinesis**	Cytokinesis ^{††}
<i>pim</i> ⁺	M15	36	10.0 \pm 2.4	6.4 \pm 2.2	1.7 \pm 0.4	1.8 \pm 0.4
<i>pim</i> ¹	M15	36	9.9 \pm 1.5	6.1 \pm 1.2	1.5 \pm 0.5	2.4 \pm 0.6
<i>thr</i> ¹	M15	10	9.6 \pm 0.7	5.2 \pm 1.0	1.4 \pm 0.3	3.0 \pm 0.5
<i>pim</i> ⁺	M16	20	7.4 \pm 0.7	4.2 \pm 0.6	1.6 \pm 0.3	1.6 \pm 0.5
<i>pim</i> ¹	M16	23	24.2 \pm 5.2 ^{**}	21.5 \pm 5.1 ^{**}	1.4 \pm 1.0	3.2 \pm 0.9
<i>pim</i> ¹ <i>dup</i> ^{al}	M16	32	18.8 \pm 5.2	11.7 \pm 4.6	2.2 \pm 0.7	3.9 \pm 1.5
<i>thr</i> ¹	M16	10	24.7 \pm 7.4 ^{**}	21.4 \pm 7.5 ^{**}	2.3 \pm 0.9	4.75 \pm 0.6

*Eggs from parents heterozygous for *pim*¹, *thr*¹ or *pim*¹ *dup*^{al}, which also carried a *His2AvD-mRFP* transgene and a gene trap insertion resulting in expression of a GFP fusion protein marking the cell cortex, were collected and used for time-lapse analysis. Homozygous mutant embryos were identified on the basis of the sister chromatid separation failure. *pim*⁺ are sibling embryos without sister chromatid separation failure.

[†]Progression through mitosis 15 (M15) or mitosis 16 (M16) was analyzed.

[‡] n =number of mitotic cells analyzed. These mitotic cells were from at least two different embryos.

[§]Time from the onset of chromosome condensation until completion of cytokinesis.

^{||}Time from the onset of chromosome condensation until end of metaphase.

**Time from the metaphase-to-anaphase transition (meta/ana, i.e. last metaphase frame) until the onset of cytokinesis (i.e. the first frame in which an equatorial constriction of the cortex was clearly apparent).

^{††}Time from the onset until completion of cytokinesis (i.e. the time from onset until completion of the equatorial constriction of the cell cortex).

^{**}Because almost half of the mitotic cells did not complete mitosis within the analyzed period the given values indicate a minimal and not the actual duration.

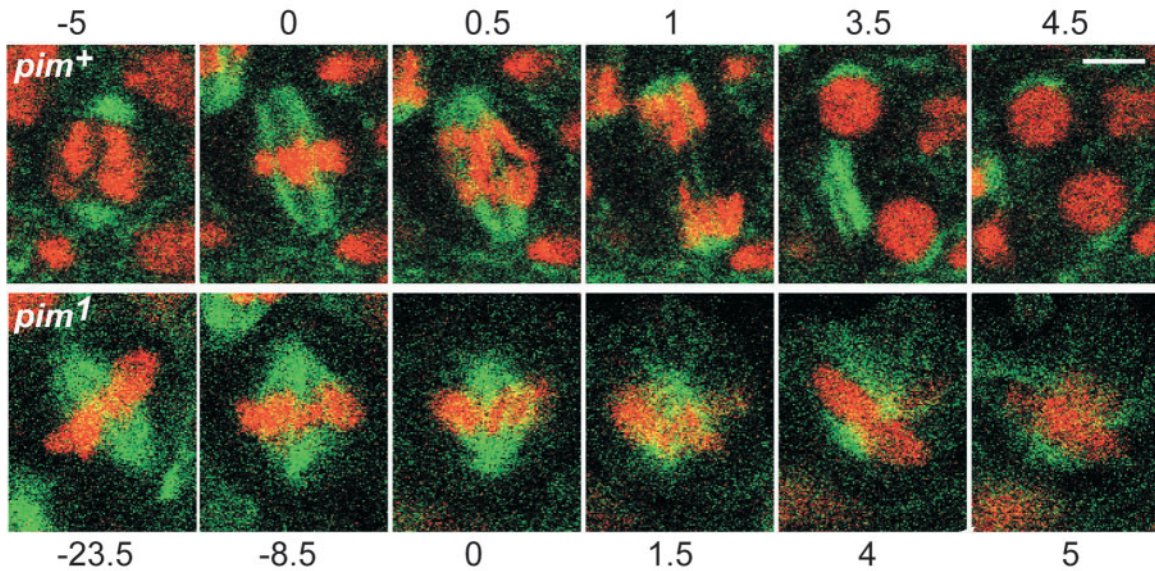


Fig. 2. Metaphase delay during mitosis 16 in *pim* mutant embryos. Time-lapse in vivo imaging was used for the analysis of progression through the sixteenth round of mitosis during *Drosophila* embryogenesis in *pim*¹ mutant (*pim*¹) and *pim*⁺ (*pim*⁺) sibling embryos expressing red fluorescent histone H2AvD-mRFP and a green fluorescent microtubule-binding protein. Selected frames of merged images are shown. Numbers above and below the frames indicate the time in minutes relative to the last metaphase frame which was set to zero. Bar in upper right frame, 5 μ m.

Diplochromosomes delay the metaphase-to-anaphase transition

After exit from mitosis 15, *pim*¹ mutants progressed through interphase 16 and entered mitosis 16 without apparent delays. However, during mitosis 16, we observed an extensive delay in the mutants both by in vivo imaging (Fig. 2, Table 1) and in fixed embryos (Fig. 3) where the mitotic index was found to be drastically increased. In *pim*¹ mutants, mitosis 16 lasts on average at least four times longer than in *pim*⁺ siblings. Therefore in *pim*¹ mutants mitosis 16 is substantially prolonged in contrast to mitosis 15, which is only slightly delayed.

We considered two potential explanations for the pronounced difference in the dynamics of mitosis 15 and 16

in *pim* mutants. In principle, the difference might reflect the dynamics of the exhaustion of the maternal *pim*⁺ contribution. The levels of residual maternally derived *pim*⁺ function during mitosis 15 might be higher than during mitosis 16. Alternatively, the unusual diplochromosomes, which are present during mitosis 16 in *pim* mutants as a consequence of the sister chromatid separation failure during the preceding mitosis 15 (Stratmann and Lehner, 1996), might trigger the mitotic spindle checkpoint because of difficulties in integrating these abnormal chromosomes in a regular bipolar manner into the mitotic spindle. In this latter case, the delay is expected to occur before the onset of cyclin B degradation which is known to be blocked by the mitotic spindle

Fig. 3. Metaphase delay during mitosis 16 in *pim* mutants is caused by diplochromosomes. (A-E) Embryos were labeled with a DNA stain (red) and anti-phospho-histone H3 (PH3, green) at the stage of mitosis 16. (A-D) The number of PH3-positive mitotic cells in a defined epidermal region was counted in 10 embryos homozygous for *pim*¹ (B), *dup*^{al} (C), double mutant for both *pim*¹ and *dup*^{al} (D), as well as in *pim*⁺ embryos (A). The resulting average number of mitotic cells (E) in the mutant and the corresponding sibling embryos are indicated by white and black bars, respectively. *dup* encodes an initiation factor for DNA replication; *dup*^{al} homozygosity inhibits S phase 16 (Whittaker et al., 2000), as well as the accumulation of mitotic figures in *pim*¹ mutants during the subsequent mitosis (see text for further explanations). In metaphase cells with maximal PH3 labeling, chromosomes were arranged in metaphase plates in *pim*¹ *dup*^{al} double mutants (inset in D). In contrast, the single chromatid chromosomes present in *dup*^{al} mutants failed to congress into a plate (inset in C), as previously described (Parry et al., 2003). Bar, 25 μ m (A-D). (F) Labeling with anti-cyclin B (green) and a DNA stain (red) demonstrates that progression through mitosis 16 is delayed before cyclin B degradation in *pim*¹ mutants. Bar, 10 μ m.

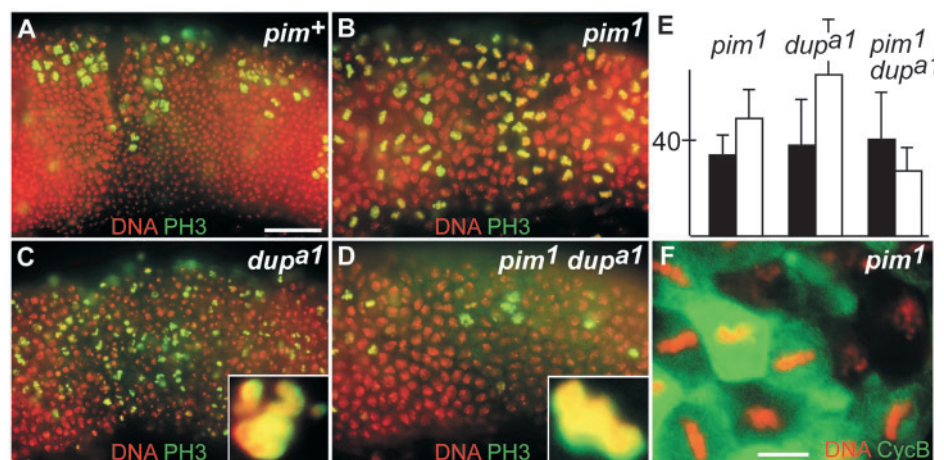
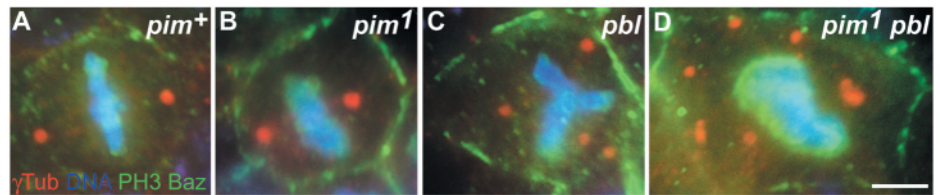


Fig. 4. Centrosome numbers in *pim* mutants. Embryos were labeled at the stage of mitosis 16 (A,B,D) or mitosis 15 (C) with a DNA stain (blue), with anti-phospho-histone H3 (PH3, green) to identify mitotic cells, with anti-Bazooka (Baz, green) to define cell boundaries, and with anti- γ -tubulin (red, γ Tub) to reveal centrosomes. Maximal projections of representative cells from a *pim*¹ mutant (B, *pim*¹), a *pbl* mutant (C, *pbl*), a *pim*¹*pbl* double mutant (D, *pim*¹ *pbl*) and a sibling *pim*⁺ embryo (A, *pim*⁺) are shown, indicating that centrosomes are duplicated in *pim*¹ mutants during cycle 16 when cytokinesis during mitosis 15 is inhibited by homozygosity for *pbl* (see text for further explanations). Bar, 3 μ m.



checkpoint (Minshull et al., 1989; Whitfield et al., 1990; Minshull et al., 1994). In the former case, however, the delay is not expected to occur before cyclin B degradation because separase is thought to exert its functions only after cyclin B and securin degradation. Immunolabeling of *pim* mutant embryos fixed at the stage of mitosis 16 clearly revealed that the great majority of mitotic cells still contained high levels of cyclin B (Fig. 3F). Moreover, in vivo imaging confirmed that the delay occurred during metaphase, clearly before the onset of anaphase (Fig. 2).

To test whether the abnormal diplochromosomes are responsible for the delay during metaphase of mitosis 16 in *pim* mutants, we analyzed embryos with mutations in both the *pim* and the *double-parked* (*dup*) gene. *dup* encodes the *Drosophila* Cdt1 homolog and is required for DNA replication (Whittaker et al., 2000). As in *pim* mutants, a *dup*⁺ maternal contribution supports normal initial development. However, *dup*^{al} mutant embryos are unable to replicate chromosomes during cycle 16 (Garner et al., 2001; Whittaker et al., 2000). *pim*¹ *dup*^{al} double mutant embryos therefore should not contain diplochromosomes at mitosis 16 and thus, if the mitotic delay in *pim* single mutants results from the presence of these abnormal chromosomes, it should not occur in the double mutants. Therefore, we analyzed the number of mitotic cells present at the stage of mitosis 16 in *pim*¹ and *dup*^{al} single and *pim*¹ *dup*^{al} double mutants. Compared to sibling control embryos (Fig. 3A,E), the number of mitotic cells was not only increased in *pim*¹ mutants (Fig. 3B,E) but also in *dup*^{al} mutants (Fig. 3C,E). The increased mitotic index in *dup*^{al} mutants has previously been described and shown to result from the presence of single chromatid chromosomes, which cannot be stably integrated in a bipolar fashion into the mitotic spindle (Parry et al., 2003; Whittaker et al., 2000). The chromosomes therefore fail to congress into a metaphase plate during mitosis 16 in *dup*^{al} mutants (Fig. 3C, inset) (Parry et al., 2003). Moreover, chromosomes are not exposed to tension within the centromeric region and therefore the mitotic spindle checkpoint remains active (Garner et al., 2001; Whittaker et al., 2000). In contrast to *pim*¹ and *dup*^{al} single mutants, we did not observe an increased number of mitotic cells in the *pim*¹ *dup*^{al} double mutants (Fig. 3D,E). In addition, chromosomes were found to congress into a metaphase plate (Fig. 3D, inset). These findings, therefore, indicate that the abnormal diplochromosomes are largely responsible for the delay observed during mitosis 16 in the *pim*¹ single mutants. This conclusion was fully confirmed by in vivo imaging of the progression through mitosis 16 in *pim*¹ *dup*^{al} double mutants (Table 1).

The dynamics of mitosis is indistinguishable in *pim* and *thr* mutants

The protein encoded by the *thr* gene corresponds to the N-terminal regulatory domain of separase proteins of other eukaryotes (Jäger et al., 2001; Jäger et al., 2004). The maternal *thr*⁺ contribution present in *thr*¹ mutants is sufficient for normal initial development until mitosis 15. However, just as in *pim* mutants, sister chromatid separation during mitosis 15 fails in *thr*¹ mutants (D'Andrea et al., 1993). With our antibodies raised against the C-terminal third of THR, we were unable to detect protein products expressed from the *thr*¹ allele, indicating that the mutant protein is either unstable or C-terminally truncated (data not shown). By in vivo imaging we analyzed whether the *thr*¹ mutation affects the dynamics of exit from mitosis. However, as observed in the *pim*¹ mutants, we detected only a slight delay during exit from mitosis 15 and 16 (Table 1). In addition, we also observed an extensive delay during metaphase 16 (Table 1). To date, neither in vivo imaging nor other analyses have revealed phenotypic differences in *pim*¹ and *thr*¹ mutants.

pim and *thr* are not required for centrosome duplication and cytokinesis

Our previous phenotypic characterizations of fixed *pim* and *thr* mutant embryos had suggested that cytokinesis during mitosis 15 is not completed in these mutants (D'Andrea et al., 1993; Stratmann and Lehner, 1996). Cleavage furrows pinching the undivided chromosomes were often observed in fixed mutant embryos at the stage of mitosis 15. However, at a later stage, during the following interphase 16, the nuclear density in the epidermal cell layer of fixed mutant embryos was found to be 1.6-fold lower than in sibling control embryos (D'Andrea et al., 1993; Stratmann and Lehner, 1996) (see below), suggesting that the cleavage furrows had failed to cut completely through the chromosomes during mitosis 15. The cleavage furrows were thus thought to have had aborted in most cells.

After such an inferred cytokinesis failure during mitosis 15 and subsequent duplication of centrosomes during cycle 16, mitotic spindles would be predicted to be tetrapolar during mitosis 16 in *pim*¹ or *thr*¹ mutant cells. In contrast to this expectation, we observed apparently bipolar mitotic spindles and normal metaphase plates during mitosis 16 in *pim*¹ and *thr*¹ mutants (Fig. 3F, and data not shown). Immunolabeling of centrosomal γ -tubulin demonstrated that the majority of the epidermal cells in *pim*¹ and *thr*¹ mutant embryos have only two and not four centrosomes at the stage of mitosis 16 (Fig. 4).

In contrast to *pim*¹ and *thr*¹ mutant embryos, in *pebble* (*pbl*)

Table 2. Centrosome number in *pim*, *thr* and *pbl* mutants

Genotype*	Stage [†]	n [‡]	Centrosome number/cell	
			2 or less (%)	More than 2 (%)
<i>pim</i> ⁺	M15	49	100	0
	M16	101	100	0
<i>pim</i> ¹	M15	51	100	0
	M16	204	85	15
<i>thr</i> ¹	M15	94	100	0
	M16	282	85	15
<i>pbl</i> ⁷⁰	M14	85	98	2
	M15	48	10	90
<i>pbl</i> ^{11D}	M15	92	5	95
	<i>pbl</i> ⁺	M15	89	100

*Embryos homozygous for either *pim*¹, *thr*¹, *pbl*⁷⁰, or *pbl*^{11D} were identified by collecting eggs from heterozygous parents with blue balancer chromosomes and scoring for absence of *lacZ* expression. *pim*⁺ and *pbl*⁺ embryos represent *lacZ*-expressing sibling embryos.

[†]Embryos were aged to the stage of mitosis 14, 15 or 16 (M14, M15 or M16, respectively) before fixation and immunolabeling.

[‡]n=number of mitotic cells analyzed.

mutants the centrosome number was found to increase to four during the cycle following a cytokinesis failure (Fig. 4, Table 2). *pbl* encodes a Rho-GEF required for cytokinesis (Hime and Saint, 1992; Lehner, 1992; Prokopenko et al., 1999). This apparent difference in centrosome behavior in *pim*¹ and *thr*¹ mutants, on the one hand, and *pbl* mutants, on the other, raised the question of whether the *Drosophila* separase complex might be required during mitosis for centrosome duplication in the following cell cycle. However, in *pim pbl* double mutants, centrosome number per cell was found to increase with each cycle (Fig. 4), indicating that centrosome duplication is not dependent on the function of the separase complex.

The observed behavior of centrosomes in *pim*¹ and *thr*¹ mutants would be readily explained, if these mutations did not interfere with completion of cytokinesis during mitosis 15. Therefore, we re-evaluated cytokinesis in *pim* mutants, this time by in vivo imaging of embryos expressing a green fluorescent cell cortex marker in addition to *His2AvD-mRFP*. Time-lapse recordings clearly demonstrated that cytokinesis is completed successfully during mitosis 15 in the great majority of the epidermal cells in both *pim*¹ and *thr*¹ mutants (Fig. 5, and data not shown). The dynamics of cytokinesis was only slightly slower in the mutants compared to sibling controls (Fig. 5, Table 1). The mass of non-separated chromosomes therefore is not a significant obstacle for cytokinesis. In about half of the cells, the cleavage furrow was observed to cut

through the chromatin mass, resulting in two daughter cells, which frequently contained unequal amounts of chromatin. In the other half of the cells, the chromatin mass moved towards one pole and cleavage resulted in an enucleate and a nucleate cell pair. Cleavage furrows were not observed to revert after mitosis 15 even during extended observation periods. During the following mitosis 16 in *pim*¹ and *thr*¹ mutants, cytokinesis was considerably more abnormal and variable from cell to cell (data not shown). Cleavage furrows were rarely observed to cut through the chromatin mass and they appeared to revert occasionally.

Progression through mitosis without separase function results in epithelial pseudostratification

Our finding that cytokinesis is completed successfully in *pim*¹ and *thr*¹ mutants, at least during mitosis 15, was a surprise in the light of the significantly lower densities of cells and nuclei within the superficial epidermal layer in these mutants during cycle 16. Based on our analysis of cytokinesis during mitosis 15, cell density before mitosis 16 should be comparable in *pim*¹ and *pim*⁺ sibling embryos and the nuclear density should be 25% lower in the mutants. However, cell and nuclear densities were significantly below these expectations. Quantification of the nuclear densities revealed a 38% reduction in *pim*¹ before mitosis 16. A comparable extensive decrease in the density of nucleated cells was also observed in *thr*¹ mutant embryos.

In principle, this more extensive reduction might result from apoptosis of the aneuploid cells generated by cytokinesis despite sister chromatid separation failure in *pim*¹ and *thr*¹ mutants. To compare the rate of apoptosis in *pim*¹ and *pim*⁺ sibling embryos we used the TUNEL assay, which detects nucleate apoptotic cells. We did not observe any difference in apoptosis between *pim*¹ and *pim*⁺ sibling embryos until after the stage of mitosis 16. Up to mitosis 16, we observed only very few apoptotic cells, in the characteristic developmental pattern of programmed cell death in both *pim*¹ and *pim*⁺ sibling embryos (Fig. 6A,B). After mitosis 16, during germband retraction, *pim*¹ embryos had slightly more apoptotic cells in regions where developmentally programmed cell death in wild-type is very rare (Fig. 6C,D). After full germband retraction, the number of TUNEL-positive cells was clearly, but still not dramatically, increased in *pim*¹ mutants (data not shown). Aneuploid cells in *pim* mutants therefore appear to undergo apoptosis eventually, but only after mitosis 16.

To quantify the cellular and nuclear densities in *pim* mutants

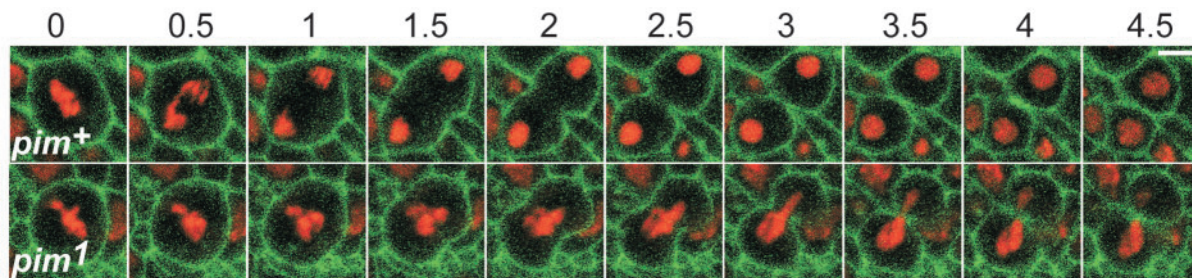


Fig. 5. Cytokinesis during mitosis 15 in *pim* mutants. Time-lapse in vivo imaging was used for the analysis of cytokinesis during the fifteenth round of mitosis during *Drosophila* embryogenesis in *pim*¹ mutant (*pim*¹) and *pim*⁺ (*pim*⁺) sibling embryos expressing red fluorescent histone H2AvD-mRFP and a green fluorescent fusion protein marking the cell cortex. Selected frames of merged images are shown. Numbers above the frames indicate the time in minutes relative to the last metaphase frame which was set to zero. Bar in upper right frame, 5 µm.

after mitosis 15, our initial attempts involved double labeling with a DNA stain and an antibody against the apical junction protein Bazooka (BAZ). In *pim*⁺ sibling embryos, each cell displayed an apical ring of anti-BAZ above a centrally located nucleus, as expected. However, in *pim*¹ mutants, nuclei were very frequently displaced relative to the apical ring of anti-BAZ staining, indicating that the cylindrical organization of the wild-type epithelial cells had been lost (data not shown). Double labeling of DNA and the cell cortex protein α -spectrin further confirmed that the epithelial organization in *pim*¹ mutants had an abnormal pseudostratified appearance after mitosis 15 but not before (Fig. 7). While single confocal sections through the nucleus of every epidermal cell could readily be obtained in *pim*⁺ sibling embryos before mitosis 16 (Fig. 7C), there were striking irregularities in the sections of *pim*¹ mutants and they never included all of the nuclei of the nucleated epidermal cells present in other planes of the z stacks (Fig. 7D).

Discussion

To address whether *Drosophila* separase complex subunits provide functions beyond sister chromatid separation during mitosis, we have further characterized the phenotypic consequences of mutations in *pim* and *thr*, which encode the *Drosophila* securin and the equivalent of the N-terminal regulatory domain of non-dipteran separases, respectively.

Our time-lapse analyses of live embryos demonstrate that progression through mitosis 15, i.e. the first mitosis during

which the maternal contribution is no longer sufficient for sister chromatid separation in the *pim* and *thr* mutants, is only marginally delayed. The duration of pro- and metaphase 15 did not appear to be affected and the time from anaphase onset until the start of cytokinesis was also not prolonged in the mutants. In contrast, completion of cytokinesis was slightly but significantly extended. This extension by about 1 minute in the *Drosophila* mutants is less than the 20–30 minutes delay during exit from mitosis that results from mutations in the *ESP1* separase gene in budding yeast (Stegmeier et al., 2002; Sullivan and Uhlmann, 2003). The difference in the extent of mitotic delays apparent in *Drosophila* and budding yeast is reduced but not eliminated when expressed relative to the overall duration of exit from mitosis, which lasts about eight times longer in budding yeast.

While sister chromatid separation is largely inhibited during mitosis 15 in *pim* and *thr* mutants, one exceptional, apparently normal division could be observed in the hundreds of analyzed cells. Therefore, the maternal *pim*⁺ and *thr*⁺ contributions are unlikely to be completely eliminated in the mutants by the time of mitosis 15. As PIM and THR are degraded during mitosis (Herzig et al., 2002; Leismann and Lehner, 2003; Stratmann and Lehner, 1996) any residual maternal contribution, which is still present during mitosis 15, is expected to be further reduced at the

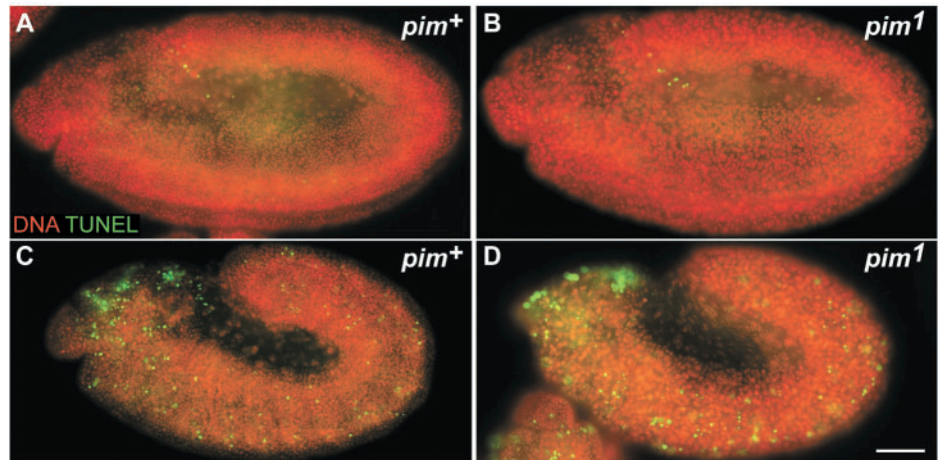


Fig. 6. Apoptosis in *pim* mutants. Embryos before (A,B) or after (C,D) progression through mitosis 16 in the dorsolateral epidermis were labeled with a DNA stain (red) and analyzed by TUNEL (green) for the presence of apoptotic cells. *pim*¹ mutant embryos (B,D) do not have more apoptotic cells than the *pim*⁺ sibling embryos (A,C), at least before mitosis 16. Bar, 50 μ m.

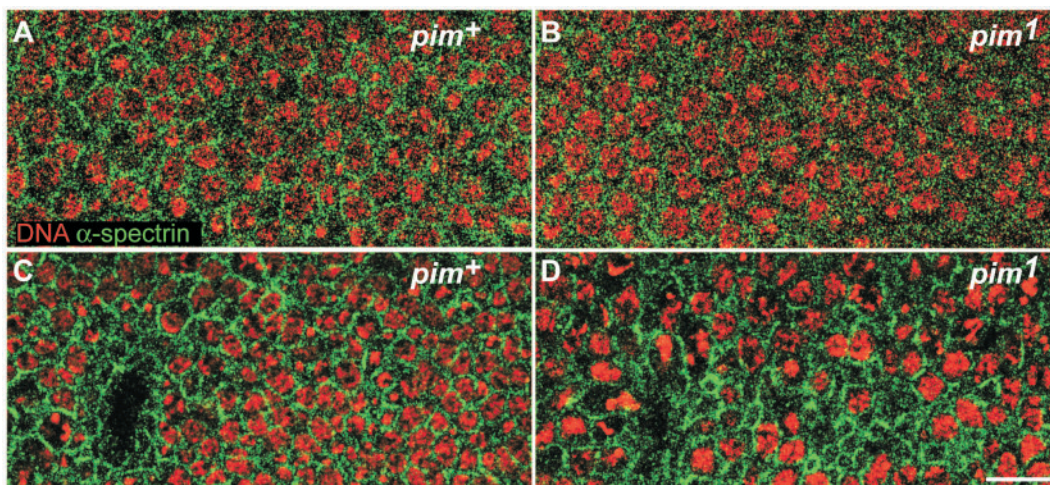


Fig. 7. Epithelial organization in *pim* mutants. Embryos before mitosis 15 (A,B) or before mitosis 16 (C,D) were labeled with a DNA stain (red) and anti- α -spectrin (green). Single confocal sections through the nuclear layer of the epidermal epithelium do not reveal differences between *pim*¹ mutant (B,D) and *pim*⁺ sibling embryos (A,C) before mitosis 15 (compare A and B). In contrast, a relatively disorganized epidermal epithelium is observed in *pim*¹ mutants before mitosis 16 (compare C and D). Bar, 10 μ m.

stage of mitosis 16. The slightly more extensive delay during cytokinesis and exit from mitosis that is observed in the mutants during mitosis 16 might therefore be taken as an indication that a complete elimination of PIM and THR might result in extensive delay. However, alternative explanations are not excluded. Exit from mitosis 16 might be kinetically abnormal not because of a further depletion of the maternal contribution but because of some indirect consequences of the mitosis 15 defects. Mutant cells appear to exit mitosis 16 after adaptation to a spindle checkpoint arrest resulting from mitosis 15 defects (see below). The adaptation mechanisms are unknown and they might have effects on mitosis exit dynamics, which are absent during normal mitosis 16. Such alternative, potential explanations for the slightly stronger delay during exit from mitosis 16 compared to mitosis 15 underscore the technical difficulties of experimental analysis after complete elimination of PIM and THR. In vertebrate systems, the effect of separase on mitotic exit kinetics has not yet been addressed. In *C. elegans*, elimination of separase to a level insufficient for sister chromatid separation does not significantly delay exit from mitosis in controlled osmotic conditions (Siomos et al., 2001).

Arguably the most striking effect on the dynamics of progression through mitosis observed in *pim* and *thr* mutants, i.e. the extensive delay during metaphase of mitosis 16, results indirectly from the failure of sister chromatid separation during mitosis 15. After replication of these non-separated chromatid pairs during S phase 16, *pim* and *thr* mutant cells enter mitosis 16 with abnormal diplochromosomes (Stratmann and Lehner, 1996). Here we demonstrate, with the help of mutations in *Drosophila* Cdt1/Dup, that inhibition of S phase 16 in *pim* mutants prevents most of the delay during metaphase 16. The metaphase extension observed in *pim* and *thr* mutants might therefore be caused by spindle checkpoint activation predominantly resulting from difficulties with bipolar integration of abnormal diplochromosomes into mitotic spindles. We do not understand why the delay during metaphase 16 is not completely reversed in the *pim dup* double mutants, but the residual delay might again reflect adaptation effects, in this case after incomplete inhibition of progression through the preceding S phase 16 (Garner et al., 2001).

Mutations in budding yeast *ESP1*, which abolish protease activity and prevent sister chromatid separation, do not necessarily eliminate activity in the FEAR pathway (Sullivan and Uhlmann, 2003). Therefore the *Drosophila* separase protein which is still present in *pim* and *thr* mutants (Herzig et al., 2002) might be sufficient, in principle, to activate a putative FEAR pathway. Thereby *Drosophila* separase might prevent more extensive mitotic delays in *pim* and *thr* mutants. However, experiments in budding yeast have demonstrated that relatively minor N-terminal truncations abolish FEAR activity of Esp1 (M. Sullivan and F. Uhlmann, personal communication). It appears unlikely, therefore, that *Drosophila* separase, which corresponds to the C-terminal protease domain of Esp1, should be able to function in a putative homologous FEAR pathway in a monomeric form without its usual complex partner THR, which corresponds to the N-terminal domain of Esp1.

In budding yeast, both the proteolytic and the FEAR activity of Esp1 contribute to spindle stability during anaphase, in part by recruiting the budding yeast INCENP-aurora B complex to

the central spindle (Pereira and Schiebel, 2003; Ross and Cohen-Fix, 2004; Sullivan et al., 2001). In *Drosophila*, INCENP and aurora B still transfer to the central spindle in *pim* and *thr* mutants during mitosis 15 (A. Herzig and C.F.L., unpublished). Moreover, in vivo imaging has not revealed severe abnormalities in microtubule organization during exit from mitosis 15. Cytokinesis also proceeded surprisingly normally in *pim* and *thr* mutants. Despite an equatorial mass of undivided chromosomes, cleavage furrows contracted rapidly and completely in the mutants during mitosis 15. Therefore, non-separated equatorial chromosomes appear to affect completion of cytokinesis to a variable extent in different cell types. In *Drosophila* and fission yeast, cleavage furrows are definitely able to cut readily through the chromosomes (Uzawa et al., 1990) (Fig. 5). In contrast, in cultured human cells, eventual regression of the cleavage furrow has been observed after expression of mutant SCC1 versions, which cannot be processed by separase (Hauf et al., 2001).

The effects on cytokinesis and spindle organization in the mutants were more prominent during mitosis 16 compared to mitosis 15. Again, as discussed for the mitotic exit kinetics above, this increase in the severity of observed defects might reflect the progressive depletion of the maternal contributions and/or indirect consequences of earlier defects. A rather stochastic segregation of undivided chromosomes during mitosis 15 might generate phenotypic variability during mitosis 16. The observation that some cells exit mitosis 16 in a manner comparable to mitosis 15, while others are more severely affected, therefore argues for indirect consequences.

An interesting aspect of the *pim* and *thr* mutant phenotype revealed by our analyses concerns epithelial organization. Cellularization during wild-type embryogenesis results in a regular monolayer of cylindrical cells, which is maintained in the epidermis throughout the three postblastoderm division cycles, 14-16. In the mutants, this regular epithelial organization is lost after mitosis 15. The abnormal pseudostratified appearance of the epidermis develops rapidly and long before apoptotic responses. The loss of epithelial organization is therefore unlikely to be a consequence of altered gene expression in the aneuploid cells. Rather the loss of separase complex function might affect epithelial organization via effects on the cytoskeleton. Since budding yeast separase has been shown to regulate microtubule stability, a similar role of the *Drosophila* separase complex remains an attractive explanation. Moreover, after mitosis 15, *pim* and *thr* mutant cells contain very variable amounts of chromatin. They contain either no nuclei or nuclei of variable sizes. Since the nucleus might function as a mechanical element within the cells, its variability might contribute to the epithelial disorganization in the mutants. In addition, even though cleavage furrows are able to cut through the undivided chromosomes quite effectively and central spindles as well as midbodies are formed, it is possible that these latter structures are not fully functional, resulting in an inhibition of the establishment of effective junctional contacts between the newly formed daughter cells. The rounding up of cells on the apical side, which occurs upon entry into mitosis, might provide a force that, in particular, displaces some of the already divided cells towards the basal side. Our phenotypic analyses in *Drosophila* embryos emphasize that a loss of separase function can have consequences that might be difficult to

observe with cultured cells. Loss of separase regulation, as for instance after overexpression of the oncogenic human securin PTTG (Melmed, 2003), might promote tumors, not only by increasing genetic instability but also by effects on tissue organization.

We thank A. Herzig for his help with experiments, X. Morin and A. Debec for providing *Drosophila* strains and E. Knust for antibodies. This work was supported by the Fonds der Deutschen Chemie and by grants from the Deutsche Forschungsgemeinschaft (DFG Le 987/3-1, 3-2, 3-3).

References

- Bardin, A. J., Visintin, R. and Amon, A. (2000). A mechanism for coupling exit from mitosis to partitioning of the nucleus. *Cell* **102**, 21-31.
- Buonomo, S. B., Clyne, R. K., Fuchs, J., Loidl, J., Uhlmann, F. and Nasmyth, K. (2000). Disjunction of homologous chromosomes in meiosis I depends on proteolytic cleavage of the meiotic cohesin Rec8 by separin. *Cell* **103**, 387-398.
- Campbell, R. E., Tour, O., Palmer, A. E., Steinbach, P. A., Baird, G. S., Zacharias, D. A. and Tsien, R. Y. (2002). A monomeric red fluorescent protein. *Proc. Natl. Acad. Sci. USA* **99**, 7877-7882.
- Ciosk, R., Zachariae, W., Michaelis, C., Shevchenko, A., Mann, M. and Nasmyth, K. (1998). An ESP1/PDS1 complex regulates loss of sister chromatid cohesion at the metaphase to anaphase transition in yeast. *Cell* **93**, 1067-1076.
- Clarkson, M. and Saint, R. (1999). A His2AvDGFP fusion gene complements a lethal His2AvD mutant allele and provides an in vivo marker for *Drosophila* chromosome behavior. *DNA Cell Biol.* **18**, 457-462.
- Cohen-Fix, O., Peters, J. M., Kirschner, M. W. and Koshland, D. (1996). Anaphase initiation in *Saccharomyces cerevisiae* is controlled by the APC-dependent degradation of the anaphase inhibitor Pds1p. *Genes Dev.* **10**, 3081-3093.
- D'Amours, D., Stegmeier, F. and Amon, A. (2004). Cdc14 and condensin control the dissolution of cohesin-independent chromosome linkages at repeated DNA. *Cell* **117**, 455-469.
- D'Andrea, R. J., Stratmann, R., Lehner, C. F., John, U. P. and Saint, R. (1993). The *three rows* gene of *Drosophila melanogaster* encodes a novel protein that is required for chromosome disjunction during mitosis. *Mol. Biol. Cell* **4**, 1161-1174.
- Dubreuil, R., Byers, T. J., Branton, D., Goldstein, L. S. and Kiehart, D. P. (1987). Drosophila spectrin. I. Characterization of the purified protein. *J. Cell Biol.* **105**, 2095-2102.
- Funabiki, H., Yamano, H., Kumada, K., Nagao, K., Hunt, T. and Yanagida, M. (1996). Cut2 proteolysis required for sister-chromatid separation in fission yeast. *Nature* **381**, 438-441.
- Garner, M., van Kreeveld, S. and Su, T. T. (2001). mei-41 and bub1 block mitosis at two distinct steps in response to incomplete DNA replication in *Drosophila* embryos. *Curr. Biol.* **11**, 1595-1599.
- Hauf, S., Waizenegger, I. C. and Peters, J. M. (2001). Cohesin cleavage by separase required for anaphase and cytokinesis in human cells. *Science* **293**, 1320-1323.
- Herzig, A., Lehner, C. F. and Heidmann, S. (2002). Proteolytic cleavage of the THR subunit during anaphase limits *Drosophila* separase function. *Genes Dev.* **16**, 2443-2454.
- Hime, G. and Saint, R. (1992). Zygotic expression of the *pebble* locus is required during the postblastoderm mitoses of *Drosophila*. *Development* **114**, 165-171.
- Jacobs, H. W., Knoblich, J. A. and Lehner, C. F. (1998). *Drosophila* Cyclin B3 is required for female fertility and is dispensable for mitosis like Cyclin B. *Genes Dev.* **12**, 3741-3751.
- Jäger, H., Herzig, A., Lehner, C. F. and Heidmann, S. (2001). *Drosophila* separase is required for sister chromatid separation and binds to PIM and THR. *Genes Dev.* **15**, 2572-2584.
- Jäger, H., Herzig, B., Herzig, A., Sticht, H., Lehner, C. F. and Heidmann, S. (2004). Structure predictions and interaction studies indicate homology of separase N-terminal regulatory domains and *Drosophila* THR. *Cell Cycle* **3**, 182-188.
- Jaspersen, S. L., Charles, J. F. and Morgan, D. O. (1999). Inhibitory phosphorylation of the APC regulator Hct1 is controlled by the kinase Cdc28 and the phosphatase Cdc14. *Curr. Biol.* **9**, 227-236.
- Lehner, C. F. (1992). The *pebble* gene is required for cytokinesis in *Drosophila*. *J. Cell Sci.* **103**, 1021-1030.
- Leismann, O. and Lehner, C. F. (2003). *Drosophila* securin destruction involves a D-box and a KEN-box and promotes anaphase in parallel with Cyclin A degradation. *J. Cell Sci.* **116**, 2453-2460.
- Leismann, O., Herzig, A., Heidmann, S. and Lehner, C. F. (2000). Degradation of *Drosophila* PIM regulates sister chromatid separation during mitosis. *Genes Dev.* **14**, 2192-2205.
- Melmed, S. (2003). Mechanisms for pituitary tumorigenesis: the plastic pituitary. *J. Clin. Invest.* **112**, 1603-1618.
- Minshull, J., Pines, J., Golsteyn, R., Standart, N., Mackie, S., Colman, A., Blow, J., Ruderman, J. V., Wu, M. and Hunt, T. (1989). The role of cyclin synthesis, modification and destruction in the control of cell division. *J. Cell Sci.* **12**, 77-97.
- Minshull, J., Sun, H., Tonks, N. K. and Murray, A. W. (1994). A MAP kinase-dependent spindle assembly checkpoint in *Xenopus* egg extracts. *Cell* **79**, 475-486.
- Morin, X., Daneman, R., Zavortink, M. and Chia, W. (2001). A protein trap strategy to detect GFP-tagged proteins expressed from their endogenous loci in *Drosophila*. *Proc. Natl. Acad. Sci. USA* **98**, 15050-15055.
- Parry, D. H., Hickson, G. R. and O'Farrell, P. H. (2003). Cyclin B destruction triggers changes in kinetochore behavior essential for successful anaphase. *Curr. Biol.* **13**, 647-653.
- Pereira, G. and Schiebel, E. (2003). Separase regulates INCENP-Aurora B anaphase spindle function through Cdc14. *Science* **302**, 2120-2124.
- Prokopenko, S. N., Brumby, A., O'Keefe, L., Prior, L., He, Y., Saint, R. and Bellen, H. J. (1999). A putative exchange factor for Rho1 GTPase is required for initiation of cytokinesis in *Drosophila*. *Genes Dev.* **13**, 2301-2314.
- Ross, K. E. and Cohen-Fix, O. (2004). A role for the FEAR pathway in nuclear positioning during anaphase. *Dev. Cell* **6**, 729-735.
- Shou, W., Seol, J. H., Shevchenko, A., Baskerville, C., Moazed, D., Chen, Z. W., Jang, J., Charbonneau, H. and Deshaies, R. J. (1999). Exit from mitosis is triggered by Tem1-dependent release of the protein phosphatase Cdc14 from nucleolar RENT complex. *Cell* **97**, 233-244.
- Siomos, M. F., Badrinath, A., Pasierbek, P., Livingstone, D., White, J., Glotzer, M. and Nasmyth, K. (2001). Separase is required for chromosome segregation during meiosis I in *Caenorhabditis elegans*. *Curr. Biol.* **11**, 1825-1835.
- Stegmeier, F., Visintin, R. and Amon, A. (2002). Separase, polo kinase, the kinetochore protein Slk19, and Spo12 function in a network that controls Cdc14 localization during early anaphase. *Cell* **108**, 207-220.
- Stratmann, R. and Lehner, C. F. (1996). Separation of sister chromatids in mitosis requires the *Drosophila* pimples product, a protein degraded after the metaphase anaphase transition. *Cell* **84**, 25-35.
- Sullivan, M. and Uhlmann, F. (2003). A non-proteolytic function of separase links the onset of anaphase to mitotic exit. *Nat. Cell Biol.* **5**, 249-254.
- Sullivan, M., Lehane, C. and Uhlmann, F. (2001). Orchestrating anaphase and mitotic exit: separase cleavage and localization of Slk19. *Nat. Cell Biol.* **3**, 771-777.
- Sullivan, M., Higuchi, T., Katis, V. L. and Uhlmann, F. (2004). Cdc14 phosphatase induces rDNA condensation and resolves cohesin-independent cohesion during budding yeast anaphase. *Cell* **117**, 471-482.
- Tinker-Kulberg, R. L. and Morgan, D. O. (1999). Pds1 and Esp1 control both anaphase and mitotic exit in normal cells and after DNA damage. *Genes Dev.* **13**, 1936-1949.
- Uhlmann, F., Lottspeich, F. and Nasmyth, K. (1999). Sister-chromatid separation at anaphase onset is promoted by cleavage of the cohesin subunit Scc1. *Nature* **400**, 37-42.
- Uhlmann, F., Wernic, D., Poupart, M. A., Koonin, E. V. and Nasmyth, K. (2000). Cleavage of cohesin by the CD clan protease separin triggers anaphase in yeast. *Cell* **103**, 375-386.
- Uzawa, S., Samejima, I., Hirano, T., Tanaka, K. and Yanagida, M. (1990). The fission yeast cut1+ gene regulates spindle pole body duplication and has homology to the budding yeast esp1 gene. *Cell* **62**, 913-925.
- Visintin, R., Craig, K., Hwang, E. S., Prinz, S., Tyers, M. and Amon, A. (1998). The phosphatase Cdc14 triggers mitotic exit by reversal of Cdk-dependent phosphorylation. *Mol. Cell* **2**, 709-718.
- Waizenegger, I. C., Hauf, S., Meinke, A. and Peters, J. M. (2000). Two distinct pathways remove mammalian cohesin from chromosome arms in prophase and from centromeres in anaphase. *Cell* **103**, 399-410.
- Wang, S. L., Hawkins, C. J., Yoo, S. J., Muller, H. A. and Hay, B. A. (1999). The *Drosophila* caspase inhibitor DIAP1 is essential for cell survival and is negatively regulated by HID. *Cell* **98**, 453-463.

Whitfield, W. G. F., Gonzalez, C., Maldonado-Codina, G. and Glover, D. M. (1990). The A- and B-type cyclins of *Drosophila* are accumulated and destroyed in temporally distinct events that define separable phases of the G2-M transition. *EMBO J.* **9**, 2563-2572.

Whittaker, A. J., Royzman, I. and Orr-Weaver, T. L. (2000). *Drosophila* double parked: a conserved, essential replication protein that colocalizes

with the origin recognition complex and links DNA replication with mitosis and the down-regulation of S phase transcripts. *Genes Dev.* **14**, 1765-1776.

Zou, H., McGarry, T. J., Bernal, T. and Kirschner, M. W. (1999). Identification of a vertebrate sister-chromatid separation inhibitor involved in transformation and tumorigenesis. *Science* **285**, 418-422.

Part B

Rapid effects of acute anoxia on spindle kinetochore interactions activate the mitotic spindle checkpoint.

Rahul Pandey, Sebastian Heeger and Christian F. Lehner

Submitted to Molecular and Cellular Biology.

Contribution to Part B

The study was designed by the last author and myself. Except for Fig. 5A, which presents findings of Sebastian Heeger, all other results are from my own experimental work. Some reagents (anti-Mps1, *Bub3* mutants) and initial experiments eventually leading to Figs. 6A,C,D,G and 7 were developed by Ulrike Großkinsky during her diploma thesis. The manuscript was written by the last author with contributions by myself.

Rapid effects of acute anoxia on spindle kinetochore interactions activate the mitotic spindle checkpoint

Rahul Pandey, Sebastian Heeger and Christian F. Lehner^{*)}

Department of Genetics, BZMB, University of Bayreuth, 95440 Bayreuth, Germany

running title: anoxia-induced spindle checkpoint arrest

^{*)} Corresponding author. Mailing address: Department of Genetics, University of Bayreuth, Universitätsstrasse 30, 95447 Bayreuth, Germany. Phone: 49 921 55 2701. Fax: 49 921 55 2710. E-mail: chle@uni-bayreuth.de.

word counts: Material and Methods (1007), Introduction, Results, Discussion (5651)

Abstract

The dramatic chromosome instability in tumor cells might reflect a synergy of spindle checkpoint defects and hypoxia. Spindle checkpoint function has already been shown to protect effectively from anoxia-induced chromosome missegregation in *C. elegans* and *D. melanogaster*. Our analyses with syncytial *D. melanogaster* embryos demonstrate that oxygen deprivation affects microtubule organization rapidly and reversibly within minutes. In addition, motor proteins (dynein, Kin-8), centrosomal proteins (Cnn, TACC) and kinetochore proteins (Cenp-C, Nuf2) are rapidly re-localized. Kinetochores congress ineffectively into the metaphase plate and are not exposed to normal pulling forces. Consequentially, the spindle checkpoint remains active, resulting in a drastic accumulation of checkpoint proteins mainly within the equatorial region. These rapid cellular effects of anoxia presumably result from reduced ATP levels since they are mimicked by inhibitors of oxidative phosphorylation. Yet the ATP decrease does not prevent motor protein and kinase activity at least initially; and in checkpoint-deficient embryos, mitosis is still completed, although accompanied by massive chromosome missegregation. The chromosome segregation machinery is therefore a more sensitive anoxia target than spindle checkpoint activity which involves ATP-consuming protein kinases. This allows the spindle checkpoint to provide protection from aneuploidies in response to acute anoxia.

Introduction

Oxygen plays a decisive role in metabolism and is particularly important in metazoans for efficient ATP production by oxidative phosphorylation. Diverse and highly adapted mechanisms have evolved to cope with oxygen limitation during development and adult life.

A well-known pathway triggered by acute and chronic hypoxia involves the activation of the HIF-1 transcription factor. This pathway has been shown to operate in a conserved manner in vertebrates and invertebrates like *C. elegans* and *D. melanogaster* (13). In addition,

experiments with these invertebrate model organisms have revealed the importance of alternative pathways especially in anoxia when oxygen levels are even further decreased. Not only nematode (37) and insect embryos (12) but also some vertebrates (38) tolerate extended periods of anoxia. In response to anoxia, they enter a state of suspended animation from which they can rapidly recover upon re-oxygenation. HIF-1 is not required in *C. elegans* for survival of anoxia, while it is clearly crucial for survival of hypoxia (24, 37). However, a screen for *C. elegans* genes required for survival of anoxia has led to the identification of *san-1* which encodes a homolog of budding yeast Mad3 (36). Mad3 is a component of the mitotic spindle checkpoint, a surveillance pathway known to monitor the bipolar integration of chromosomes into the mitotic spindle. Moreover, experiments in *D. melanogaster* demonstrated that Mps1 protein kinase, which also functions in the spindle checkpoint, is required for the mitotic arrest resulting from severe hypoxia (11).

The mitotic spindle checkpoint acts during mitosis and prevents progression into anaphase until all chromosomes are bi-oriented (for reviews see (28, 30, 40, 47)). It is activated during prometaphase of normal mitoses by kinetochores which are either not yet attached to spindle microtubules or not under physical tension. Several proteins are known to function in the spindle checkpoint. Apart from the components introduced above (Mad3, Mps1), additional protein kinases (Bub1, BubR1) and scaffold proteins (Mad1, Bub3) are involved. Moreover, in metazoans, the kinesin Cenp-E and the Rod/Zw10/Zwilch (RZZ) complex which recruits dynein-dynactin and Mad2 to the kinetochore have also been implicated in the spindle checkpoint. The molecular interactions that lead to spindle checkpoint activation are not yet understood in detail. However, it is clear that spindle checkpoint activity prevents Fzy/Cdc20-APC/C ubiquitin ligase from marking securin and B-type cyclins for rapid proteasomal degradation. Securin inhibits separase, a protease that cleaves the Scc1 subunit of the cohesin complex. Therefore, as long as the spindle checkpoint remains active, sister chromatids are

kept together by the cohesin linkage and anaphase cannot proceed. Moreover, high levels of B-type cyclin cdk activity maintain the mitotic state in the spindle checkpoint arrest.

The spindle checkpoint protects against aneuploidies. Spindle checkpoint dysfunction has been proposed to be involved in tumor formation, because excessive chromosome instability is a hallmark of a large fraction of solid human tumors. Evidence supporting this notion is increasing (28). Moreover, the spindle checkpoint might be of particular importance in tumor cells because their growth is known to be severely constrained by oxygen limitation (19, 41). As a result, areas with very low (down to zero) oxygen partial pressures exist in solid tumors, occurring either acutely or chronically (19). Based on the initial analyses in *C. elegans* and *D. melanogaster*, it is readily conceivable that it is the combination of spindle checkpoint dysfunction and severe hypoxia which generates the remarkable chromosome instability typically observed in tumor cells. At least in the two model organisms, this combination clearly results in mitotic chromosome segregation defects (11, 36). A more detailed analysis of the functional connections between anoxia and the spindle checkpoint should therefore be of interest.

The synchronous cell cycle progression of thousands of nuclei which occur during the syncytial blastoderm stage of early *Drosophila* embryogenesis provides many advantages for experimental studies. Zalokar and Erk already observed that anoxia leads to a rapid and reversible developmental arrest during these stages in wild type (50). The studies of Foe and Alberts (1985) and DiGregorio et al. (2001) clearly revealed that anoxia triggers chromatin condensation in interphase nuclei and blocks further cell cycle progression within few minutes (7, 12). Embryos which have already entered mitosis at the time of anoxia induction become arrested either in metaphase or in late telophase. A metaphase arrest is observed when anoxia is induced before the metaphase to anaphase transition, and late telophase arrest thereafter.

In principle, it is conceivable that the early and rapid activation of the mitotic spindle checkpoint in response to anoxia involves an unknown dedicated pathway directly targeting one of the spindle checkpoint components. Such a pathway would appear especially beneficial if the error-free execution of post-metaphase processes were to be more sensitive to oxygen shortage than the initial mitotic processes. In this case, spindle assembly and chromosome attachment might still occur normally after oxygen deprivation, but progression into the more oxygen-dependent anaphase would be inhibited by a dedicated anoxia-sensing spindle checkpoint activation pathway. Alternatively, the process of chromosome attachment to the mitotic spindle might be more sensitive to ATP shortage than activation of the mitotic spindle checkpoint which involves ATP-consuming protein kinases. Accordingly, already a relatively minor drop in ATP levels would result in free kinetochores or reduce tension between sister kinetochores and thereby activate the spindle checkpoint. Our analyses support this latter notion. We demonstrate that spindle and kinetochore function are indeed very rapidly affected by oxygen deprivation. Crucial components of centrosomes and spindles as well as kinetochore proteins including Cenp-C which is thought to localize exclusively and constitutively to the centromere are rapidly and dramatically re-distributed in response to anoxia.

Results

Anoxia has rapid effects on mitotic spindles

Previous analyses have demonstrated that oxygen deprivation from the normal 21% to below 2% triggers a rapid cell cycle arrest in syncytial *Drosophila* embryos (7, 9, 12). In the following, we will use the term anoxia for these conditions even though our experimental procedures do not eliminate oxygen completely. We use this term to clearly distinguish our relatively severe conditions from milder hypoxia (5-3% O₂) which although sufficient for

HIF-1 activation does not trigger rapid cell cycle and developmental arrest during *Drosophila* development (29).

Mitotic spindles and chromosomes in metaphase plates have been shown to be present in syncytial embryos arrested by anoxia induction during early mitosis (i.e. before the metaphase to anaphase transition) (7, 9, 11). However, a careful comparison revealed that the mitotic spindles present in arrested embryos fixed after a 20 minute incubation in degassed buffer were different from metaphase spindles in normoxic embryos (Fig. 1A). After anti- α -tubulin labeling, centrosomes were either not or only hardly detectable in anoxic embryos. Moreover, asters were greatly reduced or absent. In addition, spindles were narrow and contained few and only short microtubule fibers which did not extend far away from the metaphase plates. The extent of these spindle abnormalities was somewhat variable. In the majority of the anoxic embryos, abnormalities were at least as severe as in the example shown in Fig. 1A. In contrast to the mitotic spindles, we did not observe clear differences in the metaphase plate arrangement of the condensed chromosomes when comparing normoxic and anoxic embryos.

To analyze how fast spindle abnormalities develop in anoxia, we fixed embryos after a two or five minute incubation in degassed buffer. Spindles were observed to be affected already after two minutes of anoxia (Fig. 1A). After five minutes, abnormalities were more severe but still minor than after 20 minutes of anoxia. Apart from a partial centrosome detachment and a reduction of astral and centrosome-proximal spindle fibers (Fig. 1A), spindle length appeared to be slightly extended in anoxia (Fig. 1B).

To study the effects of anoxia on spindle behavior, we also performed *in vivo* imaging with embryos expressing GFP- α -tubulin (15). These embryos were made anoxic by applying a flow of N₂ (Fig. 1C) or Ar gas (data not shown). As previously described (7, 9), we observed a rapid mitotic arrest after oxygen deprivation during early mitosis. We were unable to observe clear spindle abnormalities already after two minutes, in contrast to our findings with fixed embryos. Moreover, even after prolongation of anoxia up to 20 minutes, we never

observed the almost complete elimination of spindles which was frequently apparent after 20 minutes of incubation in degassed buffer followed by fixation and anti- α -tubulin labeling. Therefore, microtubule destabilizing effects of fixation (26) might enhance the apparent effects of anoxia on spindle organization. However, after prolonged anoxia, the reduction of centrosome-proximal spindle fibers was also evident in the in vivo imaging experiments (Fig. 1C). A very similar spindle response to prolonged anoxia has also previously been observed using in vivo imaging of Ncd-GFP, a fluorescent spindle-associated *Drosophila* kinesin-14 protein (9, 44).

In vivo imaging allowed an observation of spindle behavior during recovery from anoxia. Re-oxygenation was followed by a prominent increase in the density of microtubules around centrosomes (Fig. 1C). Subsequently, the centrosomes were pulled towards the spindle resulting in a distinct shortening of spindle length (Fig. 1C). Thereafter the spindle adopted an essentially normal metaphase appearance (Fig. 1C) followed rapidly by anaphase onset (not shown). In vivo imaging with embryos expressing the centrosomal protein GFP-D-TACC (2) confirmed the characteristic spindle shortening preceding anaphase during recovery from anoxia (Fig. 1D). Spindles shortened transiently to a length below that of normoxic metaphase spindles but comparable to prophase spindles. The defective poles of metaphase spindles in anoxic embryos therefore appear to be extensively rebuilt after re-oxygenation.

The rapid spindle malfunction in response to oxygen deprivation is independent of the spindle checkpoint

To address whether the observed rapid effects of oxygen deprivation on the spindle might be cause or consequence of spindle checkpoint activation, we incubated checkpoint-deficient embryos lacking *Mps1* function (11) for 5 minutes in degassed buffer followed by fixation and anti- α -tubulin labeling. Anoxic *Mps1* mutant embryos with metaphase plates (Fig. 2A, lower panel) were found to display the same abnormalities as observed with checkpoint-

competent control embryos (Fig. 1A). Moreover, we emphasize that normoxic *Mps1* mutant embryos (Fig. 2A, upper panel) did not display the metaphase spindle abnormalities which are characteristically observed in anoxic embryos. We conclude, therefore, that the rapid initial anoxia effects on spindle organization occur independently of spindle checkpoint activation.

In vivo imaging of *Mps1* mutant embryos, in which completion of mitosis is not blocked by oxygen deprivation, allowed an analysis of the function of the mitotic apparatus in anoxia. To monitor chromosome congression and segregation, we used embryos expressing green fluorescent Cenp-A/Cid centromere protein and red fluorescent histone H2Av (17). These experiments revealed that anoxia severely impaired chromosome congression during prometaphase. Congression proved to be slow and incomplete after oxygen deprivation, while it occurred far more effectively in normoxic *Mps1* mutants (Fig. 2B)(11). Moreover, in anoxic *Mps1* mutant embryos, anaphase appeared to start with a delay but still before normal metaphase plates had formed (Fig. 2B). Anaphase was also significantly slower in anoxia. The leading centromeres moved towards the poles with an average speed of about $2.5 \mu\text{m min}^{-1}$ in anoxic *Mps1* mutants compared to about $4 \mu\text{m min}^{-1}$ in normoxic ones (in both cases s.d. = $0.25 \mu\text{m min}^{-1}$ and $n = 12$ mitotic figures from a total of 3 different embryos). Consistent with the observed pronounced congression defects, lagging chromosomes were far more frequently observed during anaphase in anoxic *Mps1* mutants (Fig. 2B)(11). These observations suggest that spindle attachment of kinetochores is impaired by anoxia.

To confirm the impaired spindle attachment of kinetochores, we compared the average separation of sister kinetochores in normoxic and hypoxic metaphase plates after immunolabeling *Mps1*⁺ embryos with antibodies against α -tubulin and Cenp-A/Cid (Fig. 2C). As previously established in cultured *Drosophila* cells and cellularized embryos (17, 31), chromosome bi-orientation in normoxic syncytial embryos was also found to be accompanied by an increase in the average separation of sister kinetochores, from $0.42 \mu\text{m}$ in prophase to $0.71 \mu\text{m}$ in metaphase (Fig. 2D). However, in anoxic metaphase plates, the average distance

between sister kinetochores (0.63 μm) was slightly (12 %) but significantly shorter than in the normoxic controls (Fig. 2D). Tension generated by the mitotic spindle, therefore, appears to be reduced in anoxia. Alternatively, it is not excluded that anoxia leads to tighter cohesion between sister chromatids. Apart from the reduced inter sister kinetochore distances, the α -tubulin and Cenp-A/Cid double labeling also demonstrated that the anoxic spindles were largely composed of kinetochore fibers which are known to be the most stable spindle fibers (32).

Effects of anoxia on centrosomal components and motor proteins

According to our microtubule analyses, the mitotic apparatus is rapidly affected by oxygen deprivation. Anoxia induction leads to a reduction of centrosome-proximal spindle fibers, centrosome detachment and slight spindle lengthening. Therefore, the centrosome appears to be especially sensitive to anoxia. To characterize centrosome behavior in response to anoxia in further detail, we examined the centrosome components Aurora A, γ -tubulin, Centrosomin (Cnn) and D-TACC. Anoxia had only a subtle effect on Aurora A and γ -tubulin (Fig. 3A). In the resulting mitotic arrest the centrosomal pool of these proteins had a more doughnut-shaped appearance with sharp outer borders while in normoxic metaphase the signal maxima were present in the centrosome center with a more graded decline towards the periphery (Fig. 3A, compare insets). These localization differences between anoxic and normoxic metaphases were far more pronounced in the case of Cnn (Fig. 3B). The characteristic flares of Cnn, which represent transport away from and back to the centrosome primarily on dynamic astral microtubules (33), were absent in anoxia. Cnn flaring on astral microtubules is known to be more extensive in interphase compared to metaphase (33). Accordingly, the anoxia-induced elimination of Cnn flares was even more striking in interphase embryos (Fig. 3C). D-TACC localization was also strongly affected by oxygen deprivation (Fig. 3D). However, D-TACC localization, which is known to stimulate astral microtubule plus end growth (2, 27, 39), was

affected in a manner opposite to Aurora A, γ -tubulin and Cnn. D-TACC was found to be far less focused to centrosomes in anoxia (Fig. 3D). By in vivo imaging using embryos expressing GFP-D-TACC (data not shown), we analyzed the dynamics of D-TACC re-localization in response to oxygen deprivation. These analyses revealed that the striking D-TACC spikes were gradually built up after oxygen deprivation during prophase. At the time when anaphase onset would have occurred in normoxic conditions, D-TACC re-distribution was subtle at most. During recovery from anoxia, GFP-D-TACC spikes were compacted back into the normal distribution within the period where centrosome fiber re-growth was apparent in the GFP- α -tubulin imaging experiments (Fig. 1C). D-TACC function at the centrosome has been shown to be regulated by Aurora A which phosphorylates an identified site on D-TACC (2). An antibody against this phospho-epitope (2) resulted in signal intensities which were not clearly altered by oxygen deprivation (data not shown), suggesting that Aurora A activity is not inhibited by anoxia.

Similar effects on spindle organization as those triggered by anoxia have been observed in Schneider cells after knock-down of the kinesin family member Kin-8 (Klp67A) or dynein heavy chain 64C, while knock-down of many other components of the mitotic apparatus resulted in additional, structurally different spindle responses (14). Therefore, we analyzed whether oxygen deprivation affects the localization of these motor proteins. Both motor proteins appeared to be rapidly and strongly affected. Oxygen deprivation induced a rapid reduction of Kin-8 levels within the equatorial spindle region already within 2 minutes (Fig. 4A). After 5 minutes of anoxia, Kin-8 spindle association was almost undetectable (Fig. 4A). With an antibody recognizing the *Drosophila* dynein light intermediate chain (D-LIC), we followed the response of dynein to anoxia. In normoxic metaphase, D-LIC was predominantly associated with the pseudo-cleavage furrows (Fig. 4B), as previously reported for dynein heavy chain (6, 45). After oxygen deprivation, D-LIC accumulated within minutes on spindle fibers in the vicinity of the kinetochores (Fig. 4B). The same behavior in response to anoxia

was also observed by in vivo imaging embryos expressing a functional D-LIC version fused to GFP (data not shown). In these experiments, we also observed D-LIC-GFP particle movement on spindle fibers towards the pole (see below), suggesting that the dynein motor activity is not eliminated, at least during the initial minutes of anoxia.

Outer and constitutive inner kinetochore proteins are re-localized in response to anoxia.

Kin-8 and dynein which are rapidly affected by anoxia are thought to provide important functions at the kinetochore (43, 46). Therefore, we characterized the response of centromere kinetochore complex components to oxygen deprivation. We did not observe rapid effects on the behavior of Cenp-A/Cid, a centromeric histone H3 variant which acts at the top of the centromere kinetochore assembly process (Fig. 2C). Surprisingly, however, the localization of Cenp-C, another constitutive centromere protein of the inner kinetochore plate, was found to be severely affected by anoxia. An anoxia-induced re-distribution of Cenp-C was observed by immunofluorescence after fixation (Fig. 5A), as well as by in vivo imaging (data not shown) of a functional EYFP-Cenp-C variant (17). Cenp-C immunolabeling with two different affinity-purified rabbit antibodies indicated that a fraction of Cenp-C is spindle-associated even in normoxic syncytial embryos (Fig. 5A, and data not shown). In anoxic embryos, this Cenp-C pool appeared to be increased and re-distributed to the centrosome-proximal spindle region (Fig. 5A). Interestingly, we observed a similar anoxia-induced re-distribution predominantly to the centrosome-proximal spindle region also for the outer kinetochore plate Ndc80/Hec1 complex component Nuf2 when analyzing the localization of a functional *Drosophila* EGFP-Nuf2 version (Fig. 5B). Therefore, we conclude that oxygen deprivation affects some important kinetochore proteins.

Kinetochore attachment to spindle fibers is thought to be regulated by the chromosomal passenger complex which includes Aurora B kinase and INCENP (48). Using antibodies against *Drosophila* INCENP (1), we were unable to detect an extensive re-localization after

anoxia induction during mitosis comparable to that observed for Cenp-C and Nuf2 (data not shown). However, we cannot exclude that anoxia affects Aurora B kinase activity.

The response of spindle checkpoint proteins to anoxia

Since anoxia has rapid effects on the mitotic apparatus, we analyzed the response of mitotic spindle checkpoint proteins. Oxygen was deprived from embryos expressing functional EGFP fusion proteins and their localization was analyzed by *in vivo* imaging as well as after fixation.

During normoxic metaphase some EGFP-Mps1 has been shown to be enriched on centrosomes and spindles and only weakly on kinetochores (11). Apart from these localized signals, diffuse specific signals are observed as well. In response to oxygen deprivation, EGFP-Mps1 strongly accumulated at kinetochores and even more pronounced in the spindle fiber overlap zone in the equatorial region (Fig. 6A, arrows). Interestingly, in about 5% of the embryos, impressive filamentous EGFP-Mps1 structures formed in the vicinity of the centrosomes in addition to the equatorial concentration (Fig. 6A, arrowheads). EGFP-Mps1 re-localization started within minutes after oxygen deprivation and reached a maximum after about 8 minutes. Recovery from anoxia (Fig. 6A) was accompanied by a return to the normal metaphase distribution before anaphase onset. We point out that the comparatively weaker signals of kinetochore- and spindle-associated EGFP-Mps1 before oxygen deprivation, as well as after re-oxygenation, were not detectable with the confocal microscope settings adjusted for detection of the drastic EGFP-Mps1 enrichment within the equatorial region during anoxia, as apparent in Fig. 6A.

While the EGFP-Mps1 filaments close to centrosomes were only formed in some of the anoxic metaphase embryos, we observed EGFP-Mps1 aggregation far more frequently in the cortical region of anoxic pre-blastoderm embryos where nuclei have not yet migrated out to the egg periphery. EGFP-Mps1 aggregation occurred in about 80% of the anoxic pre-

blastoderm embryos, usually in the form of bright dots but occasionally also in filamentous structures (Fig. 6D).

EGFP-BubR1 behavior in response to anoxia was very similar to EGFP-Mps1. In mitotic cells, enrichment also occurred within the equatorial region (Fig. 6E), although apparently less pronounced than with EGFP-Mps1. After oxygen deprivation, we also observed EGFP-BubR1 aggregation within the cortical region of pre-blastoderm embryos (data not shown), as well as filament formation around centrosomes in syncytial blastoderm embryos during mitosis (Fig. 6E), at comparable frequencies as with EGFP-Mps1. Double labeling indicated co-localization of BubR1 and EGFP-Mps1 within these aggregates (Fig. 6F). Co-localization was not perfect, however, perhaps reflecting antibody accessibility problems.

To analyze the behavior of *Drosophila* Bub3 in response to anoxia, we established an *gEGFP-Bub3* transgene which was found to rescue the recessive lethality associated with a newly identified *Bub3* mutation. Similar to EGFP-Mps1 and EGFP-BubR1, we also observed an enrichment of EGFP-Bub3 within the equatorial region in response to oxygen deprivation (Fig. 6G). However, aggregation in dots or filaments was not detected with anoxic *gEGFP-Bub3* embryos.

In metazoans, the RZZ complex which includes the Rod protein has been implicated in the mitotic spindle checkpoint and shown to recruit the Mad2 checkpoint protein to kinetochores and spindle fibers (4, 25). In response to anoxia, EGFP-Rod was strongly enriched on metaphase spindles, in particular within the equatorial region (Fig. 6H). As expected, the behavior of EGFP-Mad2 in response to anoxia was highly similar to EGFP-Rod (data not shown). The RZZ complex is also known to interact with the dynein/dynactin motor protein complex which mediates the shedding of Mad2 and presumably other spindle checkpoint proteins away from bi-oriented kinetochore along kinetochore fibers. As observed in normoxic larval neuroblasts (3), dynein behavior (Fig. 4B) appeared to be similar but not identical to the RZZ complex and Mad2 in anoxic embryos. Interestingly, with D-LIC-GFP

and EGFP-Rod (data not shown), as well as with EGFP-Mps1 (Fig. 6B), we observed particle transport along spindle fibers during the anoxia-induced metaphase arrest, suggesting that dynein motor activity is not abolished.

Spindle checkpoint activation results in Fzy/Cdc20 inhibition via Mad2 and BubR1. This inhibition prevents the APC/C-mediated degradation of securin and B-type cyclins and thereby anaphase onset. Consistent with the proposed complex formation between Fzy and activated Mad2 and BubR1, anoxia was found to result in an enrichment of EGFP-Fzy on metaphase spindles (Fig. 6I), similar to the other analyzed mitotic spindle checkpoint components. In addition, EGFP-Fzy was also found on centrosomes in anoxic metaphase embryos.

Interestingly, some spindle checkpoint components were not only re-distributed during mitosis in response to oxygen deprivation, but also during interphase. In normoxic interphase embryos, EGFP-Mps1 is very weakly enriched on centrosomes (Fig. 6C)(11). After oxygen deprivation, EGFP-Mps1 was observed in very bright and highly focused spots (Fig. 6C) which were closely associated with interphase centrosomes and possibly represent centriolar structures. The same behavior was also observed with EGFP-BubR1 (data not shown). Similarly, EGFP-Bub3 enrichment on centrosomes was not detected in normoxic but occurred strongly in anoxic interphase embryos (data not shown).

The observed re-localization of EGFP-Mps1 and EGFP-Bub3 in anoxic interphase embryos raised the possibility that oxygen deprivation activates the spindle checkpoint not only during mitosis but also during interphase. Spindle checkpoint activation in various experimental systems is correlated with an electrophoretic mobility shift of several components including *Drosophila* Mps1. Therefore, we analyzed whether oxygen deprivation during interphase leads to an Mps1 mobility shift. However, we did not detect such a shift, even though it was clearly observed during prometaphase of normal mitosis and in the anoxic metaphase arrest (Fig. 7).

From our characterization of spindle checkpoint components (Mps1, BubR1, Bub3, Rod, Mad2) and the final target (Fzy), we conclude that anoxia rapidly affects their behavior (even during interphase in the case of Mps1 and Bub3) and activates the checkpoint pathway during mitosis.

Comparison of the consequences of anoxia and metabolic inhibitors

The drop in ATP levels after oxygen deprivation has been shown to be less than 10% within the time sufficient to induce a metaphase arrest (7). This modest drop is not expected to have pronounced effects on protein kinase and motor protein activities based on biochemical analyses in vitro. Our in vivo studies strongly support the notion that these enzymes retain at least some activity after oxygen deprivation at least within the first minutes. Mitotic spindle checkpoint activation which occurs in anoxic embryos involves protein kinase activities (Mps1, BubR1) and dynein/dynactin-mediated transport. Moreover, motor activity of the *Drosophila* kinesin-14 Ncd has recently been described in oxygen-deprived embryos (44). It is conceivable, therefore, that anoxia might activate the mitotic spindle checkpoint independent of its effect on oxidative phosphorylation and ATP levels. Accordingly, inhibition of oxidative phosphorylation in the presence of oxygen would not be expected to result in spindle checkpoint activation. To address whether inhibition of oxidative phosphorylation in the presence of oxygen results in spindle checkpoint activation, we incubated syncytial embryos in medium containing azide (data not shown) or cyanide (Fig. 8). These cytochrome oxidase inhibitors were observed to have rapid effects on metaphase spindle organization and EGFP-Mps1 localization (Fig. 8A). Moreover, the effects appeared to be indistinguishable from those induced by oxygen deprivation. In addition, the metabolic inhibitors also mimicked the effects of oxygen deprivation on chromatin condensation and centrosomal EGFP-Mps1 during interphase (Fig. 8B). Therefore we conclude that spindle

checkpoint activation by anoxia is presumably caused by inhibition of oxidative phosphorylation.

Discussion

Anoxia in combination with spindle checkpoint defects drastically enhances chromosome instability in *C. elegans* and *D. melanogaster* and possibly during cancer development in humans as well. A functional spindle checkpoint has been shown to protect the model organisms very effectively from anoxia-induced aneuploidy. Our analyses with syncytial *Drosophila* embryos provide insights into the mechanism of spindle checkpoint activation by anoxia. Oxygen deprivation is shown to affect microtubule organization rapidly and reversibly within minutes. The spindle association of the motor proteins dynein and Kin-8 was changed quickly. Strikingly, the kinetochore proteins Cenp-C and Nuf2 are re-localized as well. Kinetochores congress ineffectively into the metaphase plate and do not appear to experience a normal tension. We propose that therefore the spindle checkpoint remains active, resulting in the observed massive accumulation of checkpoint proteins within the equatorial region. Since inhibitors of oxidative phosphorylation have the same effects as anoxia, it appears that spindle defects and consequential checkpoint activation and mitotic arrest result from a decrease in ATP levels. Importantly, however, ATP levels after anoxia induction are still sufficiently high, allowing motor protein and protein kinase activities at least initially. Moreover, in the absence of mitotic spindle checkpoint function, anaphase and completion of mitosis still proceed although accompanied by massive chromosome missegregation. Thus faithful chromosome segregation during mitosis appears to be exquisitely sensitive to ATP reduction, far more than spindle checkpoint activation which involves ATP-consuming protein kinases. As a consequence spindle checkpoint activation in response to acute anoxia can provide protection from aneuploidies.

Anoxia effects on spindle organization have been reported previously (9, 16, 44). However, the spindle abnormalities described in these studies were observed after prolonged exposure to anoxia of 30 minutes or longer. Our analyses in checkpoint-deficient *Mps1* mutant embryos demonstrate that the spindle abnormalities are not simply the consequence of the anoxia-induced mitotic arrest. Moreover, our description of rapid effects strongly suggests that spindle abnormalities are a cause of the mitotic arrest. While spindle abnormalities were clearly apparent in fixed embryos already after two minutes of anoxia, we did not observe them equally early by in vivo imaging. We explain this discrepancy by the lower signal to noise ratio and lower spatial resolution of our in vivo imaging experiments compared to the analyses with fixed material. Moreover, the methanol fixation applied in our experiments is known to disturb some aspects of the microtubule organization (26) and thereby it seems to enhance the apparent defects. Nevertheless, the apparent differences between mitotic spindles fixed after two minutes of incubation in either normoxic or anoxic media provide clear evidence that oxygen deprivation has rapid effects on spindles. Only rapid effects can cause a mitotic spindle checkpoint arrest in syncytial embryos because of the speed of the mitotic divisions during these developmental stages. To cause a mitotic arrest, anoxia has to be induced after entry into mitosis (otherwise it leads to an interphase arrest) and the consequences must be sensed in the embryo before the metaphase to anaphase transition which occurs only 4.5 minutes after mitosis onset (34).

The spindle abnormalities which develop within minutes after oxygen deprivation are accompanied by a reduced separation of sister kinetochores in metaphase plates. The inter-kinetochore distance in metaphase is thought to reflect the pulling forces exerted by the spindle on bi-oriented chromosomes. Accordingly, anoxia appears to reduce these pulling forces. It should be pointed out, however, that the observed decrease in the inter-kinetochore distance might also be explained by reduced chromosome elasticity. Since oxygen deprivation induces a substantial chromatin condensation at least in interphase (12), a contribution by

increased stiffness of anoxic metaphase chromosomes should not be discounted prematurely. Nevertheless, the notion of reduced pulling forces is further supported by the observation that the speed of chromosome congression in prometaphase and segregation to the poles in anaphase in the checkpoint-deficient *Mps1* mutant embryos is markedly slower during anoxic compared to normoxic mitoses.

The rapid effects of oxygen deprivation on spindles and chromosome attachment, readily explain why mitotic spindle checkpoint activity is maintained in anoxia. All the mitotic spindle checkpoint proteins analyzed (*Mps1*, *BubR1*, *Bub3*, *Rod*, *Mad2*) as well as their target *Fzy/Cdc20* accumulate strongly on anoxic spindles, predominantly in the equatorial region. A similar accumulation has been observed in normoxic embryos in response to taxol in experiments with EGFP-*BubR1*, EGFP-*Rod* and EGFP-*Mad2* (4). Moreover, *Mps1* has a low electrophoretic mobility in anoxic metaphase extracts, as also observed in normoxic metaphase and in colchicine arrest (data not shown). Interestingly, some mitotic spindle checkpoint proteins (*Mps1* and *Bub3*) were also observed to re-localize in interphase in response to anoxia. However, based on the *Mps1* behavior revealed in our immunoblotting experiments, anoxia does not appear to activate the mitotic spindle checkpoint during interphase. This further argues against a physiological link that would allow mitotic spindle checkpoint activation by anoxia independent of the effects on the mitotic apparatus.

The anoxia response of *Mps1* and *Bub3* during interphase might also reflect effects on microtubules. The same interphase response was also induced by the inhibitors of oxidative phosphorylation KCN and NaN_3 . A rapid reduction of microtubule asters induced by these various treatments therefore occurs during both mitosis and interphase. Aster reduction might reflect increased microtubule instability or reduced centrosomal nucleation activity. The centrosomal components *Cnn* and *TACC* are clearly re-organized after anoxia induction during interphase, while other components (γ -tubulin and *Aurora A*) were only subtly affected. Moreover, the *Cnn*-containing flares of pericentrosomal material, which are moved

by microtubule dynamics independent of motors during normoxia (33), are eliminated by anoxia.

We note that an opposite response of aster microtubules has been observed with mitotic mammalian cells in culture after treatment with cyanide and 2-deoxyglucose (49). These conditions are expected to induce a more drastic reduction in ATP levels because they inhibit glycolysis in addition to oxidative phosphorylation. With regard to the precise experimental conditions, we would also like to add that CO₂ was found to have slightly different consequences when it was used instead of N₂ or Ar for air displacement during in vivo imaging. In the wild, *Drosophila* deposits eggs into fermenting yeast on decaying fruits. Anoxia resulting from high CO₂ concentration is therefore likely to be of physiological relevance. After CO₂ application in prophase, we also observed a rapid and reversible arrest in metaphase. Interestingly, however, metaphase arrest occurred also in checkpoint-deficient *Mps1* mutant embryos, in contrast to the experiments with N₂, Ar or degassed buffer. Moreover, the mobility of checkpoint protein particles was found to be strongly reduced in the CO₂-induced mitotic arrest.

In addition to centrosomal proteins, anoxia affects the localization of spindle-associated protein Kin-8/KLP67A and dynein. Our observations are in accord with those of others (22, 44) and argue against the possibility that the rapid effects on these proteins reflect an inhibition of their motor activity. Similarly, our observations argue that the activity of protein kinases (like Mps1, BubR1, Aurora A) is not inhibited during the initial response to anoxia. We consider it to be likely, therefore, that the observed anoxia-induced re-localization of the proteins analyzed in our studies and including the kinetochore proteins Cenp-C and Nuf2 results from altered microtubule dynamics. However, the rapid chromatin condensation which is induced by anoxia during interphase (12) is very unlikely to be linked with microtubule dynamics, indicating the existence of sensitive anoxia targets other than microtubules.

Our finding that metabolic inhibitors (CN^- , N_3^-) and anoxia have indistinguishable early effects both in interphase and mitosis is consistent with the notion that the sensitive targets respond already to relatively minor changes in ATP levels. We also point out that the recovery dynamics of ATP levels after re-oxygenation was found to be closely correlated to resumption of mitosis (7). The behavior of the highly abundant cellular component tubulin is directly regulated by GTP which is generated from ATP. It is conceivable, therefore, that microtubule dynamics responds rather immediately to changes in ATP levels. However, further analysis will certainly be required for the identification of the sensitive targets of anoxia and the molecular details of their response.

Materials and methods

Fly stocks

The following fly strains have been described before: *Mps1¹* and *P{gEGFP-Mps1}* (11), *P{gcid-EGFP-cid}*, *P{gEYFP-Cenp-C}* and *P{His2Av-mRFP1}* (17), *w¹¹¹⁸*; *P{w^{+mC}=GAL4::VP16-nos.UTR}MVD1*, *P{w^{+mC}=UASp-GFPS65C-alphaTub84B}3* (15), *G147* (35), *P{gEGFP-Rod}*, *P{gEGFP-BubR1}*, and *P{gEGFP-Mad2}* (4), *P{Ubi-EGFP-Fzy}* (42), *P{Ubi-TACC-GFP}* (2). *P{Ubi-DLIC-GFP}* was kindly provided by Jordan Raff before publication. *P{gEGFP-Nuf2}* will be described in detail elsewhere. We used *w¹* for control experiments because all the analyzed mutations and transgenes were in a *w* mutant background. Females with *Mps1¹* germ line clones were generated using the FLP-DFS method (5) as described previously (11), and the term “*Mps1* mutant embryos” refers to the progeny derived from these females.

P{gEGFP-Bub3} lines were obtained by standard germ line transformation using a pP{CaSpeR-4} construct. For its construction, we amplified the genomic *Bub3* region from BAC RPC1-98 10L12 (21) using the primers RaS7 (5'-GAT GAATTC AGGGGAAGGACGAACTGG-3') and RaS8 (5'-ACGA TCTAGA ATGCTTGGGCAACA ATTCCGA-3') which introduced an *EcoRI* and an *XbaI* site, respectively. After digestion with *EcoRI* and *XbaI*, the amplification product was inserted into the corresponding sites of pP{CaSpeR-4} to generate *P{gBub3}* lines. To insert the EGFP coding sequence just before the initiation codon, we subcloned an *EcoRI*-*BglIII* fragment from the *P{gBub3}* construct into pLitmus28Δ*EcoRV*-*StuI*. Into the resulting cloning intermediate, we introduced restriction sites for *BamHI*, *SmaI* and *NotI* immediately upstream of the *Bub3* initiation codon by inverse PCR using the primers RP23 (5'-TGGG CCCGGGATCC TGTC AAGTTTTCTGC TAGCA-3') and RP24 (5'-GCAG CCCGGGCGGCCGC ATG CGTCCCCCAGAGTTCAA-3'). The *BamHI*-*NotI* fragment including the *SmaI* site was subsequently replaced with a *BamHI*-*NotI* fragment containing the complete EGFP coding sequence. Finally, the recombinant *EcoRI*-

*Bgl*III fragment with the EGFP sequence was used to replace the corresponding region in *P{gBub3}*. After sequence confirmation, several independent *P{gBub3}* and *P{gEGFP-Bub3}* lines were established. Complementation tests using *Bub3*²³³ mutant flies indicated that both transgenes, *P{gBub3}* and *P{gEGFP-Bub3}*, were functional. *Bub3*²³³ carries a *pBac{tTA}* mutator element (20) within the 5' UTR of *Bub3* resulting in recessive lethality at the larval/pupal interphase. *Bub3*²³³ homozygotes carrying *P{gBub3}* or *P{gEGFP-Bub3}* were found to be fully viable and fertile.

In vivo imaging

Embryos were aged to the syncytial blastoderm stages after collection on apple juice agar plates. Dechorionated embryos were lined up, immobilized on coverslips and covered with halocarbon oil. Time lapse confocal laser scanning microscopy was performed with a Leica TCS SP1 system in combination with an inverted microscope at 22-24°C in a temperature controlled room. To avoid light damage, excitation laser intensity was minimized and the pinhole was opened. In most experiments, two frames (1024 x 1024 pixels) were acquired and averaged, at 15 second intervals using a 63x glycerol immersion objective, sometimes in combination with four-fold electronic zoom magnification.

For induction of anoxia, we covered the embryos mounted under halocarbon oil on the glass coverslip with a glass cylinder (20 mm diameter, 30 mm high), which was closed on one side except for two small openings (2 mm diameter), using silicon grease for air tight sealing. Air in the glass cylinder was then displaced by applying a flow of nitrogen, argon or carbon dioxide gas via silicon tubing connected to one of the top openings and a gas bottle on the other end. Re-oxygenation was achieved by stopping the gas flow.

Immunofluorescence

Embryos were collected and aged to the appropriate developmental stage before chorion removal. To induce anoxia, half of the embryos were subsequently incubated in extensively degassed 0.7% NaCl 0.07% Triton-X-100 (NaCl-Tx) for 2 to 20 minutes. The other half of the embryos was incubated at the same time in normal NaCl-Tx for normoxic control experiments. For the inhibitor experiments, we incubated half of the de-chorionated embryos in 4 mM KCN or 4 mM NaN₃ in phosphate buffered saline (PBS) for 5 to 15 minutes. For control experiments, the other half of the embryos was incubated in 4 mM KCl in PBS for the same time. Embryos were rapidly fixed and de-vitellinized after these incubations by replacing NaCl-Tx or PBS with a 1:1 mixture of heptane and methanol. The concentration of the inhibitors of oxidative phosphorylation was chosen because 4 mM of NaCN has previously been shown to reduce ATP levels with comparable kinetics as oxygen deprivation (7).

For immunofluorescent staining we used mouse monoclonal antibody DM1A anti- α -tubulin (Sigma) at 1:8000, affinity-purified rabbit anti-Cenp-A/Cid (23) at 1:1000, affinity-purified rabbit anti Cenp-C (17) at 1:2000, rabbit anti-BubR1 (kindly provided by C. Sunkel, Universidade do Porto, Portugal) at 1:2000, rabbit anti-INCENP (1) at 1:500, rabbit anti-KLP67A (43) at 1:50, mouse monoclonal 74.1 anti-dynein intermediate chain (8)(Abcam) at 1:300, rabbit anti-Aurora A (2) at 1:250, rabbit anti-phospho-TACC (2) at 1:500, rabbit anti-Centrosomin (18) at 1:200, and mouse monoclonal GTU-88 anti- γ -tubulin (Sigma) at 1:500. DNA was labeled with 1 μ g/ml Hoechst 33258. Single focal planes or Z stacks were acquired with a Zeiss Axioplan 2 Imaging system using Zeiss AxioVision software. Adobe Photoshop was used for preparation of the figures.

Immunoblotting

Embryos were collected and aged to the syncytial blastoderm stage before chorion removal. Aliquots of embryos were incubated in either NaCl-Tx, or Schneider's *Drosophila* cell culture

medium containing 10 μ M colcemid (N-Deacetyl-N-methylcolchizin, Sigma) or in extensively de-gassed NaCl-Tx for 20 minutes. After methanol fixation and DNA staining, interphase or metaphase embryos were selected with the help of an inverted microscope and pooled before extract preparation (10). Extracts were resolved by SDS polyacrylamide gel electrophoresis. For production of rabbit antibodies against *Drosophila* Mps1, we expressed an Mps1 fragment (amino acids 150-630) in *E. coli* with an N-terminal His₆ extension. Ni-NTA chromatography was used for purification of the immunogen. Antibodies were affinity-purified after immobilization of the immunogen on CNBr-activated Sepharose (Sigma). Immunoblots were probed with affinity-purified rabbit anti-Mps1 at 1:5000 and affinity-purified rabbit anti-EGFP (kindly provided by S. Heidmann, University of Bayreuth) at 1:3000 using Hybond-ECL membranes and ECL-detection (Amersham Biosciences).

Acknowledgments

We thank F. Althoff, U. Großkinsky and R. Schittenhelm for providing reagents and help during initial experiments. We are also grateful to W. Earnshaw, D. Glover, R. Karess, T. Kaufman, J. Raff and C. Sunkel for antibodies and fly stocks. Moreover, we thank S. Heidmann for comments on the manuscript.

This work was supported by the Deutsche Forschungsgemeinschaft (DFG LE 987/4-1).

References

1. **Adams, R. R., H. Maiato, W. C. Earnshaw, and M. Carmena.** 2001. Essential roles of *Drosophila* inner centromere protein (INCENP) and aurora B in histone H3 phosphorylation, metaphase chromosome alignment, kinetochore disjunction, and chromosome segregation. *J Cell Biol* **153**:865-80.
2. **Barros, T. P., K. Kinoshita, A. A. Hyman, and J. W. Raff.** 2005. Aurora A activates D-TACC-Msps complexes exclusively at centrosomes to stabilize centrosomal microtubules. *J Cell Biol* **170**:1039-46.
3. **Basto, R., F. Scaerou, S. Mische, E. Wojcik, C. Lefebvre, R. Gomes, T. Hays, and R. Karess.** 2004. In vivo dynamics of the rough deal checkpoint protein during *Drosophila* mitosis. *Curr Biol* **14**:56-61.
4. **Buffin, E., C. Lefebvre, J. Huang, M. E. Gagou, and R. E. Karess.** 2005. Recruitment of Mad2 to the kinetochore requires the Rod/Zw10 complex. *Curr Biol* **15**:856-61.
5. **Chou, T. B., and N. Perrimon.** 1996. The autosomal FLP-DFS technique for generating germline mosaics in *Drosophila melanogaster*. *Genetics* **144**:1673-1679.
6. **Cytrynbaum, E. N., P. Sommi, I. Brust-Mascher, J. M. Scholey, and A. Mogilner.** 2005. Early spindle assembly in *Drosophila* embryos: role of a force balance involving cytoskeletal dynamics and nuclear mechanics. *Mol Biol Cell* **16**:4967-81.
7. **DiGregorio, P. J., J. A. Ubersax, and P. H. O'Farrell.** 2001. Hypoxia and nitric oxide induce a rapid, reversible cell cycle arrest of the *Drosophila* syncytial divisions. *J Biol Chem* **276**:1930-7.
8. **Dillman, J. F., 3rd, and K. K. Pfister.** 1994. Differential phosphorylation in vivo of cytoplasmic dynein associated with anterogradely moving organelles. *J Cell Biol* **127**:1671-81.

9. **Douglas, R. M., T. Xu, and G. G. Haddad.** 2001. Cell cycle progression and cell division are sensitive to hypoxia in *Drosophila melanogaster* embryos. *Am J Physiol Regul Integr Comp Physiol* **280**:R1555-63.
10. **Edgar, B. A., D. A. Lehman, and P. H. O'Farrell.** 1994. Transcriptional regulation of string(*cdc25*): a link between developmental programming and the cell cycle. *Development* **120**:3131-3143.
11. **Fischer, M. G., S. Heeger, U. Hacker, and C. F. Lehner.** 2004. The mitotic arrest in response to hypoxia and of polar bodies during early embryogenesis requires *Drosophila* Mps1. *Curr Biol* **14**:2019-24.
12. **Foe, V. E., and B. M. Alberts.** 1985. Reversible chromosome condensation induced in *Drosophila* embryos by anoxia: visualization of interphase nuclear organization. *J Cell Biol* **100**:1623-36.
13. **Gorr, T. A., M. Gassmann, and P. Wappner.** 2006. Sensing and responding to hypoxia via HIF in model invertebrates. *J Insect Physiol* **52**:349-64.
14. **Goshima, G., R. Wollman, N. Stuurman, J. M. Scholey, and R. D. Vale.** 2005. Length control of the metaphase spindle. *Curr Biol* **15**:1979-88.
15. **Grieder, N. C., M. de Cuevas, and A. C. Spradling.** 2000. The fusome organizes the microtubule network during oocyte differentiation in *Drosophila*. *Development* **127**:4253-64.
16. **Hajeri, V. A., J. Trejo, and P. A. Padilla.** 2005. Characterization of sub-nuclear changes in *Caenorhabditis elegans* embryos exposed to brief, intermediate and long-term anoxia to analyze anoxia-induced cell cycle arrest. *BMC Cell Biol* **6**:47.
17. **Heeger, S., O. Leismann, R. Schittenhelm, O. Schraidt, S. Heidmann, and C. F. Lehner.** 2005. Genetic interactions of Separase regulatory subunits reveal the diverged *Drosophila* Cenp-C homolog. *Genes Dev* **19**:2041-53.

18. **Heuer, J. G., K. J. Li, and T. C. Kaufman.** 1995. The *Drosophila* homeotic target gene centrosomin (*cnn*) encodes a novel centrosomal protein with leucine zippers and maps to a genomic region required for midgut morphogenesis. *Development* **121**:3861-3876.
19. **Hockel, M., and P. Vaupel.** 2001. Tumor hypoxia: definitions and current clinical, biologic, and molecular aspects. *J Natl Cancer Inst* **93**:266-76.
20. **Horn, C., N. Offen, S. Nystedt, U. Hacker, and E. A. Wimmer.** 2003. piggyBac-Based Insertional Mutagenesis and Enhancer Detection as a Tool for Functional Insect Genomics. *Genetics* **163**:647-61.
21. **Hoskins, R. A., C. R. Nelson, B. P. Berman, T. R. Lavery, R. A. George, L. Ciesiolka, M. Naemuddin, A. D. Arenson, J. Durbin, R. G. David, P. E. Tabor, M. R. Bailey, D. R. DeShazo, J. Catanese, A. Mammoser, K. Osoegawa, P. J. de Jong, S. E. Celniker, R. A. Gibbs, G. M. Rubin, and S. E. Scherer.** 2000. A BAC-based physical map of the major autosomes of *Drosophila melanogaster*. *Science* **287**:2271-4.
22. **Howell, B. J., B. F. McEwen, J. C. Canman, D. B. Hoffman, E. M. Farrar, C. L. Rieder, and E. D. Salmon.** 2001. Cytoplasmic dynein/dynactin drives kinetochore protein transport to the spindle poles and has a role in mitotic spindle checkpoint inactivation. *J Cell Biol* **155**:1159-72.
23. **Jäger, H., M. Rauch, and S. Heidmann.** 2005. The *Drosophila melanogaster* condensin subunit Cap-G interacts with the centromere-specific histone H3 variant CID. *Chromosoma* **113**:350-361.
24. **Jiang, H., R. Guo, and J. A. Powell-Coffman.** 2001. The *Caenorhabditis elegans* hif-1 gene encodes a bHLH-PAS protein that is required for adaptation to hypoxia. *Proc Natl Acad Sci U S A* **98**:7916-21.

25. **Karess, R.** 2005. Rod-Zw10-Zwilch: a key player in the spindle checkpoint. *Trends Cell Biol* **15**:386-92.
26. **Kellogg, D. R., T. J. Mitchison, and B. M. Alberts.** 1988. Behaviour of microtubules and actin filaments in living *Drosophila* embryos. *Development* **103**:675-86.
27. **Kinoshita, K., T. L. Noetzel, L. Pelletier, K. Mechtler, D. N. Drechsel, A. Schwager, M. Lee, J. W. Raff, and A. A. Hyman.** 2005. Aurora A phosphorylation of TACC3/maskin is required for centrosome-dependent microtubule assembly in mitosis. *J Cell Biol* **170**:1047-55.
28. **Kops, G. J., B. A. Weaver, and D. W. Cleveland.** 2005. On the road to cancer: aneuploidy and the mitotic checkpoint. *Nat Rev Cancer* **5**:773-85.
29. **Lavista-Llanos, S., L. Centanin, M. Irisarri, D. M. Russo, J. M. Gleadle, S. N. Bocca, M. Muzzopappa, P. J. Ratcliffe, and P. Wappner.** 2002. Control of the hypoxic response in *Drosophila melanogaster* by the basic helix-loop-helix PAS protein similar. *Mol Cell Biol* **22**:6842-53.
30. **Lew, D. J., and D. J. Burke.** 2003. The spindle assembly and spindle position checkpoints. *Annu Rev Genet* **37**:251-82.
31. **Logarinho, E., H. Bousbaa, J. M. Dias, C. Lopes, I. Amorim, A. Antunes-Martins, and C. E. Sunkel.** 2004. Different spindle checkpoint proteins monitor microtubule attachment and tension at kinetochores in *Drosophila* cells. *J Cell Sci* **117**:1757-71.
32. **McIntosh, J. R., E. L. Grishchuk, and R. R. West.** 2002. Chromosome-microtubule interactions during mitosis. *Annu Rev Cell Dev Biol* **18**:193-219.
33. **Megraw, T. L., S. Kilaru, F. R. Turner, and T. C. Kaufman.** 2002. The centrosome is a dynamic structure that ejects PCM flares. *J Cell Sci* **115**:4707-18.
34. **Minden, J. S., J. W. Agard, J. W. Sedat, and B. M. Alberts.** 1989. Direct cell lineage analysis in *Drosophila melanogaster* by time lapse three dimensional optical microscopy of living embryos. *J. Cell Biol.* **109**:505-516.

35. **Morin, X., R. Daneman, M. Zavortink, and W. Chia.** 2001. A protein trap strategy to detect GFP-tagged proteins expressed from their endogenous loci in *Drosophila*. *Proc Natl Acad Sci U S A* **98**:15050-5.
36. **Nystul, T. G., J. P. Goldmark, P. A. Padilla, and M. B. Roth.** 2003. Suspended animation in *C. elegans* requires the spindle checkpoint. *Science* **302**:1038-41.
37. **Padilla, P. A., T. G. Nystul, R. A. Zager, A. C. Johnson, and M. B. Roth.** 2002. Dephosphorylation of cell cycle-regulated proteins correlates with anoxia-induced suspended animation in *Caenorhabditis elegans*. *Mol Biol Cell* **13**:1473-83.
38. **Padilla, P. A., and M. B. Roth.** 2001. Oxygen deprivation causes suspended animation in the zebrafish embryo. *Proc Natl Acad Sci U S A* **98**:7331-5.
39. **Peset, I., J. Seiler, T. Sardon, L. A. Bejarano, S. Rybina, and I. Vernos.** 2005. Function and regulation of Maskin, a TACC family protein, in microtubule growth during mitosis. *J Cell Biol* **170**:1057-66.
40. **Pinsky, B. A., and S. Biggins.** 2005. The spindle checkpoint: tension versus attachment. *Trends Cell Biol* **15**:486-93.
41. **Pouyssegur, J., F. Dayan, and N. M. Mazure.** 2006. Hypoxia signalling in cancer and approaches to enforce tumour regression. *Nature* **441**:437-43.
42. **Raff, J. W., K. Jeffers, and J. Y. Huang.** 2002. The roles of Fzy/Cdc20 and Fzr/Cdh1 in regulating the destruction of cyclin B in space and time. *J Cell Biol* **157**:1139-49.
43. **Savoian, M. S., M. K. Gatt, M. G. Riparbelli, G. Callaini, and D. M. Glover.** 2004. *Drosophila* Klp67A is required for proper chromosome congression and segregation during meiosis I. *J Cell Sci* **117**:3669-77.
44. **Sciambi, C. J., D. J. Komma, H. N. Skold, K. Hirose, and S. A. Endow.** 2005. A bidirectional kinesin motor in live *Drosophila* embryos. *Traffic* **6**:1036-46.

45. **Sharp, D. J., H. M. Brown, M. Kwon, G. C. Rogers, G. Holland, and J. M. Scholey.** 2000. Functional coordination of three mitotic motors in *Drosophila* embryos. *Mol Biol Cell* **11**:241-53.
46. **Sharp, D. J., G. C. Rogers, and J. M. Scholey.** 2000. Cytoplasmic dynein is required for poleward chromosome movement during mitosis in *Drosophila* embryos. *Nat Cell Biol* **2**:922-30.
47. **Taylor, S. S., M. I. Scott, and A. J. Holland.** 2004. The spindle checkpoint: a quality control mechanism which ensures accurate chromosome segregation. *Chromosome Res* **12**:599-616.
48. **Vader, G., R. H. Medema, and S. M. Lens.** 2006. The chromosomal passenger complex: guiding Aurora-B through mitosis. *J Cell Biol* **173**:833-7.
49. **Wadsworth, P., and E. D. Salmon.** 1988. Spindle microtubule dynamics: modulation by metabolic inhibitors. *Cell Motil Cytoskeleton* **11**:97-105.
50. **Zalokar, M., and I. Erk.** 1976. Division and migration of nuclei during early embryogenesis of *Drosophila melanogaster*. *J. Microbiol. Cell.* **25**:97-109.

Figure Legends

FIG. 1. Mitotic spindle organization in anoxia.

(A) Early *Drosophila* embryos during the synchronous syncytial blastoderm cycles were incubated in either normoxic (+O₂) or anoxic (-O₂) buffer for 2, 5 or 20 minutes (2', 5', 20') before fixation and labeling with anti- α -tubulin (Tub) and a DNA stain (DNA). Metaphase embryos reveal an increasing reduction of centrosome-proximal spindle fibers during anoxia. Bar = 10 μ m.

(B) The pole to pole distances in metaphase spindles (in μ m on y-axis +/- s.d.) after incubation (2 minutes) in either normoxic (white bars) or anoxic (black bars) buffer before fixation and immunolabeling (see A) was measured during mitosis 10, 11, 12 and 13. At least 25 different spindles from at least 5 different embryos were measured and averaged for each bar.

(C) Selected frames are shown after time lapse in vivo imaging of embryos expressing α -tubulin-GFP. Time in minutes after prometaphase onset is indicated in the lower left corners. In the presence of oxygen (+O₂, top row), the last metaphase frame is reached after 3.5 minutes, followed by anaphase (not shown). In the embryo made anoxic at the start of mitosis (-O₂, lower row), a metaphase arrest is maintained until after re-oxygenation (+O₂, lower row). The last frame before re-oxygenation at 15 minutes reveals the loss of centrosome-proximal spindle fibers (arrowheads) and a reduced spindle width (dashed lines) in comparison to normoxic metaphase spindles. Re-oxygenation is followed by a pronounced increase in centrosomal fibers (18 minutes, arrow) and spindle shortening (21 minutes) before an apparently normal metaphase spindle (27 minutes) precedes anaphase (not shown).

(D) The intercentrosomal distance in mitotic spindles was determined after in vivo imaging of embryos expressing GFP-D-TACC starting in prophase. Anaphase onset in normoxic conditions (x-x) is indicated by the open arrow. During the metaphase arrest in anoxic

conditions (o-o), the intercentrosomal distance extends slightly beyond normoxic metaphase values. Re-oxygenation (indicated by arrowhead +O₂) is followed by a pronounced shortening and eventual anaphase onset (black arrow). The given distances at each time point are average values of five different spindles observed in representative embryos.

FIG. 2. Mitotic spindle function in anoxia.

(A) Spindle checkpoint-deficient embryos lacking Mps1 protein kinase function were incubated during the synchronous syncytial blastoderm cycles in either normoxic (+O₂) or anoxic (-O₂) buffer for 5 minutes before fixation and labeling with anti- α -tubulin (Tub) and a DNA stain (DNA). The effects of anoxia on metaphase spindles do not depend on spindle checkpoint function (compare with Fig. 1A). Bar = 10 μ m.

(B) Progression through mitosis was analyzed by in vivo imaging of *Mps1* mutant embryos expressing a green fluorescent Cenp-A/Cid centromere protein (Cenp-A) and a red fluorescent histone H2A variant (Histone H2Av) in either normoxic (+O₂, top row) or anoxic (-O₂, bottom row) conditions. Time in minutes starting in early prometaphase is indicated in the lower left corners of the selected frames. Chromosome congression in anoxia is slow and incomplete at the time of anaphase onset. Subsequent chromosome segregation is also slow. Some of the frequent lagging centromeres are indicated by arrowheads. Bar = 10 μ m.

(C,D) Spindle checkpoint-competent embryos were incubated during the synchronous syncytial blastoderm cycles in either normoxic (+O₂) or anoxic (-O₂) buffer for 5 minutes before fixation and labeling with antibodies against α -tubulin (Tub), Cenp-A (Cenp-A) and a DNA stain (DNA). The relative resistance of kinetochore fibers against anoxia-induced depolymerization is illustrated with representative metaphase figures (C). Bar = 5 μ m.

Moreover, inter sister kinetochore distances were measured (n = 125 sister kinetochore pairs from at least 18 different embryos) and the average (in μ m +/- s.d.) in prophase (pro) or

metaphase (meta) is given in (D). The average distance in normoxic (+O₂) and anoxic (-O₂) metaphase was found to be distinct ($p < 0.0001$ in t test; $n = 125$). We did not detect significant variation in the average sister kinetochore separation with developmental stage (mitosis 11-13).

FIG. 3. Centrosome structure in anoxia.

Syncytial blastoderm embryos were incubated (20 minutes) in either normoxic (+O₂) or anoxic (-O₂) buffer before fixation and immunolabeling.

- (A) anti-Aurora A kinase (AurA), anti- γ -tubulin (γ -Tub) and DNA (DNA) during metaphase
 (B) anti-Centrosomin (Cnn) and DNA (DNA) during metaphase and (C) during interphase
 (D) GFP-D-TACC (TACC), anti- γ -tubulin (γ -Tub) and DNA (DNA) during metaphase.

Insets in the lower left corners show a representative centrosome at higher magnification after labeling with anti-AurA (A) and anti-Cnn (B and C). Bars = 10 μ m.

FIG. 4. Motor proteins in anoxia.

Syncytial blastoderm embryos were incubated in either normoxic (+O₂) or anoxic (-O₂) buffer for 2 or 5 minutes before fixation and immunolabeling.

- (A) anti-Kinesin 8/Klp67A (KLP67A), anti- α -tubulin (Tub) and DNA stain (DNA). Klp67A decreases rapidly in the central spindle region in response to anoxia.
 (B) dynein light intermediate chain-GFP (DLIC) and DNA. Dynein accumulates rapidly at metaphase plates (arrowhead) in response to anoxia. Bars = 10 μ m.

FIG. 5. Kinetochore proteins in anoxia.

Syncytial blastoderm embryos were incubated in either normoxic (+O₂) or anoxic (-O₂) buffer for 20 minutes before fixation and immunolabeling.

- (A) anti-Cenp-C (Cenp-C) and DNA stain (DNA).

(B) EGFP-Nuf2 (Nuf2) and DNA stain (DNA) in *gEGFP-Nuf2* embryos.

In response to anoxia, Cenp-C and EGFP-Nuf2 accumulate on spindles predominantly in the centrosome-proximal region. Bar = 10 μm .

FIG. 6. Spindle checkpoint proteins in anoxia.

(A) Selected frames after in vivo imaging of an embryo expressing EGFP-Mps1 (Mps1) and histone H2Av-mRFP (H2Av). Time in minutes is indicated in the frames showing the merged images in the bottom panel. Anoxia ($-\text{O}_2$) was induced at $t = 1.75$ minutes after the onset of chromosome condensation during entry into mitosis. The resulting EGFP-Mps1 accumulation within the equatorial region of metaphase figures (arrows) and in centrosome-associated filaments (arrowheads) is indicated. The embryo was re-oxygenated ($+\text{O}_2$) at $t = 9.75$ minutes during the metaphase arrest, resulting in EGFP-Mps1 disappearance and completion of mitosis. Bar = 10 μm .

(B) Frames showing EGFP-Mps1 at high magnification within the equatorial region of a metaphase figure during the anoxia-induced mitotic arrest. Time in seconds is indicated within each frame. An EGFP-Mps1 particle moving along the spindle is indicated by arrowheads.

(C) High magnification views of single nuclei from syncytial *gEGFP-Mps1* embryos during interphase. The embryos were fixed and labeled with anti- γ -tubulin (γ -Tub) and DNA stain (DNA) after a 20 minute incubation in either normoxic ($+\text{O}_2$) or anoxic ($-\text{O}_2$) buffer. The weak centrosomal EGFP-Mps1 (Mps1) signals in normoxic embryos (arrowhead), as well as the strong signals in sub-centrosomal dots in anoxic embryos (arrow) are indicated. Bar = 10 μm .

(D) EGFP-Mps1 signals (Mps1) in cortical regions of pre-blastoderm embryos which were fixed after a 20 minute incubation in either normoxic ($+\text{O}_2$) or anoxic ($-\text{O}_2$) buffer. Anoxia induced filamentous or dot-like EGFP-Mps1 aggregates. Bar = 5 μm .

(E) *EGFP-BubR1* embryos were fixed and labeled with anti- γ -tubulin (γ -Tub) and DNA stain (DNA) after a 20 minute incubation in either normoxic (+O₂) or anoxic (-O₂) buffer. In response to anoxia, EGFP-BubR1 (BubR1) accumulates within the equatorial region of metaphase figures and in peri-centrosomal filaments (arrowhead). Bar = 5 μ m.

(F) *gEGFP-Mps1* embryos were fixed and labeled with anti-BubR1 (BubR1) and DNA stain (DNA) after a 20 minute incubation in anoxic (-O₂) buffer. EGFP-Mps1 (Mps1) and anti-BubR1 signals largely overlap in the in peri-centrosomal filaments (arrowhead).

(G,H,I) *EGFP-Bub3* (G), *EGFP-Rod* (H), or *EGFP-Fzy* (I) embryos were fixed after a 20 minute incubation in either normoxic (+O₂) or anoxic (-O₂) buffer and labeled with a DNA stain (G-I; DNA) and anti- α -tubulin (H; Tub). Bar = 5 μ m.

FIG. 7. Mps1 modification in response to anoxia.

gEGFP-Bub3 embryos were fixed and labeled with DNA stain (DNA) after a 20 minute incubation in either normoxic (+O₂) or anoxic (-O₂) buffer. Syncytial blastoderm embryos during interphase (i) or metaphase (m) were sorted using a microscope. Anoxic interphase embryos were further sorted into early interphase (ie) and late interphase (il) based on the appearance of chromatin which is condensed into a meshwork during early interphase and into distinct chromatids during late interphase. Sorted embryos were used for extract preparation and immunoblotting with anti-Mps1 (Mps1) and anti-GFP (Bub3).

FIG. 8. Spindle checkpoint activation by cytochrome oxidase inhibitor.

gEGFP-Mps1 embryos were incubated in either absence (- CN) or presence (+ CN) of cyanide for 5 (A) or 15 (B) minutes before fixation and labeling with anti- α -tubulin (Tub) and a DNA stain (DNA). Cyanide induces re-organization of EGFP-Mps1 (Mps1), microtubules and chromatin during metaphase (A) and interphase (B) which is indistinguishable from the effects of anoxia. Bar = 5 μ m.

Figure 1

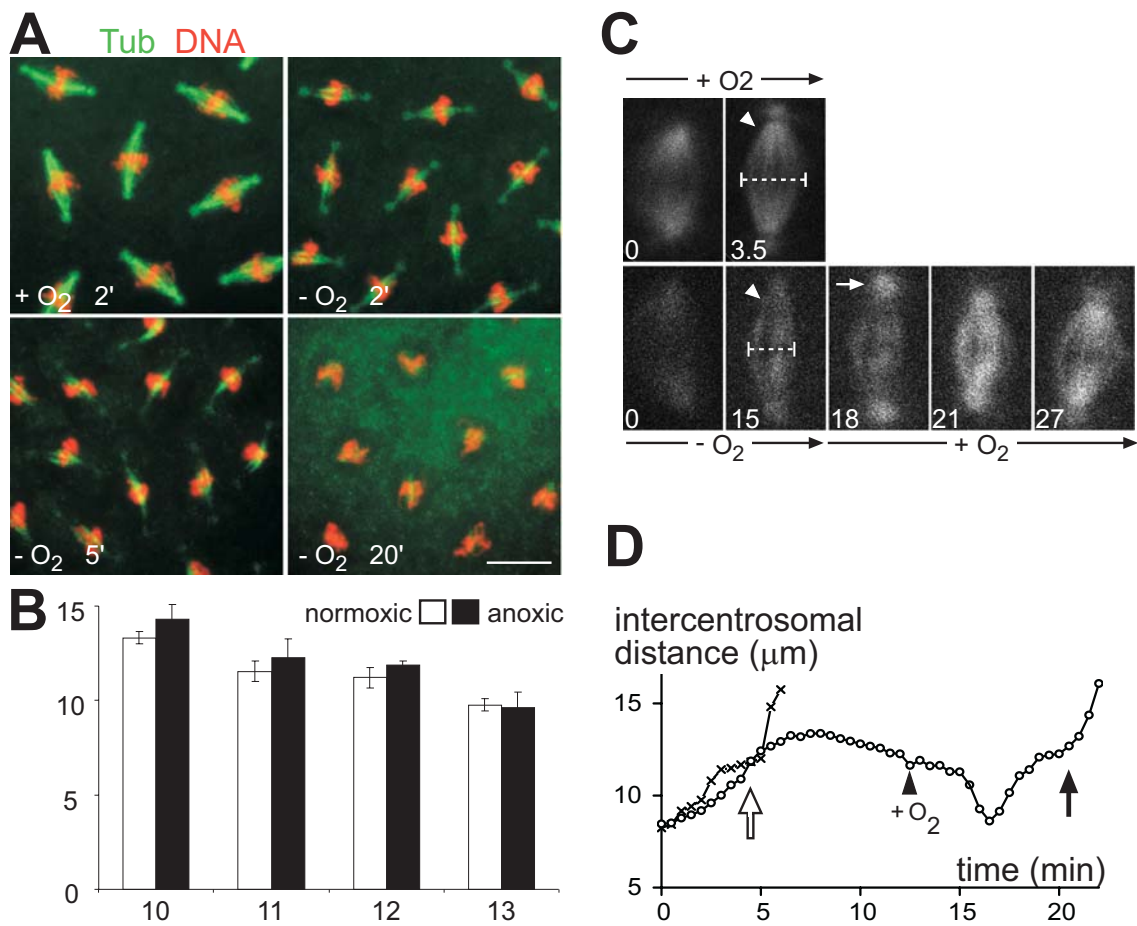


Figure 2

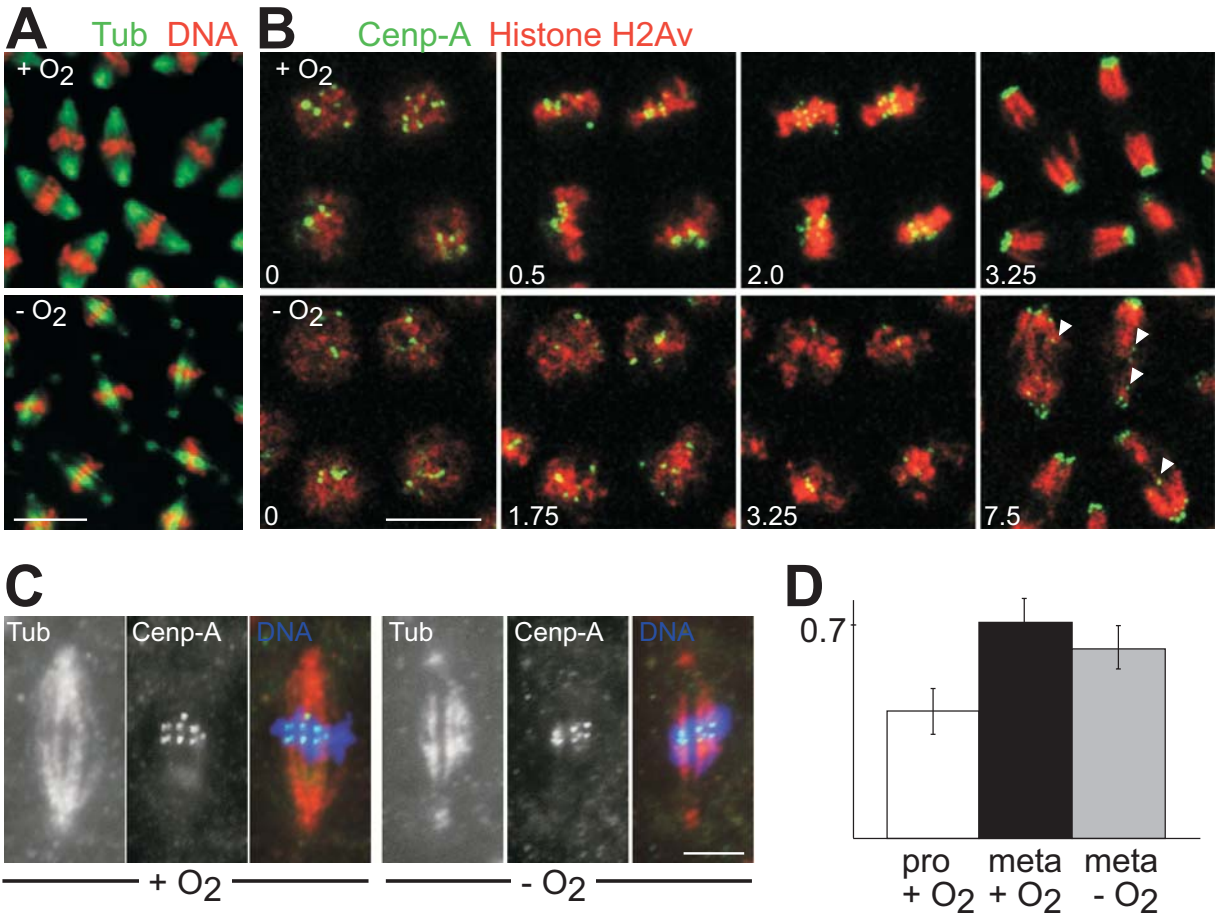


Figure 3

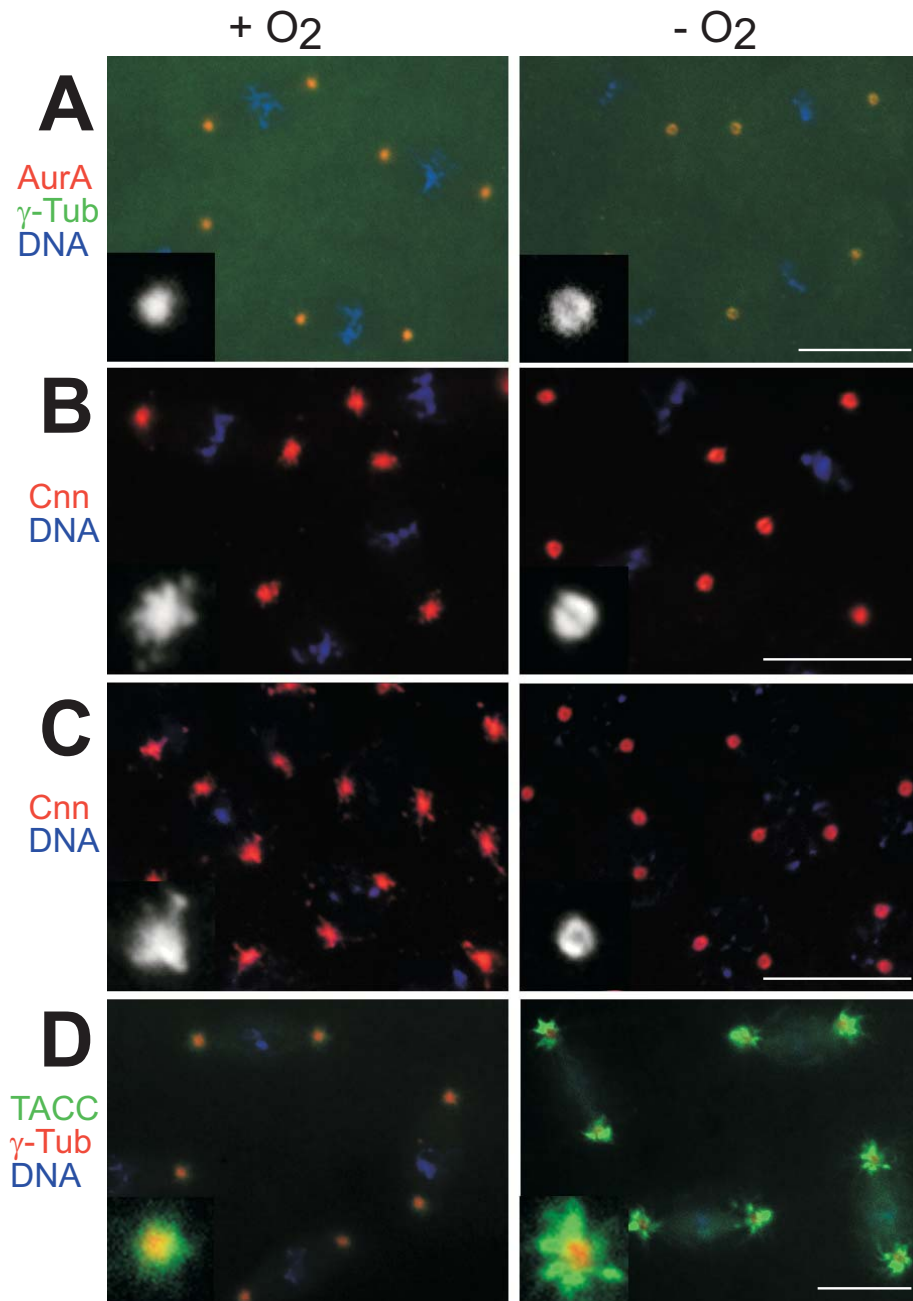


Figure 4

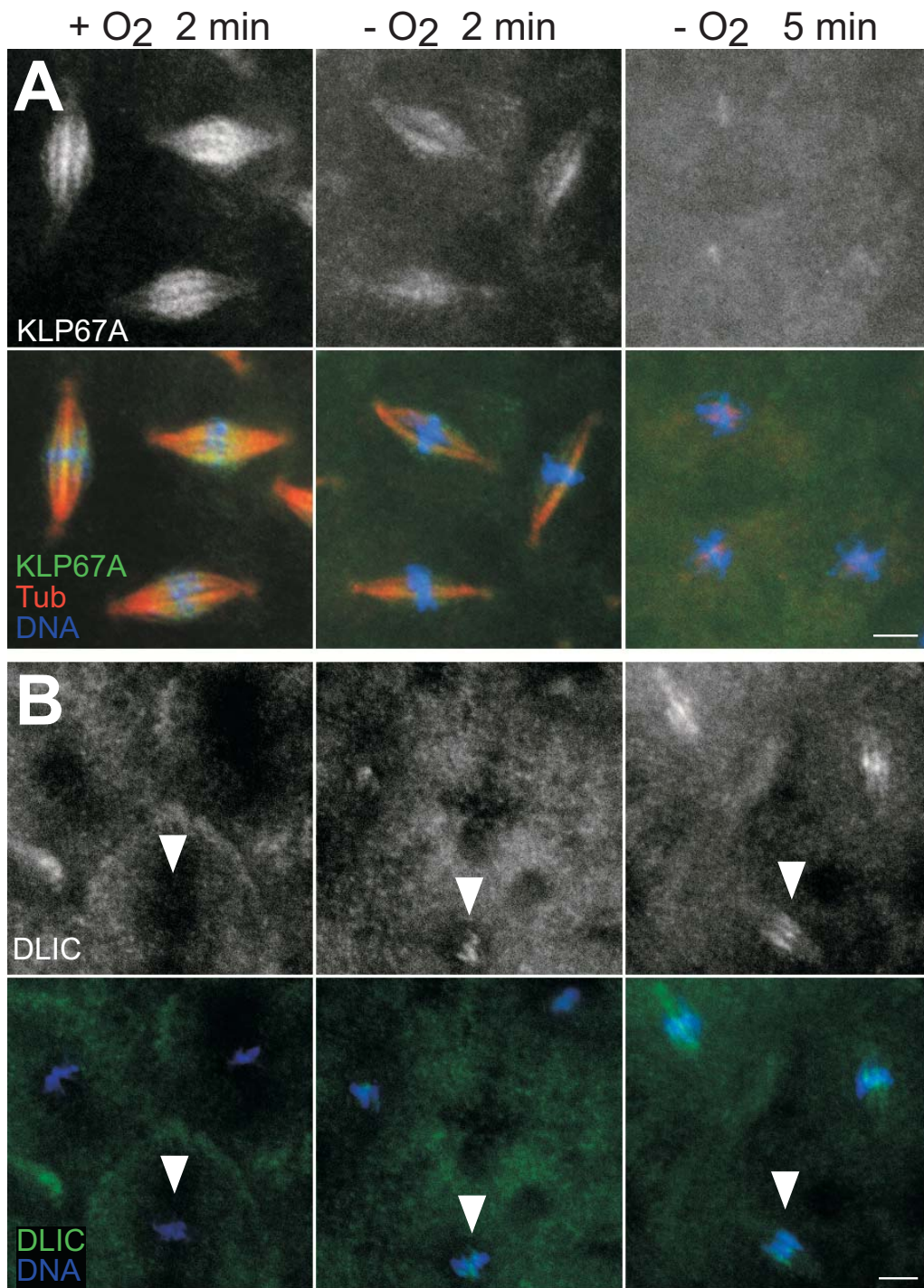


Figure 5

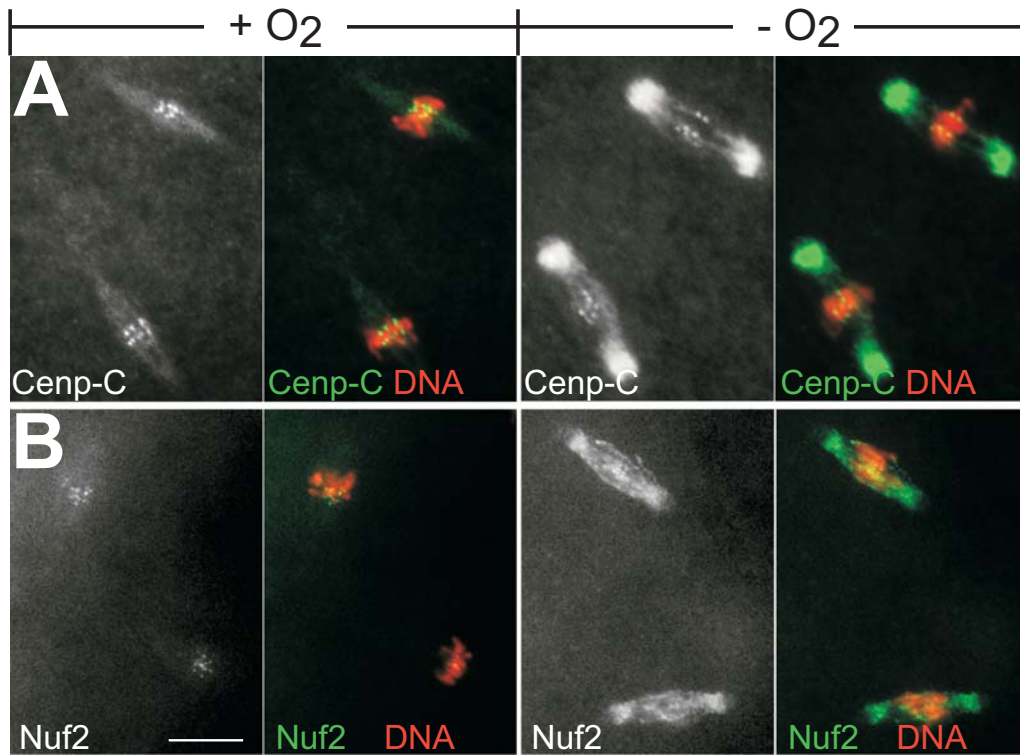


Figure 6

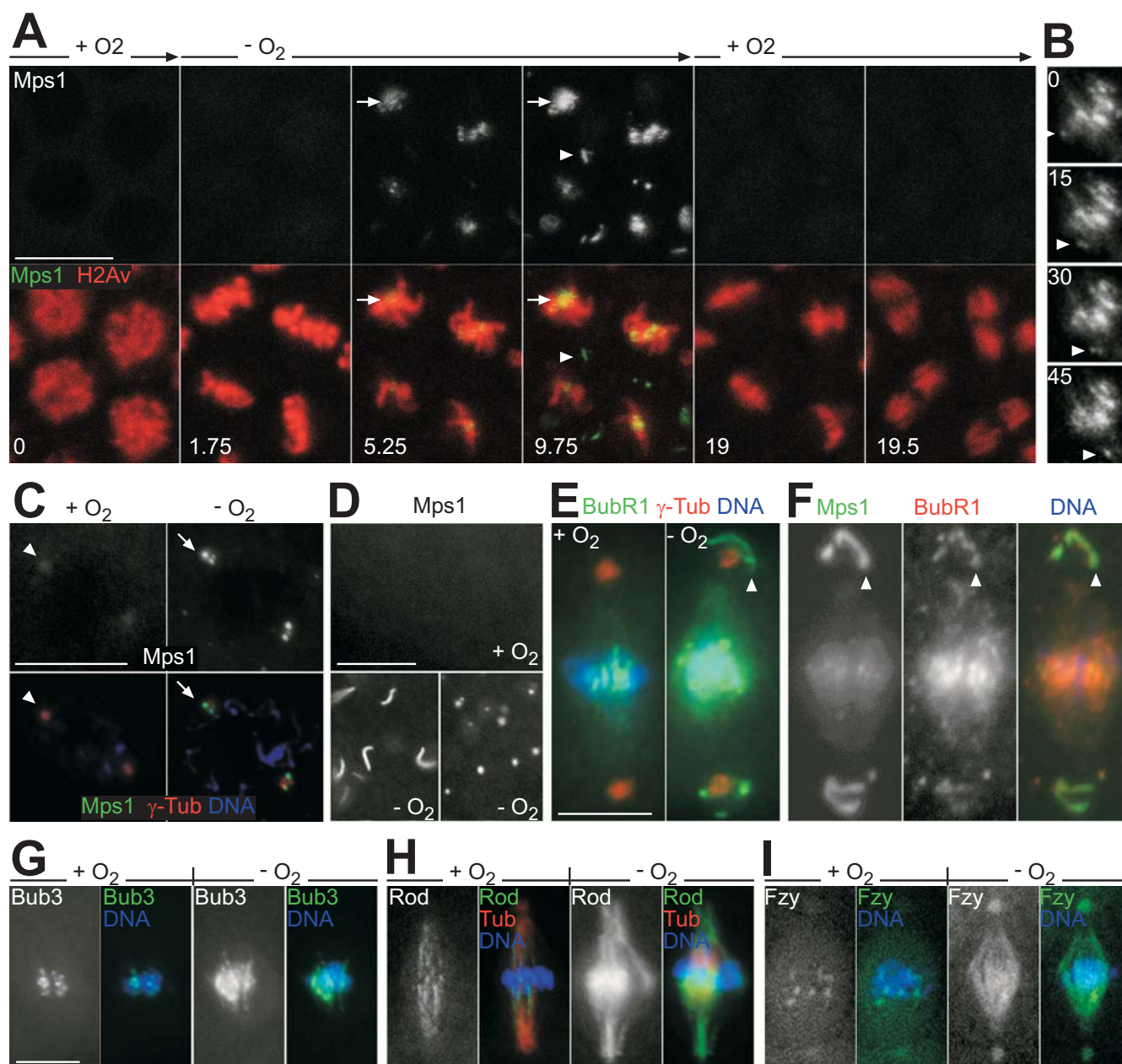


Figure 7

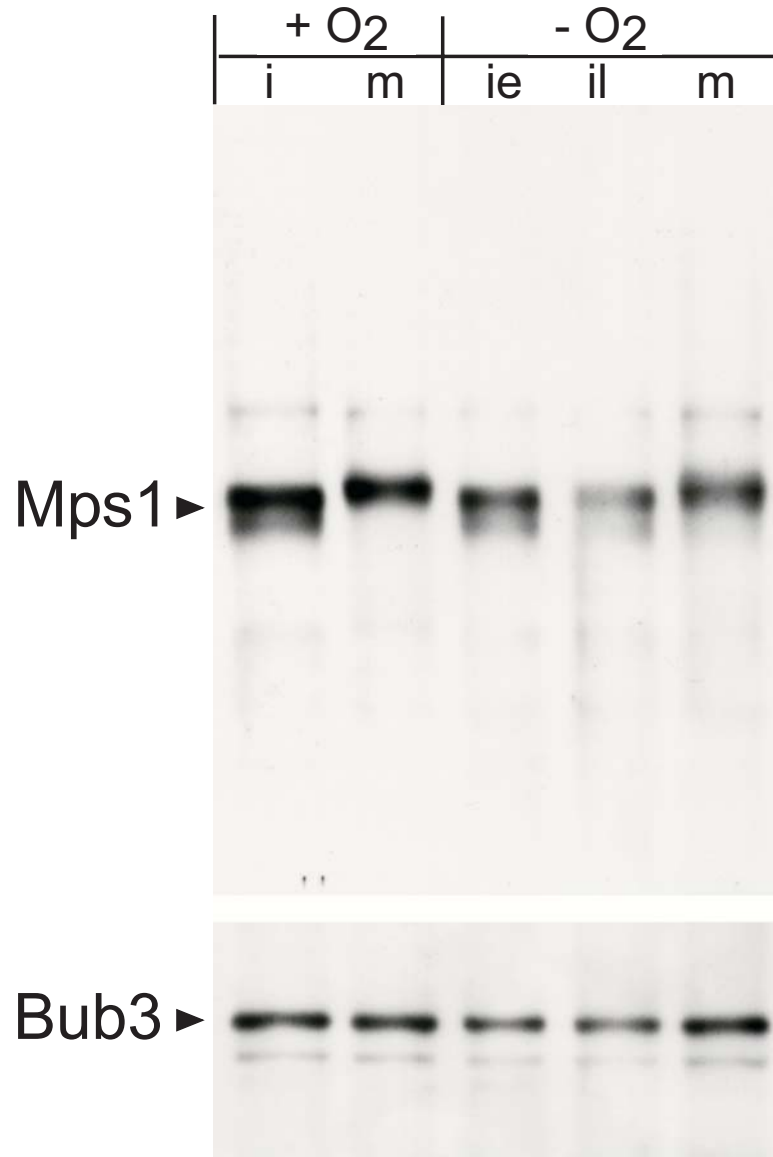
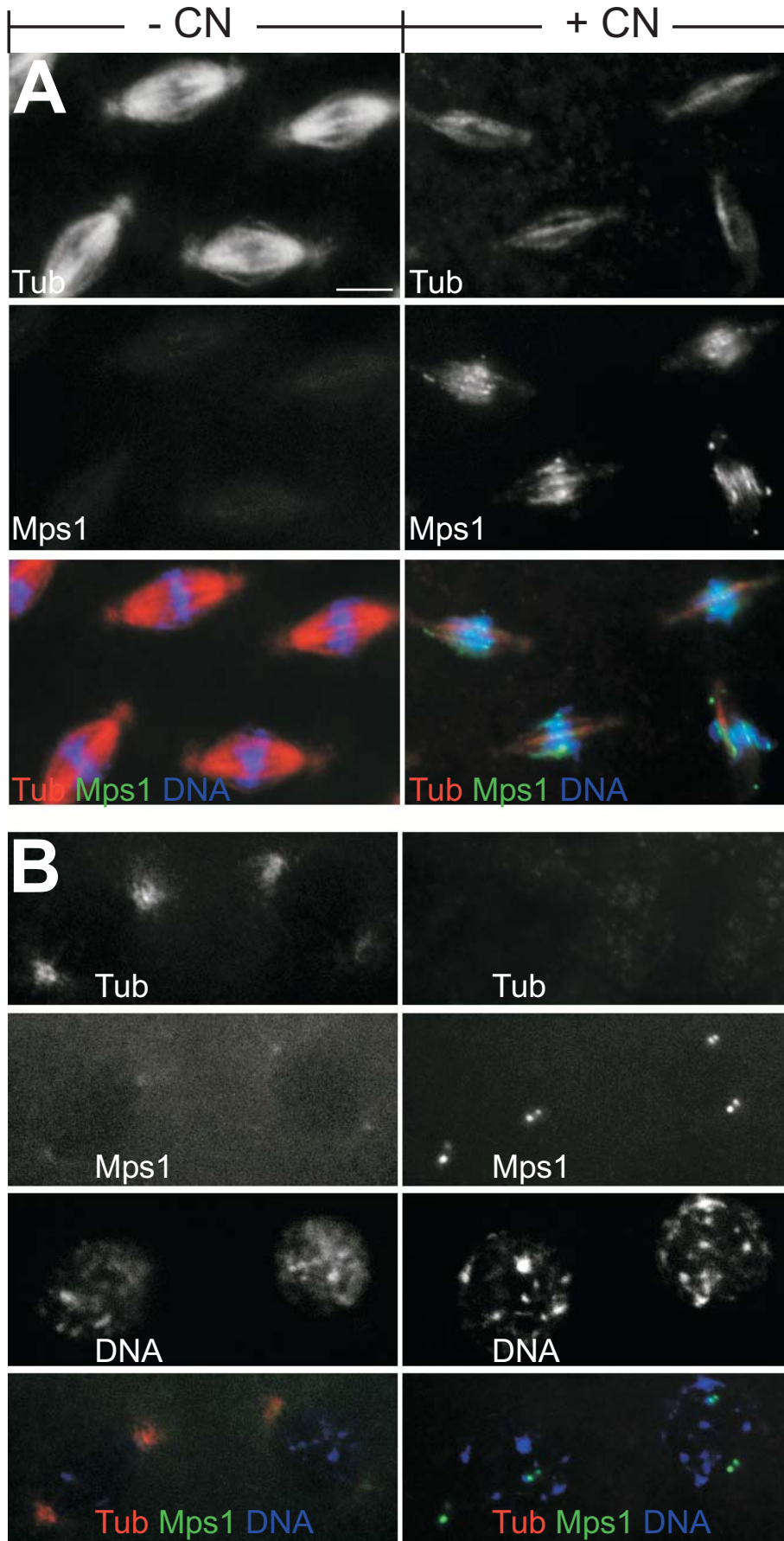


Figure 8



Part C

Identification of cold-sensitive processes during embryogenesis and genome regions important for cold survival of *Drosophila melanogaster*.

Rahul Pandey, André Koch and Christian F. Lehner

Manuscript is not yet submitted.

Contribution to Part C

The study was designed by the last author and myself. The results of this part are primarily from my work with some contributions (in particular during the deficiency screen) by André Koch during his diploma thesis.

The manuscript was written by the last author and myself.

Identification of cold-sensitive processes during embryogenesis and genome regions important for cold survival of *Drosophila melanogaster*

Rahul Pandey, André Koch and Christian F. Lehner¹⁾

Department of Genetics, BZMB, University of Bayreuth, 95440 Bayreuth, Germany

1) author for correspondence:

Christian Lehner

Department of Genetics

University of Bayreuth

Universitaetsstr. 30

95447 Bayreuth

Germany

phone: +49 921 55 2701

fax: +49 921 55 2710

e-mail: chle@uni-bayreuth.de

running title: cold sensitivity of *Drosophila* embryogenesis

Summary

Animal development succeeds only within a limited temperature range. The developmental processes, which are most cold-sensitive and form limits of adaptation, are poorly understood in particular at a molecular level. We demonstrate that the early embryonic stages are the most cold-sensitive period during development of the model organism *Drosophila melanogaster*. Cytological analyses indicate that mitotic divisions are highly cold-sensitive. Moreover, the spindle checkpoint which protects from progression through aberrant mitoses in the presence of spindle damage is shown to be required for normal cold survival. Apart from the syncytial mitoses, gastrulation processes were recognized as another especially sensitive target affected during development at low temperatures. Finally, we report the results of a genetic screen for the identification of genomic regions important for cold survival. Eleven deficiencies with molecularly defined breakpoints were found to exert a dominant maternal-effect on cold sensitivity.

Key Words: cold sensitivity, early embryogenesis, mitosis, Mps1, spindle checkpoint

Introduction

Temperature is a pervasive determinant of biological processes. However, the effects of temperature on developmental processes in metazoans have rarely been addressed at a cellular or molecular level, even though the great majority of animal species is poikilotherm and often confronted with extensive temperature variations, especially when terrestrial. While an extensive literature has been generated on the evolutionarily conserved, molecular response to heat shocks (Morimoto 1998), comparable studies of cold temperature effects have been largely restricted to prokaryotes (Weber and Marahiel 2003), yeast (Al-Fageeh and Smales 2006) and plants (Yamaguchi-Shinozaki and Shinozaki 2006). Earlier studies in bacteria have emphasized the importance of membrane fluidity, translation and metabolism in the context of cold responses. Cold-induced reduction of lipid mobility results in a decrease of membrane fluidity which may amount to a phase transition from a liquid crystalline to a more rigid gel-like state. Apart from membrane fluidity, translation has been shown to be affected strongly at low temperatures (Weber and Marahiel 2003). Insights into metabolic reactions in response to cold shocks in bacteria are still limited. However, at least initially, cold shock appears to create a transient state of metabolic excess (Weber and Marahiel 2003).

In higher organisms, adaptation to temperature extremes often involves intricate behavioural responses including mating and egg deposition. After egg laying, however, embryogenesis occurs often at ambient temperature. In species like *D. melanogaster*, temperature during embryogenesis can therefore easily and rapidly change in the wild. For example, *Drosophila* females lay their eggs preferentially at dusk which is frequently followed by extensive temperature drops within a few hours. While some studies have addressed the temperature range for survival also in the model organism *D. melanogaster* (Hoffmann et al. 2003), the molecular processes which constitute adaptations and limitations for development at low temperatures are almost completely unknown. For an understanding

of such molecular processes, an identification of the genes involved will be helpful. A genome-wide analysis of cold response is likely to take us closer to unravelling the pathways crucial for cold survival in higher eukaryotes.

Here, we have initiated an analysis of this intriguing problem in *D. melanogaster*. The temperature range allowing complete development from egg to adult has been reported to be between 11 and 32°C in *D. melanogaster* (David et al. 1971). Successive generations, however, are obtained only between 13 and 29°C, because males are sterile when grown either at or below 12°C (David et al. 1971; Cohet 1973; Chakir et al. 2002). Accordingly, the bottleneck for population growth at low temperatures appears to be male fertility in *D. melanogaster*. However, in these studies, eggs were collected for several hours at 25°C followed by a shift to lower temperatures. As a result, cold sensitivity of the very early embryonic stages before down-shift has never been addressed. These initial stages are dominated by a very rapid progression through thirteen tailored mitotic cycles (Foe and Alberts 1983). The early cycles lack gap phases. Moreover, cytokinesis is omitted, resulting in a syncytium with synchronously dividing nuclei. At the optimal growth temperature of 25°C, the initial mitoses 1-8 occur every 8 minutes followed by a gradual slow-down to 20 minute cycle time during cycles 9-13 (Foe and Alberts 1983). The last syncytial mitosis 13 which occurs two hours after egg deposition is followed by cellularization. This process compensates for the omission of cytokinesis. During cellularization, the majority of the nuclei which migrate to the egg periphery during the syncytial cycles become enveloped with cell membranes. Gastrulation starts thereafter, three hours after egg deposition (Foe and Alberts 1983).

Here we demonstrate that the initial syncytial division cycles of *Drosophila* embryogenesis are the most cold-sensitive developmental stages. We provide evidence indicating that mitosis is a sensitive target of low temperatures. Moreover, we report the results of a genetic screen

aimed at an eventual identification of genes important for cold survival during the early embryonic stages.

Results

The syncytial stages of early *Drosophila* embryogenesis are maximally cold-sensitive

To evaluate the cold sensitivity of early embryonic stages with their specialized mitotic cycles, we collected eggs from *w*¹ females for 30 minutes at 25°C followed by a 12 hour incubation at 9°C and subsequent development again at 25°C. This low temperature exposure at 9°C was found to reduce the rate with which larvae hatch from eggs to a few percent (Fig. 1) compared to more than 90% after continuous development at 25°C. Interestingly, the detrimental effect of the 12 hour incubation at 9°C was only observed during the early embryonic stages. The later it was imposed the lesser was its effect (Fig. 1). A maximal cold sensitivity was observed during the syncytial cycles. Cold sensitivity during cellularization and gastrulation was lower than during the syncytial cycles but still higher than during the remaining embryogenesis where the transient 9°C exposure no longer reduced the larval hatch rate significantly.

To analyze the cold sensitivity of the syncytial stages in further detail, we varied the temperature during the 12 hour cold exposure period from 8 to 12°C (Fig. 2). Progression through the syncytial stage was found to have a steep temperature dependency. Temperatures below 10°C were confirmed to reduce larval hatch rates by more than 80%. In contrast, a 12°C incubation caused a much milder reduction of only 20%.

Low temperatures interfere with normal progression through the syncytial cycles

Earlier reports indicated that the initial stages of *Drosophila* embryogenesis proceed even at 9°C (Houchmandzadeh et al. 2002). Whether progression through the syncytial cycles is

entirely normal or already defective at this low temperature has not been clarified in this report. Our observation of a dramatic reduction of the larval hatch rate after incubation at 9°C suggested an occurrence of abnormalities. To characterize progression through the syncytial cycles at low temperatures, we collected 0.5-1 hour eggs at 25°C and incubated these at 9°C, followed by fixation and DNA labeling. In addition, we incubated aliquots of embryos in parallel at 12°C which reduces larval hatch rates only modestly. For control, we also fixed an aliquot of embryos immediately after egg collection before incubation at low temperatures. As expected, these control embryos displayed the expected normal pattern of regularly spaced nuclei either in interphase (Fig. 3A,B) or in mitosis (Fig. 3C,D). These regular patterns were no longer observed after 4 hours at 9°C. Although the extent of abnormalities varied from embryo to embryo, the spacing between nuclei was clearly irregular in all interphase and mitotic embryos which frequently also displayed regional mitotic asynchrony (Fig. 3E-H). In contrast, after 4 hours of incubation at 12°C, embryos during interphase or mitosis displayed an almost normal nuclear pattern with occasional irregularities restricted to regions of only few nuclei (Fig. 3I-L). After 8 hours at 9°C, embryos were on the one hand severely affected with a chaotic pattern of DNA staining (Fig. 3P,Q). In these embryos, both the spacing between nuclei as well as the shape of individual nuclei was highly irregular. On the other hand, in the majority of the embryos, however, the number of nuclei had clearly increased between 4 and 8 hours at 9°C and the nuclear pattern in these embryos in either interphase or mitosis was more regular in general than after 4 hours at 9°C (Fig. 3M-O). After 24 hours at 9°C, some embryos appeared to have reached cellularization (Fig. 3R-T). However, the nuclear surface layer was clearly irregular (Fig. 3S) and the interior was almost completely filled up with yolk nuclei (Fig. 3T). In contrast, the embryos aged for 8 hours at 12°C, which also had reached cellularization, had a normal, regular surface layer and far fewer yolk nuclei more restricted within the central region (Fig. 3U-W). These observations indicate that 9°C

are not entirely incompatible with progression through syncytial cycles. However, many nuclei appear to undergo aberrant mitoses, in particular early after the temperature down-shift. Moreover, as described previously (Sullivan et al. 1993) (Sibon et al. 2000; Takada et al. 2003), the products of these abnormal mitoses appear to sink into the yolk interior during subsequent development, explaining the nuclear irregularities at the periphery and the overcrowding with yolk nuclei in the interior. In addition, we find that progression through the syncytial cycles is only mildly affected at 12°C.

The apparent, more severe damage observed soon after the temperature down-shift to 9°C suggested that initial cold shock effects might be largely responsible for the defects. Accordingly, progression through syncytial cycles might be less affected by gradual temperature reduction. Rapid cold shocks during early development certainly represent a highly artificial condition which is never experienced in the wild. However, gradual temperature changes are clearly of physiological relevance. Female flies deposit their eggs preferentially at dusk. Consequentially, the eggs must often experience a gradual temperature decline during the night in the wild. Cooling rates of up to about 0.1°C per minute can readily occur after dusk. Therefore, we investigated whether embryos are adapted to cope with gradual temperature reductions. 0.5-1 hour eggs collected and aged at 25°C were placed in a programmable incubator and cooled from 20°C to 9°C within two hours, i.e. with a cooling rate just below 0.1°C per minute. For comparison, 0.75-1.25 hour eggs collected and aged at 25°C were rapidly cooled to 9°C, as during the previous experiments. Aliquots of embryos were fixed and analyzed 0, 4 and 8 hours after the onset of the temperature down-shift. Unexpectedly, based on the extent of nuclear irregularities apparent at the 4 and 8 hour time points (Fig. 4), rapid and gradual temperature reduction appeared to cause comparable damage.

The spindle but not the DNA damage checkpoint protects against cold damage

The mitotic problems at 9°C might perhaps result at least in part from a reduced stability of spindle microtubules. Microtubules are known to be cold-sensitive structures (Brinkley and Cartwright 1975; Rieder 1981). Therefore, we double labeled embryos that had been fixed 0.5 hours after a temperature down-shift to 9°C with anti- α -tubulin and a DNA stain. Microtubule and chromatin appearance in embryos which had already completed the syncytial division cycles and were at the stage of cellularization did not appear to be affected (compare Fig. 5A and E). However, clear abnormalities were detected in embryos which had not yet completed the syncytial division cycles. The pattern of interphase nuclei displayed irregularities reflecting defects during a preceding mitosis. Regions with nuclei in the process of sinking into the interior (Fig. 5F, arrow) were observed, as well as detached centrosomes left behind by such nuclei (Fig. 5F, arrowhead). About 20% of the embryos appeared to be in an abnormal mitotic state characterized by highly condensed chromatin (Fig. 5G). Moreover, this abnormally condensed chromatin mass appeared to be surrounded by an intact nuclear envelope, as suggested by the exclusion of microtubules radiating out from spindle-like asters organized from opposite poles (Fig. 5G). At 25°C, spindle microtubules contact chromosomes before a comparable chromatin condensation has been reached (Fig. 5B). According to these observations, therefore, nuclear envelope breakdown appears to be slow or blocked after a shift to 9°C. Embryos with more normal mitotic figures were also observed after a shift to 9°C, and some of their abnormal features indicated that spindle function might also be compromised at low temperature. For example, during late anaphase, central spindles were much weaker than at 25°C (compare Fig. 5D and H).

For a further evaluation of the cold sensitivity of spindle microtubules in syncytial *Drosophila* embryos, we performed in vivo imaging with *G147*, *His2AvD-mRFP* embryos which express a red fluorescent histone variant and green fluorescent microtubule-associated

protein (Pandey et al. 2005). Eggs were collected and mounted for in vivo imaging at 25°C, followed by transfer to a microscope in a cold room at 4°C. Thereby, we observed spindle microtubules to disappear within minutes (Fig. 5I). Spindle destabilization was more pronounced in anaphase compared to metaphase spindles (Fig. 5I, ana). Moreover, some embryos were still observed to progress from metaphases into abnormal anaphases which were accompanied by chromatin bridging (Fig. 5I, meta/ana). Alternatively, chromosomes started to decondense in metaphase without any signs of anaphase (Fig. 5I, meta). These observations clearly confirm that severe temperature reductions prevent successful mitosis.

Although suggestive, our characterization of mitotic spindles cannot prove that these structures are an especially sensitive target of harmful temperature reductions. Therefore, for a further evaluation of this suggestion, we studied the role of the mitotic spindle checkpoint for cold survival. Spindle defects are known to activate the mitotic spindle checkpoint which protects from progression through abnormal anaphases and consequential damage (Lew and Burke 2003; Taylor et al. 2004; Kops et al. 2005; Pinsky and Biggins 2005). Therefore, the spindle checkpoint is expected to be of particular importance for successful development at low temperatures if this condition really results in spindle malfunction. Conversely, embryos lacking spindle checkpoint function are predicted to display an increased cold sensitivity. To address the importance of the spindle checkpoint, we analysed embryos lacking Mps1. The protein kinase Mps1 is known to be required for mitotic spindle checkpoint function also in *Drosophila* (Fischer et al. 2004). Therefore, we carefully analyzed the larval hatch rates of *Mps1^l* mutant eggs exposed to 11°C for a 12 hour incubation (followed by recovery at 25°C) or after continuous incubation at 25°C. The ratio between the hatch rates with and without cold exposure was found to be 0.19 (Fig. 6A). In contrast, this ratio was found to be 0.5 with *w^l* control embryos (Fig. 6A). Therefore, we conclude that *Mps1^l* mutant embryos are

significantly more cold-sensitive than control embryos. Moreover, this finding indicates that mitotic spindles are indeed a preferred target of harmful temperature reductions.

While microscopic analyses readily detect many mitotic defects, most other processes occurring during the syncytial stages are not effectively scrutinized thereby. Apart from mitotic spindles, therefore, additional targets with high sensitivity to low temperature might readily exist. Since DNA replication is also monitored by dedicated checkpoint pathways, we sought to apply the same experimental approach in case of this fundamental process, as before with mitotic spindle function. Two inter-connected checkpoint pathways monitor the integrity of DNA. A first checkpoint is primarily activated by single stranded DNA which occurs during DNA replication and certain DNA repair processes. The *Drosophila* Grapes/Chk1 protein kinase is required for this pathway (Sibon et al. 1997). Since this pathway has an essential developmental function during syncytial stages, mutant embryos die even after continuous development at 25°C (Sibon et al. 1997). However, the *Drosophila* Loki/Chk2 protein kinase, which functions in a pathway primarily activated by double stranded DNA breaks, is not essential for syncytial development at 25°C (Masrouha et al. 2003). Therefore, we analysed whether loss of *chk2* function results in an increased cold sensitivity. However, unlike *Mps1^l* mutants, *chk2* mutant embryos were not found to be more cold-sensitive than *w^l* control embryos (Fig. 6A).

Gastrulation is a cold-sensitive process

Our findings with embryos exposed to temperatures below 10°C demonstrate that the syncytial stages represent the most cold-sensitive stage during *Drosophila* development. Moreover, low temperature effects on mitotic spindle function might explain this special sensitivity at least in part. However, our experiments have also clearly revealed a relatively high cold sensitivity of embryos during cellularization and gastrulation when far fewer

mitoses occur than during the syncytial division cycles 1-13. Although less detrimental than during the syncytial division cycles, cold sensitivity during cellularization and gastrulation is significantly higher than during subsequent embryogenesis, as revealed by larval hatch rates (Fig. 1). Analysis of embryos exposed to temperatures above 10°C clearly confirmed the cold sensitivity of embryos during cellularization and gastrulation. When 0.5-1 hour embryos were exposed to 12°C before fixation and analysis, we observed only mild defects during the syncytial cycles (Fig. 3). Nuclear counts in embryos incubated for increasing time periods at 12°C indicated that cycle times were extended by a factor of about 7. However, after successful progression through the syncytial cycles, all embryos proceeded through a morphologically clearly abnormal gastrulation at 12°C (Fig. 7). It appears that these striking gastrulation defects are at least in part corrected after returning embryos to 25°C, since our larval hatch rate determination revealed that only 50% of the embryos exposed to 12°C during gastrulation failed to hatch to the larval stage (Fig. 1).

Identification of genomic regions required for cold survival

Progression through the early embryonic stages is largely controlled by the maternal genome. Apart from a few exceptional genes, which are mostly required for pattern formation and sex determination, zygotic genes are not expressed during the syncytial division cycles (ten Bosch et al. 2006). Widespread activation of zygotic gene expression is not observed before the cellular blastoderm stage. Accordingly, the maternal genome is also expected to determine the extent of cold sensitivity of the early syncytial stages. Therefore, we initiated a genetic approach towards an eventual identification of genes important for cold survival by assaying the cold sensitivity of progeny from females carrying chromosomal deficiencies in a heterozygous state. If a given deficiency also deletes a gene important for cold survival, progeny of deficient females might suffer from increased cold sensitivity. For our screen, we

used a collection of deficiencies with molecularly defined breakpoints in an isogenic background (Parks et al. 2004; Thibault et al. 2004). This deficiency collection covers about 56% of the *Drosophila* genome. Eggs were collected at 25°C for 30 minutes from each deficiency stock and one half of the eggs was then transiently incubated at 11°C for 12 hours, while the other half was kept continuously at 25°C. After larval hatch rate determination, we calculated the ratio between embryogenesis survival without and with cold exposure as a measure of cold sensitivity (CS). These assay conditions were chosen because they were found to result in a CS of 0.5 with our *w¹* control strain (Fig. 6A). After an initial round of screening, where CS was determined for each deficiency by averaging two independent assays, we found 44 deficiency stocks with CS values which were two standard deviations below the average CS (Fig. 6B, and Suppl. Table 1). In addition, 12 deficiency stocks appeared to have an increased cold resistance (CS = 0.9-1.1). 32 out of the cold-sensitive deficiency stocks were selected for a further test of reproducibility. These deficiencies were chosen since in addition to high CS, they were associated with low standard deviation and a healthy egg laying rate (~60 eggs in 30 minutes from ~200 females). Interestingly, 11 of these deficiencies were reproducibly found to have CS values two standard deviations below the average CS (Table 1). These findings suggest that a genetic strategy for the identification of genes important for cold survival should be feasible.

Discussion

To our knowledge, previous analyses have missed the especially pronounced cold sensitivity of the early syncytial stages of *Drosophila* development. Our results suggest that the bottleneck for *Drosophila* population growth at low temperatures is the progression through the syncytial stages rather than male fertility, as previously thought (David et al. 1971; Cohet 1973; Chakir et al. 2002). Considering that *Drosophila* females are known to

deposit their eggs at dusk, which can be followed by a rapid and extensive temperature drop during the ensuing night, the maximal cold sensitivity of the early developmental stages might appear as maladaptation. However, careful analyses of egg laying behavior of females kept with physiological temperature cycles might reveal behavioural responses.

Some characteristic features of the early syncytial stages stipulate plausible reasons for their special sensitivity to low temperatures. These initial embryonic stages rely on maternally contributed mRNA and protein stores and they proceed before the activation of wide-spread transcription. Therefore, the powerful transcriptional level of regulation cannot be used for adaptation to temperature changes. Moreover, the exponential genome amplification during the syncytial division cycles is much faster than at any other developmental stage by about one order of magnitude or more. The error-prone, complicated processes of DNA replication and mitosis which are of paramount importance for genetic stability are temporally compressed and therefore presumably also more vulnerable during the syncytial stages. Our analyses during successive developmental stages revealed a very impressive correlation of cold sensitivity with progression through the syncytial division cycles.

Some of our cytological observations are consistent with the notion that DNA replication might be compromised at low temperatures. Telophase figures present in embryos fixed 30 minutes after a temperature shift from 25°C to 9°C often contained chromatin bridges which might reflect incomplete replication during the preceding S phase (data not shown). However, without further analyses, it is not excluded that these chromatin bridges might also result in part or completely from chromosome separation and segregation defects during mitosis.

Our analyses provide clear evidence for mitotic defects resulting in response to a temperature decrease. About 20% of the embryos appeared to be in an abnormal mitotic state with abnormally advanced chromosome condensation and spindle asters but intact nuclear envelope. The known significance of lipid membrane fluidity in the context of bacterial, yeast

and plant cold sensitivity (Weber and Marahiel 2003) might provide a hint for the molecular basis of the nuclear envelope breakdown problems apparent in cold-treated *Drosophila* embryos. In addition, we find clear evidence for cold effects on spindle function. For instance, anti- α -tubulin labeling clearly revealed poorly formed central spindles during late anaphase. These weak central spindles were also present in anaphase figures without chromatin bridges, excluding the possibility that they result as secondary consequences from earlier DNA replication defects. Moreover, our experiments with *Mps1* mutants demonstrate that the mitotic spindle checkpoint, a surveillance pathway which monitors spindle assembly as well as chromosome attachment and bi-orientation within the spindle, is important for efficient cold survival.

While exposure of normal syncytial embryos to temperatures below 11°C killed 50% or more, progression through the initial embryonic division cycles and cellularization appeared to be almost normal already at 12°C although about sevenfold slower compared to 25°C. However, gastrulation was clearly abnormal at 12°C. The morphological processes of gastrulation are unlikely to create a higher functional demand on cytoskeletal dynamics and metabolism than mitosis and cellularization. We suspect therefore that a particular cold sensitivity of the expression of distinct genes might cause the observed gastrulation problems.

We emphasize that the observed abnormalities during early embryogenesis were detected irrespective of the rate of cooling. Because eggs were transferred into low temperature incubators on the apple juice agar plates used for collection, their cooling was clearly not instantaneous even in the experiments without controlled slow cooling. Since the initial cytological defects appeared to be somewhat more severe than those observed later during the incubation at low temperatures, we assume that these defects are in part but not exclusively caused by a cold shock.

Many developmental processes cannot be studied by our microscopic analyses and therefore we have also initiated an unbiased genetic approach to identify genes crucial for cold survival. As a first step, we have screened through a collection of chromosomal deficiencies. Thereby we found 11 chromosomal regions in the *Drosophila* genome, which are important for cold survival. We also found 12 deficiencies that appeared to confer maternal effect cold resistance. While it is not excluded that the *Drosophila* genome also includes genes which lower cold sensitivity, we would like to discuss the effect of overaged embryos on our CS assays in this context. Depending on the physiological state, and potentiality on the genotype as well, females can retain their eggs before oviposition. Such overaged eggs are expected to be less cold-sensitive if they have already developed to the later, less cold-sensitive developmental stages before egg deposition. Therefore, deficiencies which increase the frequency of overaged eggs will score as cold resistant in our assay. Further analyses will be required to rule out this potential complication.

We also would like to point out that the zygotic genotype can of course influence the observed cold sensitivity, even though this zygotic genotype is not of importance during the syncytial stages when we have applied the cold treatment in our screen. The zygotic genotype can of course influence the efficiency with which the defects acquired during the syncytial stages are repaired during subsequent development. Moreover, the defects acquired during the syncytial stages can synergize with zygotic effects. Cytological analysis demonstrating that a particular deficiency results in more severe defects already during the syncytial stages will be required to unequivocally identify chromosomal regions with a maternal effect on cold sensitivity during the syncytial stages.

Materials and methods

Fly stocks

We used w^1 as control because all other mutant and transgenic strains analyzed had a w mutant background. *G147*, *His2AvD-mRFP* has been described previously (Pandey et al. 2005). Females with *Mps1¹* germ line clones were generated using the FLP-DFS method (Chou and Perrimon 1996) as described previously (Fischer et al. 2004), and term “*Mps1¹* mutant embryos” refers to progeny derived from these females after mating with w^1 males. The flies completely lacking *loki/chk2* function were w ; *Df(2L)be408*, *P{w+, CG10728+}/Df(2L)pr2b*, *P{w+, barren+}* (Masrouha et al. 2003). The deficiency collection (Parks et al. 2004) was kindly provided by the Bloomington *Drosophila* Stock Center at Indiana University. The analyzed deficiency stocks are listed in Supplementary Table 1.

Larval hatch rate determination and maternal effect cold sensitivity screen

For larval hatch rate experiments (Fig. 1,2), eggs were collected for 30 minutes at 25°C on apple juice agar plates. Agar with eggs was divided into several pieces which were subjected to specific incubation programs at defined times and temperatures. In the experiments described in Fig.1, we incubated one aliquot continuously at 25°C for an additional 30 minutes followed by fixation, DNA staining and microscopy. Eggs which did not contain multiple nuclei were scored as unfertilized. The ratio of fertilized eggs in the sample was determined and used as a correction factor in the calculation of larval hatch rates. All other aliquots were aged at 25°C to the desired times and exposed to 9°C for 12 hours. After 30 hours of recovery at 25°C, we counted the hatched and unhatched eggs on the agar. Hatch rates were calculated as the ratio of hatched eggs to the total number of fertilized eggs. The number of eggs N per time point and experiment was between 35-190. In the experiments described in Fig. 2, one half of the egg collection was incubated continuously at 25°C while the other half was transiently exposed for 12 hours to either 8, 9, 10, 11, or 12°C. After 30 hours of recovery at 25°C, the hatched and unhatched eggs on the agar were counted. The

number of eggs N per temperature and experiment was between 44-120. For the deficiency screen, eggs were collected from balanced parents which were 3-5 day old adults. One half of the collection was transiently incubated for 12 hours at 11°C and returned to 25°C for subsequent development. The other half was incubated continuously at 25°C. All values (total number of eggs analyzed, hatch rates, number of experiments, standard deviations) obtained during the primary and secondary deficiency screens are given in the Supplementary Table 1 and 2, respectively. All incubations were performed by placing the eggs on the collection plates into temperature-controlled incubators.

In vivo imaging and immunofluorescence

Syncytial *G147*, *His2AvD-mRFP* embryos were collected at 25°C and in vivo imaging was performed essentially as described previously (Herzig et al. 2002) in a cold room at 4°C. For the analysis of fixed embryos, we collected eggs for 30 minutes at 25°C on apple juice agar plates which were then divided into various slices and incubated for the desired times at the wished temperatures. For control of the cooling rate, we placed the eggs on the agar plate into a programmable temperature-controlled incubator. The embryos were then dechorionated in 100% bleach during 6 and 2.5 minutes, respectively, at 9 and 12°C, followed by fixation in methanol. All solutions used during the fixation procedure were pre-cooled to the given incubation temperatures. DNA was labeled with 1 µg/ml Hoechst 33258. For immunofluorescent staining we used mouse monoclonal antibody DM1A anti- α -tubulin (Sigma) at 1:8000. Single focal planes were acquired with a Zeiss Axioplan 2 Imaging system using Zeiss AxioVision software. Adobe Photoshop was used for preparation of the figures.

Acknowledgements

We thank B. Suter for the loki mutant stock and the members of the lab for help during the screen. This work was supported by the Deutsche Forschungsgemeinschaft (DFG LE 987/4-1).

References

- Al-Fageeh, M.B. and Smales, C.M. 2006. Control and regulation of the cellular responses to cold shock: the responses in yeast and mammalian systems. *Biochem J* **397**(2): 247-259.
- Brinkley, B.R. and Cartwright, J., Jr. 1975. Cold-labile and cold-stable microtubules in the mitotic spindle of mammalian cells. *Ann N Y Acad Sci* **253**: 428-439.
- Chakir, M., Chafik, A., Moreteau, B., Gibert, P., and David, J.R. 2002. Male sterility thermal thresholds in *Drosophila*: *D. simulans* appears more cold-adapted than its sibling *D. melanogaster*. *Genetica* **114**(2): 195-205.
- Chou, T.B. and Perrimon, N. 1996. The autosomal FLP-DFS technique for generating germline mosaics in *Drosophila melanogaster*. *Genetics* **144**: 1673-1679.
- Cohet, Y. 1973. Stérilité mâle provoquée par une basse température de développement chez *Drosophila melanogaster*. *C R Acad Sci Paris* **276**: 3343-3345.
- David, J., Arens, M.F., and Cohet, Y. 1971. Stérilité mâle à haute température chez *Drosophila melanogaster*: nature, progressivité, réversibilité des effets de la chaleur. *C R Acad Sci Paris* **272**: 1007-1010.
- Fischer, M.G., Heeger, S., Hacker, U., and Lehner, C.F. 2004. The mitotic arrest in response to hypoxia and of polar bodies during early embryogenesis requires *Drosophila* Mps1. *Curr Biol* **14**(22): 2019-2024.
- Foe, V.E. and Alberts, B.M. 1983. Studies of nuclear and cytoplasmic behaviour during the five mitotic cycles that precede gastrulation in *Drosophila* embryogenesis. *J Cell Sci* **61**: 31-70.
- Herzig, A., Lehner, C.F., and Heidmann, S. 2002. Proteolytic cleavage of the THR subunit during anaphase limits *Drosophila* separase function. *Genes Dev* **16**(18): 2443-2454.
- Hoffmann, A.A., Sorensen, J.G., and Loeschke, V. 2003. Adaptation of *Drosophila* to temperature extremes: bringing together quantitative and molecular approaches. *J Therm Biol* **28**: 175-216.
- Houchmandzadeh, B., Wieschaus, E., and Leibler, S. 2002. Establishment of developmental precision and proportions in the early *Drosophila* embryo. *Nature* **415**(6873): 798-802.
- Kops, G.J., Weaver, B.A., and Cleveland, D.W. 2005. On the road to cancer: aneuploidy and the mitotic checkpoint. *Nat Rev Cancer* **5**(10): 773-785.
- Lew, D.J. and Burke, D.J. 2003. The spindle assembly and spindle position checkpoints. *Annu Rev Genet* **37**: 251-282.
- Masrouha, N., Yang, L., Hijal, S., Larochelle, S., and Suter, B. 2003. The *Drosophila* *chk2* gene loki is essential for embryonic DNA double-strand-break checkpoints induced in S phase or G2. *Genetics* **163**(3): 973-982.
- Morimoto, R.I. 1998. Regulation of the heat shock transcriptional response: cross talk between a family of heat shock factors, molecular chaperones, and negative regulators. *Genes Dev* **12**(24): 3788-3796.
- Pandey, R., Heidmann, S., and Lehner, C.F. 2005. Epithelial re-organization and dynamics of progression through mitosis in *Drosophila* separase complex mutants. *J Cell Sci* **118**(Pt 4): 733-742.
- Parks, A.L., Cook, K.R., Belvin, M., Dompe, N.A., Fawcett, R., Huppert, K., Tan, L.R., Winter, C.G., Bogart, K.P., Deal, J.E., Deal-Herr, M.E., Grant, D., Marcinko, M., Miyazaki, W.Y., Robertson, S., Shaw, K.J., Tabios, M., Vysotskaia, V., Zhao, L., Andrade, R.S., Edgar, K.A., Howie, E., Killpack, K., Milash, B., Norton, A., Thao, D., Whittaker, K., Winner, M.A., Friedman, L., Margolis, J., Singer, M.A., Kopczynski,

- C., Curtis, D., Kaufman, T.C., Plowman, G.D., Duyk, G., and Francis-Lang, H.L. 2004. Systematic generation of high-resolution deletion coverage of the *Drosophila melanogaster* genome. *Nat Genet* **36**(3): 288-292.
- Pinsky, B.A. and Biggins, S. 2005. The spindle checkpoint: tension versus attachment. *Trends Cell Biol* **15**(9): 486-493.
- Rieder, C.L. 1981. The structure of the cold-stable kinetochore fiber in metaphase PtK1 cells. *Chromosoma* **84**(1): 145-158.
- Sibon, O.C., Kelkar, A., Lemstra, W., and Theurkauf, W.E. 2000. DNA-replication/DNA-damage-dependent centrosome inactivation in *Drosophila* embryos. *Nat Cell Biol* **2**(2): 90-95.
- Sibon, O.C.M., Stevenson, V.A., and Theurkauf, W.E. 1997. DNA-replication checkpoint control at the *Drosophila* midblastula transition. *Nature* **388**: 93-97.
- Sullivan, W., Daily, D.R., Fogarty, P., Yook, K.J., and Pimpinelli, S. 1993. Delays in anaphase initiation occur in individual nuclei of the syncytial *Drosophila* embryo. *Mol Biol Cell* **4**: 885-896.
- Takada, S., Kelkar, A., and Theurkauf, W.E. 2003. *Drosophila* checkpoint kinase 2 couples centrosome function and spindle assembly to genomic integrity. *Cell* **113**(1): 87-99.
- Taylor, S.S., Scott, M.I., and Holland, A.J. 2004. The spindle checkpoint: a quality control mechanism which ensures accurate chromosome segregation. *Chromosome Res* **12**(6): 599-616.
- ten Bosch, J.R., Benavides, J.A., and Cline, T.W. 2006. The TAGteam DNA motif controls the timing of *Drosophila* pre-blastoderm transcription. *Development* **133**(10): 1967-1977.
- Thibault, S.T., Singer, M.A., Miyazaki, W.Y., Milash, B., Dompe, N.A., Singh, C.M., Buchholz, R., Demsky, M., Fawcett, R., Francis-Lang, H.L., Ryner, L., Cheung, L.M., Chong, A., Erickson, C., Fisher, W.W., Greer, K., Hartouni, S.R., Howie, E., Jakkula, L., Joo, D., Killpack, K., Laufer, A., Mazzotta, J., Smith, R.D., Stevens, L.M., Stuber, C., Tan, L.R., Ventura, R., Woo, A., Zakrajsek, I., Zhao, L., Chen, F., Swimmer, C., Kopczynski, C., Duyk, G., Winberg, M.L., and Margolis, J. 2004. A complementary transposon tool kit for *Drosophila melanogaster* using P and piggyBac. *Nat Genet* **36**(3): 283-287.
- Weber, M.H. and Marahiel, M.A. 2003. Bacterial cold shock responses. *Sci Prog* **86**(Pt 1-2): 9-75.
- Yamaguchi-Shinozaki, K. and Shinozaki, K. 2006. Transcriptional Regulatory Networks In Cellular Responses And Tolerance To Dehydration And Cold Stresses. *Annu Rev Plant Biol* **57**: 781-803.

Figure legends

Figure 1. Cold sensitivity during *Drosophila* embryogenesis

Eggs were collected at 25°C for 30 minutes and aged to the desired stages before the incubation temperature was transiently lowered to 9°C for 12 hours. After subsequent development at 25°C, the rate of larval hatching from the eggs was determined. Average hatch rates (%) from three experiments and standard deviations are shown.

Figure 2. Temperature dependence of successful progression through the early embryonic stages

Embryos were collected for 30 minutes at 25°C and transiently incubated for 12 hours at a specific low temperature. After subsequent development at 25°C, the rate of larval hatching from the eggs was determined. Hatch rates obtained after low temperature incubations were normalized to the hatch rate observed after continuous development at 25°. Averages of two experiments with standard deviations are shown.

Figure 3. Cytological analysis of low temperature effects on early embryogenesis

0.5-1 hour embryos were fixed and labeled with a DNA stain either immediately (A-D) or after incubation at 9°C for 4 (E-H), 8 (M-Q) and 12 hours (R-T) or after incubation at 12°C for 4 (I-L) and 8 hours (U-W). Syncytial embryos before cold exposure displayed a regular nuclear spacing in interphase (A,B) and mitosis (C,D). For a detailed explanation of the defects observed after cold exposure (E-W) see text. Bars in A and B = 50 and 10 µm, respectively.

Figure 4. Effects of cooling rate

Early syncytial embryos were cooled from 20 to 9°C either slowly (A,B) or rapidly (C,D), followed by fixation and DNA labeling. Both slow as well as rapid cooling caused comparable damage after 4 (compare A and C) and 8 hours (compare B and D) of cold exposure. Bar = 50 μm .

Figure 5. Effects of low temperature on microtubules and cell cycle progression

Embryos were fixed either without a preceding exposure to low temperature (A-D) or 30 minutes after a temperature down shift to 9°C (E-G). Anti- α -tubulin labeling is shown in green, DNA staining in red. See text for further explanations. Bar = 10 μm .

(I) *G147*, *His2AvD-mRFP* embryos expressing a red fluorescent histone variant and a green fluorescent microtubule-associated protein (Pandey et al. 2005) were collected and mounted for in vivo imaging at 25°C. In vivo imaging was started as soon as possible after a transfer to a microscope in a cold room at 4°C. Selected frames are shown for metaphase (meta), metaphase to anaphase transition (meta/ana) and anaphase (ana). Time in minutes is shown. Bar = 5 μm .

Figure 6. The spindle checkpoint but not the Chk2-DNA-damage checkpoint is important for cold survival

(A) 0-0.5 hour embryos which were either w^1 (w^1 , control), *Mps1¹* mutant (*Mps1¹*) or *chk2* mutant (*chk2*) were incubated either continuously at 25°C or transiently at 11°C for 12 hours before a return to 25°C. Larval hatch rates were determined and the cold sensitivity (CS) of the different genotypes was estimated by calculating the ratio of the observed hatch rates with and without cold exposure. The bars indicate CS average and standard deviation of 8, 5 and 2 independent experiments in case of w^1 , *Mps1¹* and *chk2*, respectively.

(B) Results from the maternal effect cold sensitivity screen with a collection of chromosomal deficiencies (Parks et al. 2004). The bar graph shows number of deficiencies (y-axis) plotted against the CS range (x-axis). Dotted lines delimitate the region with CS values within +/- two standard deviations of the mean.

Figure 7. Gastrulation is a cold-sensitive process

Embryos were collected for 30 minutes at 25°C and incubated either further at 25°C (A) or at 12°C (B) until the stages of gastrulation. DNA was labeled after fixation. Bar = 50 μm.

Table I. Chromosomal regions important for successful progression through early embryogenesis at low temperature

Symbol	Estimated cytology (Release 3)	Sequence coordinates (Release 3)	Number of genes deleted	CS \pm σ
<i>w</i> ¹	-	-	-	0.5 \pm 0.13
<i>Df(3R)Exel9014</i>	95B1;95D1	3R:19589500..19759383	22	0.21 \pm 0.08
<i>Df(3R)Exel6192</i>	94B11;94D3	3R:18483028..18715579	37	0.13 \pm 0.03
<i>Df(2R)Exel9043</i>	37E1;37E1	2R:19416148..19430995	5	0.16 \pm 0.09
<i>Df(2L)Exel9044</i>	36C10;36C11	2L:17480597..17582843	8	0.23 \pm 0.04
<i>Df(2L)Exel8036</i>	36B1;36C9	2L:16769571..17428338	61	0.23 \pm 0.02
<i>Df(2L)Exel7067</i>	36A12;36B2	2L:16706459..16802992	37	0.14 \pm 0.12
<i>Df(2L)Exel8026</i>	31F5;32B1	2L:10509084..10854392	63	0.20 \pm 0.05
<i>Df(2L)Exel8022</i>	30B3;30B5	2L:9380364..?	8	0.22 \pm 0.11
<i>Df(2L)Exel7027</i>	26F5;27B1	2L:6657034..6779122	30	0.16 \pm 0.15
<i>Df(2L)Exel7024</i>	26A1;26A8	2L:5890506..5972368	23	0.18 \pm 0.04
<i>Df(2L)Exel8010</i>	24C8;24D4	2L:3880550..4023894	9	0.16 \pm 0.06

Figure 1

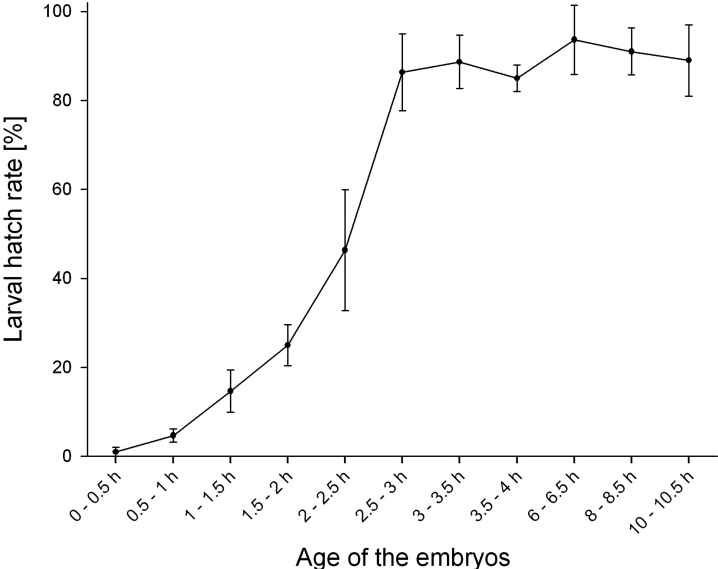


Figure 2

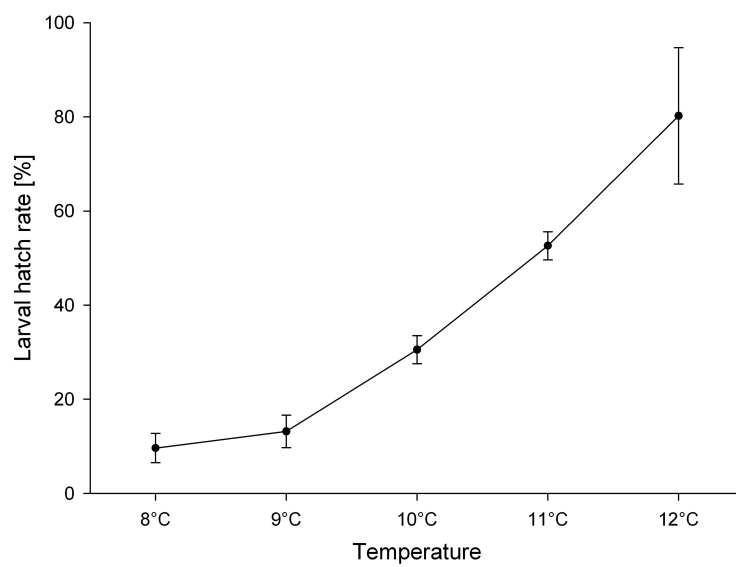


Figure 3

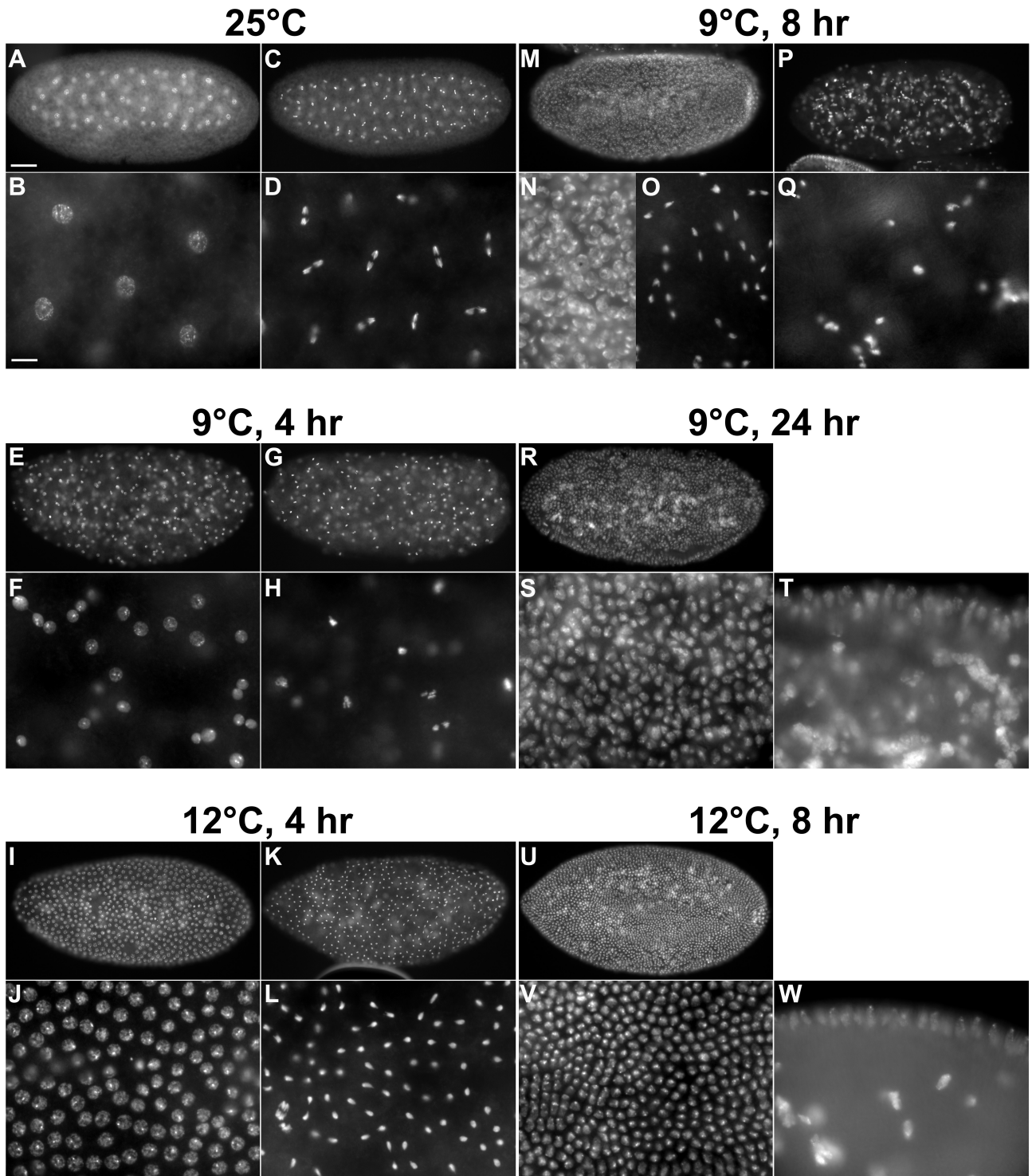


Figure 4

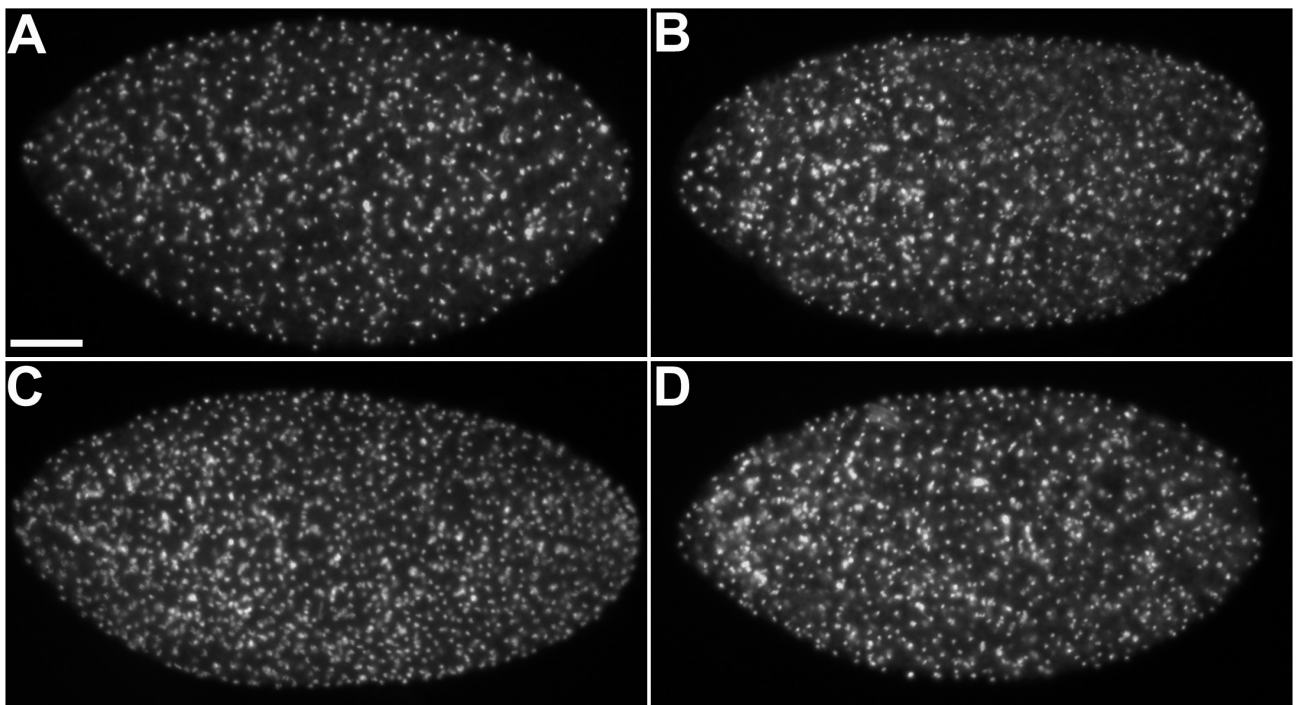


Figure 5

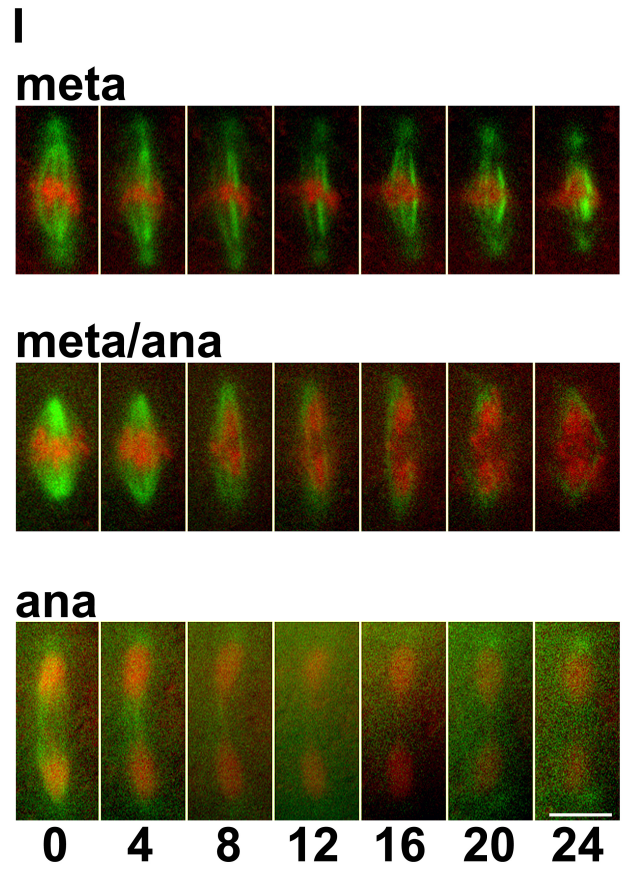
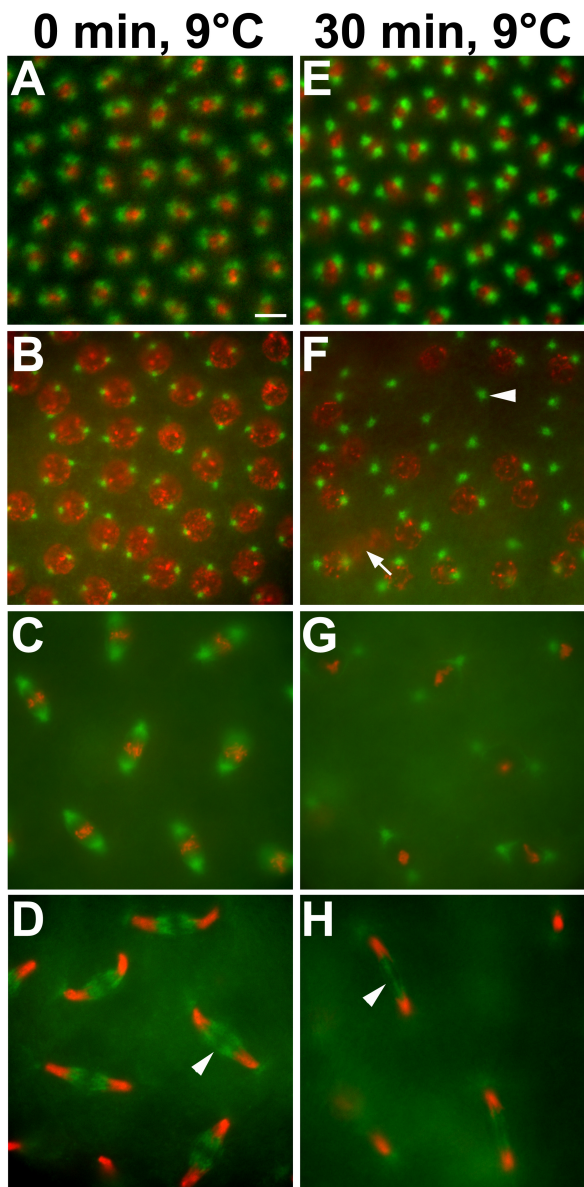


Figure 6

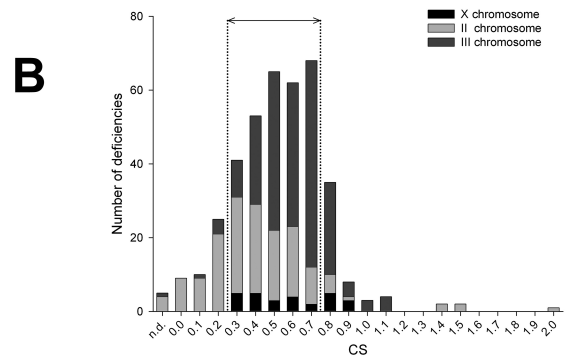
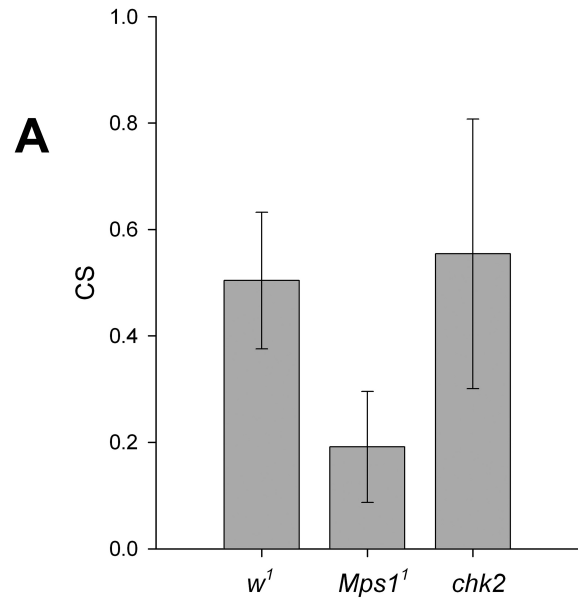
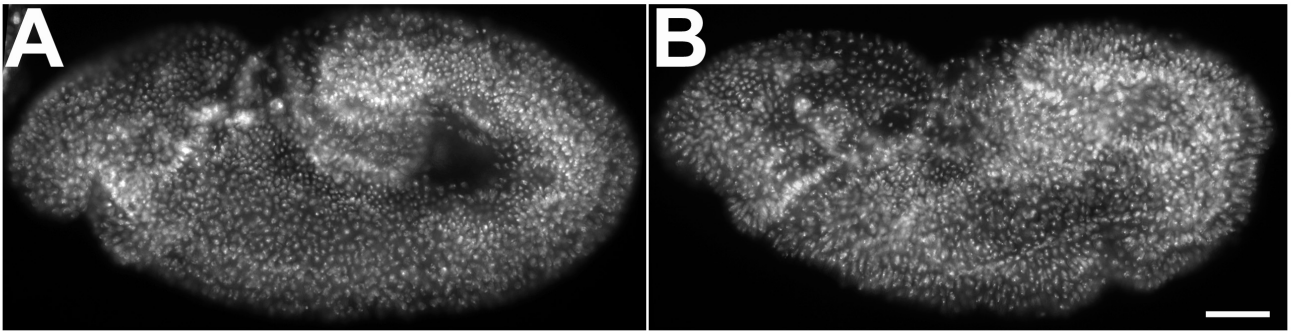


Figure 7



Supplementary table 1:Abbreviations and their meaning:

LHR: Larval Hatch Rate; \bar{O} Egg number: average number of hatched and unhatched eggs analysed. " \bar{O} LHR" and " σ LHR" represent the average LHR and standard deviation, respectively, of two independent experiments. N: total number of eggs evaluated.

The values of two independent experiments (1 and 2) are shown.

Symbol	Estimated Cytology (R3)	Sequence Coordinates (R3)	Ø Egg number	1. LHR 25°C (%)	N	1. LHR 11°C (%)	N	2. LHR 25°C (%)	N	2. LHR 11°C (%)	N	Ø LHR 25°C (%)	Ø LHR 11°C (%)	σ LHR 25°C	σ LHR 11°C	CS
Df(2R)Exel6061	48F5;49A6	2R:7326213..7502158	11	0	8	0	18	0	16	0	2	0	0	0.0	0.0	n.d
Df(2R)Exel6059	47C3;47D6	2R:5939114..6250668	5	0	3	0	8	0	3	0	7	0	0	0.0	0.0	n.d
Df(2R)Exel6051	42D4;42E4	2R:1933545..2053928	17	0	3	0	52	0	6	0	6	0	0	0.0	0.0	n.d
Df(2R)Exel7177	59C3;59D2	2R:18112252..18247566	14	0	14	0	23	82	11	0	8	41	0	40.9	0.0	0.00
Df(2R)Exel6065	53D14;53F9	2R:11920903..12161294	8	33	9	0	8	17	6	0	9	25	0	8.3	0.0	0.00
Df(2L)Exel7027	26F5;27B1	2L:6657034..6779122	70	19	83	0	63	16	80	0	53	18	0	1.5	0.0	0.00
Df(2L)Exel6015	26B9;26C1	2L:6080576..?	26	14	7	0	48	0	23	0	25	7	0	7.1	0.0	0.00
Df(2L)Exel7067	36A12;36B2	2L:16706459..16802992	34	22	33	0	31	10	42	0	29	16	0	6.1	0.0	0.00
Df(2L)Exel6035	35A3;35B2	2L:14283121..14452399	6	0	12	0	3	50	6	0	2	25	0	25.0	0.0	0.00
Df(2L)Exel7075	37D2;37E1	2L:?.19430995	4	67	3	0	0	0	5	0	6	33	0	33.3	0.0	0.00
Df(2R)Exel7174	58E5;58F3	2R:17558161..17687264	53	48	67	0	50	45	40	2	53	46	1	1.4	0.9	0.02
Df(2R)Exel7184	60B12;60C4	2R:19182947..19301415	40	32	28	3	38	21	47	0	45	27	1	5.4	1.3	0.05
Df(2R)Exel9043	37E1;37E1	2R:19416148..19430995	33	49	37	0	16	48	27	6	53	48	3	0.3	2.8	0.06
Df(2R)Exel6079	59A3;59B1	2R:17772917..17841872	75	7	70	0	110	6	33	1	88	7	1	0.5	0.6	0.09
Df(2L)Exel8016	25E6;25F2	2L:5547264..5651500	49	27	26	4	56	35	60	2	54	31	3	4.0	0.9	0.09
Df(2L)Exel7042	30B10;30C1	2L:9515175..9615216	103	13	93	1	99	25	103	3	117	19	2	6.2	0.8	0.09
Df(2R)Exel6285	52A4;52B5	2R:10547243..10739931	108	31	116	4	109	29	102	3	104	30	3	0.8	0.4	0.11
Df(2L)Exel8010	24C8;24D4	2L:3880550..4023894	134	35	191	5	106	31	120	3	119	33	4	1.9	0.7	0.12
Df(2R)Exel9026	52A13;52A13	2R:10632353..10639555	75	41	70	6	49	28	103	3	76	35	4	6.6	1.7	0.13
Df(3R)Exel6192	94B11;94D3	3R:18483028..18715579	107	66	104	6	102	70	115	12	108	68	9	1.6	3.1	0.13
Df(2L)Exel6014	25F5;26A3	2L:5797539..5936895	38	59	39	7	15	61	31	11	65	60	9	1.2	2.1	0.14
Df(2L)Exel8022	30B3;30B5	2L:9380364..?	85	40	78	3	87	45	64	9	110	43	6	2.8	2.8	0.15
Df(2R)Exel7178	59D5;59D10	2R:18335053..18439482	85	31	119	6	94	46	70	5	57	38	6	7.3	0.6	0.15
Df(2L)Exel7024	26A1;26A8	2L:5890506..5972368	108	41	112	8	118	49	106	5	95	45	7	4.0	1.6	0.15
Df(2L)Exel7039	29D5;29F1	2L:8521355..8794191	148	41	101	8	143	33	179	3	168	37	6	3.8	2.7	0.15
Df(2R)Exel6063	52F6;53C3	2R:11251613..11450240	8	14	7	10	10	50	2	0	14	32	5	17.9	5.0	0.16
Df(2L)Exel6022	30B5;30B11	2L:9439878..9552718	31	23	34	7	29	19	31	0	30	21	3	2.2	3.3	0.16
Df(2L)Exel7043	30D1;30F1	2L:9852245..9932618	103	60	101	9	100	62	99	11	112	61	10	0.6	0.9	0.16
Df(2L)Exel7029	27C4;27D4	2L:6914374..7014892	20	27	15	0	12	11	37	6	16	19	3	7.9	3.1	0.17
Df(2R)Exel7121	49B5;49C1	2R:7635400..7744466	64	29	59	8	74	17	59	0	63	23	4	5.9	4.1	0.18
Df(2L)Exel8026	31F5;32B1	2L:10509084..10854392	120	45	110	16	103	47	151	2	116	46	9	0.8	6.9	0.19
Df(2R)Exel6053	43D5;43E9	2R:2594454..2726696	6	25	4	11	9	33	3	0	8	29	6	4.2	5.6	0.19

Df(3R)Exel9014	95B1;95D1	3R:19589500..19759383	107	55	97	5	105	57	107	17	117	56	11	1.2	6.2	0.20
Df(2L)Exel7071	37A1;37A4	2L:18667136..18773903	52	27	56	5	66	30	43	7	44	29	6	1.7	1.1	0.20
Df(3L)Exel6114	67B10;67C5	3L:9466175..9652180	59	47	45	6	98	22	56	8	38	35	7	12.5	1.0	0.20
Df(2L)Exel7034	28E1;28F1	2L:8063541..8197397	106	42	163	12	52	49	122	7	85	46	9	3.4	2.2	0.20
Df(2L)Exel7016	23E5;23F5	2L:3347386..3466062	58	25	68	2	42	43	89	12	34	34	7	8.8	4.7	0.21
Df(2R)Exel7176	59B4;59C2	2R:17932540..18079391	47	48	62	7	45	59	29	16	50	54	11	5.1	4.7	0.21
Df(2L)Exel7049	32B1;32C1	2L:10845856..10967695	105	37	89	9	109	35	113	6	110	36	8	1.3	1.4	0.22
Df(2L)Exel9044	36C10;36C11	2L:17480597..17582843	86	59	73	11	70	47	89	12	112	53	12	5.9	0.1	0.22
Df(2R)Exel8049	45F1;46A1	2R:4612208..?	157	43	160	13	191	38	165	5	112	40	9	2.8	3.6	0.22
Df(2L)Exel8036	36B1;36C9	2L:16769571..17428338	70	17	65	7	106	25	40	3	69	21	5	4.0	1.9	0.23
Df(2L)Exel7002	21B4;21B7	2L:203089..?	45	51	39	11	72	33	21	8	49	42	10	9.0	1.5	0.23
Df(3L)Exel6101	64B5;64B11	3L:4364118..4520041	42	35	29	4	50	13	32	7	57	24	6	11.0	1.5	0.23
Df(3R)Exel6176	89E11;89F1	3R:12879395..12974859	74	24	114	5	59	18	57	5	65	21	5	3.1	0.2	0.24
Df(2R)Exel6283	42E7;43A1	2R:2100923..2207951	40	50	18	12	25	51	82	12	33	51	12	0.6	0.1	0.24
Df(2L)Exel8019	27E2;27E4	2L:7132386..7194548	144	35	161	12	112	44	197	8	104	40	10	4.1	2.0	0.24
Df(3R)Exel6210	98E1;98F5	3R:24490049..24806106	98	41	104	8	112	31	68	10	107	36	9	5.2	1.1	0.25
Df(2R)Exel7185	60C8;60D3	2R:19454631..19559225	101	38	120	12	89	29	95	5	101	33	9	4.0	3.7	0.26
Df(2L)Exel9040	30C1;30C1	2L:9605894..9614757	109	31	104	6	108	28	113	9	110	30	8	1.2	1.3	0.26
Df(2R)Exel7164	57A6;57A9	2R:15645883..15730562	109	17	106	3	112	17	107	6	112	17	4	0.1	1.8	0.26
Df(2L)Exel9064	30B4;30B5	2L:9407898..9423708	111	66	103	13	104	76	103	25	134	71	19	4.9	6.4	0.27
Df(2R)Exel8047	44D4;44D5	2R:3661047..3710236	117	53	145	15	104	48	105	12	112	50	13	2.7	1.9	0.27
Df(2R)Exel6050	42C7;42D4	2R:1801711..1933545	99	40	75	8	109	39	111	13	100	39	11	0.6	2.4	0.27
Df(2L)Exel8033	35B1;35B8	2L:14437873..14975673	63	42	107	5	56	33	40	15	47	37	10	4.8	4.8	0.27
Df(3R)Exel6275	88D1;88D7	3R:10549505..10744000	187	50	127	15	333	51	108	13	181	51	14	0.3	1.3	0.28
Df(2L)Exel6021	29F7;29B1	2L:8981539..9168395	19	27	15	7	27	22	18	6	16	24	7	2.2	0.6	0.28
Df(3R)Exel7283	83B7;83C2	3R:1474080..1572399	74	43	65	4	93	47	47	21	90	45	13	1.9	8.4	0.28
Df(2R)Exel7171	58C1;58D2	2R:17179553..17286801	93	55	86	14	108	46	71	15	107	51	14	4.1	0.5	0.29
Df(3R)Exel6204	96F9;97A6	3R:21821474..22076526	45	72	39	16	50	67	36	24	55	69	20	2.6	3.8	0.29
Df(1)Exel6241	8A2;8B2	X:8448820..8545575	155	54	112	22	159	64	197	12	151	59	17	5.4	5.0	0.29
Df(2R)Exel8056	49D1;49E1	2R:7807732..7958786	60	51	73	11	61	59	44	21	63	55	16	4.2	4.6	0.29
Df(2L)Exel8024	31A2;31B1	2L:10049350..10232253	104	44	94	11	120	32	90	12	113	38	11	5.7	0.3	0.29
Df(2R)Exel7182	60A13;60A16	2R:18993012..19035692	23	25	20	3	30	16	19	9	23	20	6	4.6	2.7	0.29
Df(1)Exel6236	5A12;5C2	X:5420362..5510936	141	37	122	10	117	21	137	7	189	29	9	7.9	1.7	0.30

Df(1)Exel6255	20A1;20B1	X:21191136..21450529	72	85	88	29	75	85	66	21	57	85	25	0.2	4.1	0.30
Df(2R)Exel6078	58B1;58D1	2R:17083091..17241194	108	29	102	5	115	32	103	13	113	31	9	1.3	4.0	0.30
Df(2L)Exel8012	25B1;25B8	2L:4839530..4970209	111	24	105	9	103	20	127	5	107	22	7	1.7	2.0	0.30
Df(2L)Exel6045	38A4;38A7	2L:19742803..19913216	25	45	20	7	30	31	32	17	18	38	12	6.9	5.0	0.31
Df(1)Exel6240	6B2;6C4	X:6284339..6410234	86	80	71	29	106	75	91	19	75	78	24	2.8	5.3	0.31
Df(2L)Exel7014	23C4;23D1	2L:2972223..?	96	39	121	12	84	49	72	15	105	44	14	4.9	1.7	0.31
Df(2L)Exel7063	35D2;35D4	2L:15404136..15722529	51	15	27	7	42	24	51	5	84	19	6	4.4	1.2	0.31
Df(3R)Exel6211	98F5;98F6	3R:24806106..24879352	71	52	25	18	129	53	32	15	98	53	17	0.6	1.3	0.32
Df(2L)Exel6013	25F2;25F5	2L:5650844..5797539	95	30	125	12	58	33	82	8	113	32	10	1.3	2.1	0.32
Df(2L)Exel7023	25E5;25F1	2L:5516600..5586449	111	50	121	16	105	52	109	17	107	51	17	1.4	0.3	0.32
Df(2L)Exel8034	35C5;35D2	2L:15242799..15418050	80	46	61	14	92	38	60	13	106	42	14	3.8	0.5	0.32
Df(2R)Exel7124	49F10;50A1	2R:?.?.?	120	44	134	14	112	43	111	14	121	44	14	0.4	0.1	0.32
Df(3L)Exel6097	63E3;63F2	3L:?.?.3805762	35	73	11	24	74	59	32	19	21	66	22	7.0	2.5	0.33
Df(3R)Exel6157	86B1;86B3	3R:6175954..6209627	112	57	129	0	0	42	165	32	155	50	16	7.1	16.1	0.33
Df(3L)Exel6115	68E1;68F2	3L:11779552..12039402	118	53	128	16	105	63	138	22	102	58	19	5.0	3.0	0.33
Df(2L)Exel6003	21D3;21E3	2L:827838..1075745	26	58	26	13	16	53	19	24	42	55	18	2.5	5.7	0.33
Df(1)Exel6226	1E3;1F2	X:891664..1079814	121	69	102	27	200	61	79	17	101	65	22	3.9	4.8	0.33
Df(2R)Exel6058	44C4;44D1	2R:3388275..3505491	18	33	6	12	25	22	9	7	30	28	9	5.6	2.7	0.34
Df(2R)Exel7150	54E1;54E9	2R:12779988..12845757	51	66	70	22	45	56	41	19	47	61	21	4.8	1.5	0.34
Df(3R)Exel6162	87A1;87B5	3R:7713484..8106824	98	47	109	15	100	42	59	15	124	45	15	2.2	0.2	0.34
Df(3R)Exel6159	86C3;86C7	3R:6464635..6715093	99	56	100	14	85	45	38	21	174	50	17	5.6	3.3	0.35
Df(2L)Exel7072	37A2;37B6	2L:18731653..18922025	70	37	46	12	66	20	86	8	80	28	10	8.6	2.3	0.35
Df(2L)Exel7007	22B1;22B5	2L:1718642..1911641	106	34	101	17	120	38	105	8	98	36	12	2.2	4.3	0.35
Df(2R)Exel6082	60C4;60C7	2R:19301465..19413345	117	62	106	19	121	51	109	21	130	57	20	5.4	0.9	0.35
Df(3L)Exel6106	64D6;64E2	3L:5567583..5650310	83	59	64	22	99	52	86	17	84	56	20	3.5	2.5	0.35
Df(2R)Exel7131	50E4;50F6	2R:9294393..9423952	124	64	135	27	138	71	110	21	112	67	24	3.6	3.1	0.35
Df(3L)Exel6116	68F2;69A2	3L:12039402..12161528	50	49	49	17	64	39	36	14	52	44	16	5.0	1.5	0.35
Df(2L)Exel6002	21D2;21D3	2L:716750..827838	42	35	46	18	34	30	47	5	39	32	11	2.5	6.3	0.35
Df(3R)Exel6165	87B5;87B10	3R:8106824..8268866	36	23	22	13	45	36	25	8	53	29	10	6.6	2.9	0.36
Df(3R)Exel6184	92A5;92A11	3R:15289202..15467055	130	62	103	41	222	69	104	7	91	66	24	3.5	17.0	0.36
Df(3R)Exel6183	91E4;91F8	3R:14853135..14989788	162	49	102	27	82	50	130	9	335	50	18	0.5	8.9	0.36
Df(3R)Exel6161	86E14;86E18	3R:7394952..7495415	114	64	111	19	110	74	135	31	99	69	25	5.1	6.1	0.37
Df(3R)Exel6181	91C5;91D5	3R:14566207..14749762	97	31	62	9	97	25	129	11	98	28	10	2.9	1.0	0.37

Df(3L)Exel6102	64B15;64C5	3L:4670346..4954252	124	69	127	21	129	58	126	26	112	64	24	5.5	2.5	0.37
Df(2L)Exel6046	38C2;38C7	2L:20174828..20418799	113	33	95	14	116	31	131	10	111	32	12	0.7	1.9	0.37
Df(2R)Exel6070	57A6;57B3	2R:15646492..15879577	111	17	121	3	104	24	116	13	104	21	8	3.4	4.8	0.37
Df(2R)Exel6055	43F1;44A4	2R:2947245..3121912	125	25	122	12	123	28	144	7	109	26	10	1.6	2.4	0.37
Df(1)Exel6253	18D13;18F2	X:19393976..19519673	123	66	168	27	111	65	114	22	100	65	25	0.6	2.5	0.37
Df(2L)Exel9032	31A3;31B1	2L:10126595..10191401	117	52	111	19	113	52	141	20	102	52	20	0.2	0.1	0.38
Df(2L)Exel8005	22B2;22B8	2L:1739625..2011801	128	25	102	11	201	37	102	12	106	31	12	6.4	0.7	0.38
Df(2L)Exel6032	33C2;33D4	2L:12055718..12259715	63	31	59	10	63	11	63	6	65	21	8	9.7	1.7	0.38
Df(2R)Exel7153	55B9;55C1	2R:13215178..13294288	124	68	183	28	106	70	99	24	106	69	26	1.0	2.4	0.38
Df(3R)Exel8178	95F8;96A6	3R:20087584..?	113	41	105	21	102	60	100	18	146	50	19	9.5	1.4	0.38
Df(2L)Exel7021	25B3;25B9	2L:4908197..4971870	102	45	86	26	97	36	153	6	71	41	16	4.7	10.1	0.39
Df(2L)Exel6033	33E4;33F2	2L:12412330..12644663	48	35	34	15	67	18	38	6	51	27	10	8.4	4.5	0.39
Df(1)Exel6227	1F2;2B1	X:1079814..1236256	182	66	204	37	208	64	203	14	111	65	25	1.1	11.8	0.39
Df(3R)Exel6149	85A2;85A5	3R:4303326..4495369	166	17	201	12	206	30	81	6	175	23	9	6.4	2.9	0.40
Df(2L)Exel6048	39B4;39D1	2L:21207015..21279263	141	35	130	12	111	25	191	12	130	30	12	5.1	0.3	0.40
Df(2R)Exel7094	44A4;44B4	2R:3121912..3192490	46	14	58	15	33	30	44	2	48	22	9	7.9	6.5	0.40
Df(3R)Exel6198	95E5;95F8	3R:19957748..20087584	89	55	49	31	84	57	108	14	113	56	23	1.2	8.4	0.40
Df(2L)Exel6043	37C5;37D7	2L:19139810..19401643	49	12	43	10	79	24	25	4	48	18	7	6.2	3.0	0.40
Df(2R)Exel6076	57D13;57F3	2R:16423078..16650632	51	11	53	0	57	0	49	5	44	6	2	5.7	2.3	0.40
Df(2L)Exel8013	25B8;25B10	2L:4968176..4993514	107	41	99	17	168	31	26	13	135	36	15	5.3	2.0	0.41
Df(2L)Exel7078	38C7;38D4	2L:20427920..20650366	89	46	106	18	62	49	98	21	91	48	19	1.4	1.6	0.41
Df(3R)Exel6173	88D7;88E1	3R:10744000..10920182	85	86	92	49	81	77	66	17	101	82	33	4.3	16.3	0.41
Df(2L)Exel9031	28B4;28C1	2L:7629980..7652622	83	27	103	13	120	13	60	4	50	20	8	6.9	4.3	0.41
Df(3L)Exel6109	65C3;65D3	3L:6702642..6903068	11	58	12	25	8	50	4	19	21	54	22	4.0	3.0	0.41
Df(2L)Exel6036	35B1;35B2	2L:14391863..14472809	37	36	45	17	35	39	36	13	30	37	15	1.7	1.9	0.41
Df(1)Exel6239	5F2;6B1	X:6084709..?	179	57	213	28	111	49	215	16	177	53	22	4.0	6.1	0.41
Df(3R)Exel6265	85F10;85F16	3R:5915198..6015388	118	47	124	13	117	47	114	26	116	47	19	0.3	6.5	0.41
Df(3R)Exel6163	87A1;87A4	3R:7712923..7824992	137	61	109	22	102	61	185	29	150	61	25	0.5	3.5	0.41
Df(1)Exel7468	18B7;18C8	X:18995472..19240597	15	36	14	26	19	27	15	0	13	31	13	4.5	13.2	0.42
Df(2L)Exel8004	21F4;22A3	2L:1291874..1556764	83	25	81	15	109	35	92	10	48	30	13	5.0	2.1	0.42
Df(3L)Exel6130	73B5;73D1	3L:16610171..16755528	180	39	216	12	213	39	150	21	139	39	17	0.2	4.3	0.42
Df(2R)Exel9060	52E9;52F1	2R:11206583..11222576	50	34	35	19	47	39	31	12	85	36	15	2.2	3.7	0.42
Df(3R)Exel6170	87F10;87F14	3R:9509984..9638571	96	67	76	22	149	69	62	36	97	68	29	1.1	7.0	0.43

Df(3R)Exel6215	99F6;99F8	3R:?.26378570	100	56	89	28	140	59	22	21	149	58	25	1.5	3.2	0.43
Df(3L)Exel6112	66B5;66C8	3L:8055183..8317534	14	33	3	19	21	44	18	14	14	39	17	5.5	2.5	0.43
Df(3R)Exel6164	87B5;87B10	3R:8106824..8268866	73	31	52	12	126	32	37	15	78	32	14	0.8	1.7	0.43
Df(1)Exel6234	4F10;5A2	X:5169157..5257225	75	88	78	42	73	89	64	35	84	89	38	0.3	4.0	0.43
Df(3R)Exel6197	95D8;95E5	3R:19847806..19957748	25	44	9	17	18	58	31	28	43	51	22	6.8	5.6	0.43
Df(3R)Exel6264	85D24;85E5	3R:5376443..5530688	203	62	172	29	286	60	113	24	242	61	27	0.7	2.7	0.44
Df(2L)Exel7080	38F3;39A2	2L:20831286..21072486	111	34	106	17	124	17	109	6	104	26	11	8.3	5.6	0.44
Df(3R)Exel6200	96A20;96B4	3R:20585721..20711086	90	41	76	17	101	41	69	19	115	41	18	0.1	1.1	0.44
Df(2R)Exel7128	50C5;50C9	2R:8866670..8962541	135	32	117	17	140	23	172	7	109	27	12	4.2	4.9	0.45
Df(3L)Exel8098	64A12;64B6	3L:4240055..4386729	107	29	134	12	69	40	101	19	125	34	15	5.2	3.8	0.45
Df(2R)Exel7157	55E2;55E11	2R:13685242..13794491	80	20	60	3	76	10	82	11	102	15	7	5.1	4.1	0.45
Df(2R)Exel7139	52D11;52E4	2R:11062435..11174989	150	63	134	32	181	58	160	23	124	60	27	2.6	4.7	0.45
Df(3L)Exel6092	62F5;63A3	3L:2801874..3027791	83	80	75	32	93	76	76	39	89	78	36	2.0	3.5	0.46
Df(3R)Exel6169	87F2;87F10	3R:9369382..9509698	110	49	86	22	115	59	150	28	87	54	25	4.9	2.9	0.46
Df(3R)Exel6273	94B2;94B11	3R:18347158..18483028	112	57	108	27	154	54	80	25	106	56	26	1.8	1.0	0.46
Df(3R)Exel6263	84E6;84E13	3R:?.3945752	199	48	170	26	247	47	117	18	261	48	22	0.6	3.6	0.46
Df(3R)Exel6175	89A1;89A8	3R:11491766..11746833	81	78	86	41	115	69	61	27	63	73	34	4.5	6.9	0.46
Df(3L)Exel6132	74B2;74D2	3L:17370461..17481906	135	24	164	13	164	31	154	12	57	28	13	3.4	0.6	0.46
Df(2R)Exel7123	49D5;49E6	2R:7926924..8045896	121	30	146	17	121	25	107	8	109	28	13	2.5	4.5	0.46
Df(2R)Exel7169	58A3;58B1	2R:16905802..17083181	122	61	144	26	108	69	102	34	132	65	30	3.8	4.1	0.46
Df(3R)Exel8159	88A4;88B1	3R:9809255..10085668	179	62	146	23	239	63	129	34	202	62	29	0.6	5.4	0.46
Df(3R)Exel8155	87A4;87A9	3R:7819284..7939466	79	71	49	28	82	78	82	41	102	75	35	3.3	6.6	0.46
Df(2R)Exel8059	51A4;51B1	2R:?.9639309	65	24	38	20	49	39	44	8	130	31	14	7.5	6.0	0.46
Df(2L)Exel6047	39A2;39B4	2L:21072486..21213863	69	19	74	6	106	11	19	8	75	15	7	4.2	1.2	0.46
Df(3R)Exel7378	99F8;100A5	3R:26378312..26610043	113	44	102	31	119	55	113	15	118	49	23	5.4	7.9	0.47
Df(3R)Exel9055	89C7;89C7	3R:12275012..12279438	94	56	78	33	108	65	75	24	114	61	29	4.5	4.8	0.47
Df(3R)Exel6166	87C5;87C7	3R:8504772..?	94	28	25	14	144	24	58	11	150	26	12	1.9	1.6	0.47
Df(3R)Exel6218	100B2;100B4	3R:26984227..27126307	131	48	85	23	222	49	79	23	139	49	23	0.6	0.0	0.47
Df(3L)Exel6090	62E2;62E4	3L:2398010..2470792	34	71	34	19	16	64	47	45	40	68	32	3.5	13.0	0.47
Df(3R)Exel6214	99D5;99E2	3R:25914470..26018056	24	47	32	31	29	57	23	18	11	52	25	4.8	6.4	0.48
Df(3R)Exel6276	86E14;86E18	3R:7394904..7495415	83	73	75	33	101	74	57	37	99	74	35	0.2	2.4	0.48
Df(3L)Exel6096	63E3;63E4	3L:3523212..3574487	113	75	147	39	98	78	99	34	106	77	37	1.5	2.5	0.48
Df(3R)Exel6267	88B1;88C2	3R:10103677..10307581	108	76	41	31	127	68	138	37	124	72	34	3.7	2.8	0.48

Df(2L)Exel7031	27F3;28A1	2L:7357207..7487723	39	36	25	16	51	11	36	7	44	24	11	12.4	4.4	0.48
Df(2R)Exel7173	58D4;58E5	2R:17424002..17557688	102	59	106	20	118	61	72	37	110	60	29	0.8	8.5	0.48
Df(2R)Exel6067	55F8;56A1	2R:13921755..14011006	104	44	144	23	117	45	67	19	88	44	21	0.5	1.9	0.48
Df(2R)Exel7158	55E9;55F6	2R:13769246..13893448	92	73	67	34	102	72	87	36	111	73	35	0.4	0.9	0.48
Df(3R)Exel6213	99C5;99D1	3R:25692182..25827836	106	66	77	34	100	65	127	30	118	66	32	0.4	2.2	0.48
Df(3R)Exel9013	95B1;95B5	3R:19539216..19601221	176	54	173	37	115	63	252	19	165	59	28	4.2	9.0	0.49
Df(3R)Exel7326	88F7;89A5	3R:11363141..?	105	78	104	42	95	77	112	33	109	77	38	0.5	4.5	0.49
Df(1)Exel6242	10D1;10D7	X:11356858..11450275	113	61	142	25	114	63	71	35	125	62	30	1.1	4.9	0.49
Df(3R)Exel6269	89B17;89D2	3R:12131453..12328472	111	49	139	28	79	45	93	18	133	47	23	1.9	4.9	0.49
Df(3R)Exel8157	87D8;87D10	3R:8838454..8877526	138	47	133	29	136	57	104	22	180	52	26	4.7	3.9	0.49
Df(3R)Exel6208	97E5;97E11	3R:22972573..23068609	66	72	18	40	82	73	44	31	119	72	36	0.3	4.6	0.49
Df(3R)Exel6155	85F1;85F10	3R:5754529..5915198	108	71	77	30	87	65	100	37	169	68	34	3.2	3.7	0.49
Df(2R)Exel7135	51E2;51E11	2R:10193681..10326667	141	40	134	23	161	46	108	20	162	43	21	3.0	1.6	0.49
Df(2R)Exel6057	44B9;44C4	2R:3235398..3388275	67	13	61	11	88	27	45	8	72	20	10	6.8	1.5	0.50
Df(2R)Exel6062	49E6;49F1	2R:8045896..8099900	92	37	101	17	86	30	79	16	100	34	17	3.1	0.7	0.50
Df(3R)Exel6270	89D2;89D8	3R:12328472..12528639	115	75	116	44	105	92	60	39	180	83	42	8.3	2.2	0.50
Df(3L)Exel6099	63F7;64A5	3L:3906112..4054622	122	66	120	30	99	64	117	35	153	65	33	1.0	2.5	0.50
Df(2R)Exel6284	51B1;51C2	2R:9638476..9829295	49	25	36	26	86	45	20	9	53	35	18	10.0	8.1	0.50
Df(2L)Exel6277	23A2;23B1	2L:2670261..2800669	67	43	35	24	93	54	68	25	72	49	24	5.8	0.7	0.50
Df(3R)Exel6212	99A1;99A5	3R:25030263..25103319	46	50	16	20	102	44	25	28	40	47	24	3.0	3.9	0.50
Df(3L)Exel6104	64C10;64D1	3L:5144105..5325370	136	89	150	36	138	86	116	52	139	88	44	1.5	8.0	0.50
Df(3R)Exel8153	86E8;86E14	3R:7261649..7394911	130	61	134	33	127	60	91	28	167	61	31	0.4	2.5	0.50
Df(3R)Exel6272	93A7;93B13	3R:16783442..16938073	83	40	25	22	94	63	117	30	94	52	26	11.6	3.7	0.50
Df(3R)Exel6180	91B5;91C5	3R:14410136..14566207	182	38	99	18	95	41	187	22	345	40	20	1.4	2.2	0.51
Df(2L)Exel7006	21F2;21F4	2L:1159863..1312727	106	69	102	34	142	81	102	42	78	75	38	6.4	4.3	0.51
Df(3R)Exel6172	88D5;88D7	3R:10643968..10744000	76	69	87	39	82	59	66	26	69	64	33	4.9	6.5	0.51
Df(3R)Exel6196	95C12;95D8	3R:19738513..19847806	69	60	67	32	96	59	54	28	60	59	30	0.2	2.0	0.51
Df(3L)Exel6087	62A2;62A7	3L:1459303..1567510	73	78	68	26	78	78	58	54	89	78	40	0.0	14.0	0.51
Df(3R)Exel6288	87F14;88A4	3R:9638571..9809255	88	59	93	28	97	60	45	34	116	60	31	0.4	2.9	0.52
Df(2R)Exel7098	44D5;44E3	2R:3710229..3794377	125	51	144	29	139	51	104	23	113	51	26	0.1	3.2	0.52
Df(3R)Exel6209	98D6;98E1	3R:24416263..24490049	148	75	128	40	100	81	131	41	234	78	41	3.0	0.5	0.52
Df(3L)Exel6123	70D7;70E4	3L:14358721..14563315	180	58	247	23	162	65	163	42	149	62	32	3.4	9.4	0.52
Df(2L)Exel8021	29C1;29D1	2L:8395127..?	105	59	100	33	105	62	113	30	100	60	32	1.5	1.7	0.52

Df(3L)Exel6095	63E1;63E3	3L:3441238..?	63	77	66	35	81	77	39	46	65	77	41	0.0	5.5	0.53
Df(3L)Exel6128	72D8;72D10	3L:16078533..16166207	152	33	203	24	195	61	155	25	55	47	25	14.4	0.7	0.53
Df(2L)Exel6005	22A3;22B1	2L:1556764..1738914	108	21	119	9	76	27	114	17	121	24	13	3.1	3.7	0.53
Df(3R)Exel6153	85D21;85E1	3R:5338758..5457662	143	27	186	21	196	37	130	13	61	32	17	4.8	4.2	0.54
Df(1)Exel6225	1D4;1E3	X:743500..892365	145	57	118	36	225	66	128	31	107	62	33	4.8	2.4	0.54
Df(3L)Exel6103	64C5;64C10	3L:4954344..5144105	54	57	56	28	89	68	19	40	53	63	34	5.5	6.0	0.54
Df(3R)Exel6217	100A6;100A7	3R:26635749..26703333	119	61	70	28	147	53	154	35	106	57	31	4.1	3.5	0.55
Df(1)Exel6254	19C3;19D1	X:20003330..20141181	113	67	130	47	112	58	108	21	103	63	34	4.3	13.0	0.55
Df(3R)Exel6185	92E2;92F1	3R:16135262..16376403	109	66	68	37	115	79	156	42	97	73	40	6.3	2.4	0.55
Df(2R)Exel7142	53A4;53C4	2R:11352979..11488939	61	24	54	26	70	38	37	8	83	31	17	6.9	8.6	0.55
Df(2L)Exel6029	32E4;32F2	2L:11347474..11434633	19	17	29	13	15	25	20	10	10	21	12	3.9	1.7	0.55
Df(3L)Exel9008	76B3;76B11	3L:?.19585752	127	45	161	26	122	51	111	27	113	48	27	3.3	0.6	0.56
Df(2L)Exel6024	30C1;30C9	2L:9605840..9774447	29	9	22	11	36	26	23	9	35	18	10	8.5	1.3	0.56
Df(3R)Exel6146	84C8;84D9	3R:2988428..3317338	151	44	229	27	181	63	141	34	53	54	30	9.5	3.7	0.56
Df(3R)Exel6188	93F8;93F14	3R:17691952..17859431	96	35	74.0	26	123	36	89	14	98	36	20	0.4	5.9	0.57
Df(3L)Exel6107	64E5;64F5	3L:5712322..5861852	121	53	105	30	134	51	109	29	137	52	30	1.0	0.5	0.57
Df(2L)Exel7069	36C10;36D1	2L:17460094..17751608	140	27	146	20	125	34	181	15	109	31	17	3.2	2.7	0.57
Df(3L)Exel6129	72F1;73A2	3L:16360572..16432436	166	50	227	26	233	53	151	33	52	51	29	1.6	3.5	0.57
Df(2R)Exel7145	53C13;53D14	2R:11795219..11910346	136	34	151	24	105	39	176	18	113	36	21	2.7	3.1	0.57
Df(1)Exel6223	1C4;1D2	X:527419..666687	154	69	172	37	199	59	105	36	139	64	36	4.8	0.4	0.57
Df(2L)Exel6025	30C9;30E1	2L:9774447..9889765	31	31	51	25	20	33	27	12	25	32	19	1.0	6.5	0.57
Df(2R)Exel6069	56B5;56C11	2R:14205669..14389343	30	39	33	12	33	25	24	25	28	32	19	7.2	6.4	0.58
Df(2L)Exel7015	23D1;23E3	2L:3039204..3302819	119	61	109	33	125	64	126	40	117	63	36	1.4	3.7	0.58
Df(3R)Exel7308	86E1;86E8	3R:7069696..7264890	120	42	142	23	101	54	109	33	126	48	28	5.9	5.3	0.58
Df(3L)Exel6110	65E4;65E8	3L:7054335..7115713	67	76	45	47	114	66	47	36	61	71	42	5.0	5.5	0.58
Df(1)Exel6245	11E11;11F4	X:13050532..13142304	120	82	119	49	127	74	109	42	123	78	46	3.6	3.3	0.58
Df(3R)Exel6179	91A5;91B5	3R:14223265..14410136	105	67	115	47	77	58	80	26	146	62	36	4.7	10.4	0.58
Df(2R)Exel7162	56F11;56F16	2R:?.15377347	116	49	114	23	119	47	120	33	111	48	28	1.2	5.3	0.58
Df(3L)Exel9009	76B5;76B11	3L:19459595..19585752	110	66	102	27	103	57	116	45	119	61	36	4.4	8.7	0.59
Df(3L)Exel6119	70B2;70C2	3L:13434803..13624373	176	38	168	26	165	52	164	27	208	45	26	7.2	0.4	0.59
Df(2L)Exel7040	29F1;29F6	2L:8790226..?	151	50	105	36	238	47	135	21	126	48	28	1.1	7.7	0.59
Df(3R)Exel7310	86F6;87A1	3R:7584321..7712831	69	24	41	11	61	29	85	20	89	27	16	2.5	4.4	0.59
Df(3L)Exel9011	76B8;76B11	3L:19532970..19585752	80	67	81	31	52	64	106	46	82	65	39	1.3	7.8	0.59

Df(3L)Exel6108	65A9;65A11	3L:6177612..?	94	67	121	42	105	67	103	37	46	67	40	0.0	2.5	0.59
Df(3R)Exel6280	94E5;94E11	3R:19007696..19112013	119	64	134	39	98	68	111	40	134	66	39	2.1	0.4	0.59
Df(2L)Exel6012	25D5;25E6	2L:5298217..5547264	27	38	8	22	27	35	20	21	53	36	21	1.3	0.7	0.59
Df(3L)Exel6093	63C1;63D3	3L:3231085..3398761	118	78	102	47	148	72	108	42	112	75	45	3.0	2.5	0.59
Df(3R)Exel6143	82E4;82E8	3R:776723..912501	149	48	210	27	159	44	156	27	70	46	27	2.0	0.0	0.59
Df(3R)Exel7327	89A8;89B3	3R:11727182..11867302	54	42	52	27	56	38	37	21	72	40	24	2.2	3.0	0.59
Df(2R)Exel7092	43E5;43E12	2R:?.?.2769608	85	8	73	4	102	16	91	11	74	12	7	4.1	3.4	0.60
Df(2L)Exel6044	37F2;38A4	2L:19554192..19742803	40	9	34	0	46	14	49	14	29	12	7	2.7	6.9	0.60
Df(3L)Exel6136	77B2;77C6	3L:20228768..20411746	142	26	137	21	132	38	125	17	175	32	19	6.0	2.3	0.60
Df(3R)Exel7284	83C4;83D2	3R:1641741..1833508	102	80	95	44	91	62	106	41	114	71	43	8.9	1.4	0.60
Df(3R)Exel7317	87B10;87C3	3R:8266959..8456337	126	60	156	48	126	67	120	28	101	63	38	3.2	10.3	0.60
Df(1)Exel7463	17C2;17D3	X:18265524..18472392	16	56	16	45	29	33	6	9	11	45	27	11.5	17.9	0.60
Df(3R)Exel6219	100B4;100B8	3R:27126307..27277252	132	66	129	42	193	71	115	40	92	69	41	2.7	1.1	0.60
Df(2R)Exel7137	52B1;52C8	2R:?.?.10922973	156	49	167	29	196	61	111	38	149	55	33	6.1	4.8	0.61
Df(3R)Exel6186	93E6;93F1	3R:17435102..17536460	102	36	78	13	100	20	127	21	101	28	17	8.1	3.9	0.61
Df(3R)Exel9020	100A4;100A5	3R:26571483..26610037	178	50	156	29	203	60	105	39	248	55	34	5.0	5.1	0.61
Df(3R)Exel7313	87A9;87B5	3R:7933857..8106601	149	57	164	46	105	72	114	34	213	64	40	7.6	6.0	0.62
Df(3R)Exel6182	91D5;91E4	3R:14749762..14853135	42	37	41	13	55	21	47	23	26	29	18	7.7	5.2	0.62
Df(1)Exel6231	3A2;3A3	X:2144526..2226073	140	67	135	51	158	65	161	31	107	66	41	1.4	10.2	0.62
Df(3L)Exel6091	62E8;62F5	3L:2636892..2801874	94	65	119	31	103	57	54	45	101	61	38	4.0	7.0	0.62
Df(3R)Exel6171	87F14;88A4	3R:9638639..9809255	16	33	15	14	14	33	12	27	22	33	21	0.0	6.5	0.62
Df(3R)Exel7309	86E17;86F1	3R:7472871..7541884	184	77	142	45	399	75	113	50	80	76	47	0.8	2.6	0.62
Df(3L)Exel9046	76A5;76A6	3L:19240259..19279447	128	69	83	48	100	90	108	51	219	79	50	10.6	1.6	0.63
Df(3R)Exel6206	97E1;97E5	3R:22885211..22972573	35	48	33	26	38	44	32	31	35	46	29	2.4	2.6	0.63
Df(2R)Exel6066	53F9;54B6	2R:12161294..12458367	94	8	98	9	119	15	85	5	73	12	7	3.6	1.9	0.63
Df(3R)Exel7305	86C6;86C7	3R:6606294..6698001	97	85	87	52	101	82	73	53	125	84	53	1.4	0.2	0.63
Df(2L)Exel6008	22F3;23A3	2L:2487220..2747946	53	39	28	32	66	32	74	13	45	36	23	3.4	9.2	0.63
Df(3L)Exel9061	76C3;76C3	3L:19669767..19679586	127	82	170	42	125	81	108	61	106	82	51	0.1	9.9	0.63
Df(2L)Exel6011	25C8;25D5	2L:5139829..5298217	121	32	93	22	105	36	121	21	163	34	21	1.6	0.5	0.63
Df(3R)Exel6274	94E4;94E11	3R:18991826..19112013	91	34	79	21	95	54	84	35	107	44	28	9.7	6.8	0.63
Df(2R)Exel6064	53C10;53D2	2R:11675358..11892799	27	26	35	9	46	14	7	17	18	20	13	5.7	4.0	0.63
Df(3R)Exel6194	94F1;95A4	3R:19201557..19457785	113	65	120	43	111	55	105	33	117	60	38	4.9	5.0	0.64
Df(3L)Exel6086	61C9;61E1	3L:730438..940280	137	69	219	51	101	83	114	46	112	76	49	7.0	2.5	0.64

Df(3R)Exel6152	85C11;85D2	3R:4983814..5073219	170	42	204	21	182	31	143	25	149	36	23	5.4	1.7	0.64
Df(3L)Exel6088	62B4;62B7	3L:1774992..1857014	70	62	105	39	65	71	21	46	88	67	43	4.5	3.5	0.64
Df(2R)Exel6077	57F10;58A3	2R:16757519..16915579	63	20	46	5	116	17	35	19	54	18	12	1.2	6.7	0.65
Df(3L)Exel6120	70D1;70D3	3L:14008541..14139743	133	58	115	40	137	55	152	33	126	57	37	1.5	3.4	0.65
Df(3L)Exel6094	63D2;63E1	3L:3339771..3441238	90	83	113	48	87	93	71	66	88	88	57	5.0	9.0	0.65
Df(3R)Exel6199	95F8;96A2	3R:20087584..20266334	59	46	68	36	83	51	43	27	41	48	31	2.8	4.7	0.65
Df(3R)Exel6150	85A5;85B6	3R:4495369..4753498	143	35	194	30	152	37	166	17	58	36	23	0.8	6.2	0.65
Df(3L)Exel9007	76B3;76B11	3L:19373570..19585752	43	50	24	28	46	58	60	43	40	54	35	4.2	7.1	0.65
Df(2R)Exel7170	58B1;58C1	2R:?.17179480	114	50	121	29	112	50	101	37	123	50	33	0.0	4.4	0.65
Df(3R)Exel7357	96A2;96A13	3L:20266334..20467403	119	49	129	24	112	42	113	36	120	46	30	3.2	5.9	0.66
Df(2L)Exel6017	27E4;27F5	2L:7194548..7410235	86	36	105	29	106	32	62	16	69	34	23	2.0	6.7	0.66
Df(3L)Exel8101	65A3;65A9	3L:6002147..6177581	51	54	46	37	60	63	30	41	68	59	39	4.5	2.3	0.66
Df(3L)Exel6098	63F2;63F7	3L:3805762..3906112	40	72	29	46	46	70	33	48	52	71	47	1.0	1.0	0.66
Df(3R)Exel9036	85D11;85D11	3R:5153013..5165744	105	50	143	36	73	58	116	36	89	54	36	3.7	0.2	0.66
Df(3L)Exel6133	75B4;75B11	3L:17965582..18088200	179	56	174	25	229	61	155	52	159	58	39	2.4	13.7	0.66
Df(3R)Exel8152	86D7;86D9	3R:6979890..7026020	142	66	160	48	152	63	102	38	152	64	43	1.8	5.3	0.66
Df(3L)Exel9003	73D1;73D4	3L:16755521..16820440	126	61	170	35	113	55	116	43	105	58	39	3.0	4.2	0.66
Df(3L)Exel9034	66A22;66B3	3L:7940663..8014087	113	77	143	57	117	92	87	55	105	84	56	7.5	1.0	0.67
Df(3R)Exel7330	89B19;89D2	3R:12177467..12298862	117	52	85	36	100	46	170	30	111	49	33	2.6	3.1	0.67
Df(2L)Exel7011	22E1;22F3	2L:2355484..2485014	101	28	120	27	107	46	81	22	96	37	24	9.1	2.6	0.67
Df(3L)Exel9045	76D1;76D2	3L:19764603..19782460	129	71	142	26	151	60	114	61	108	65	44	5.7	17.3	0.67
Df(2R)Exel7095	44B3;44C2	2R:3185406..3293210	154	41	135	23	123	42	146	33	212	42	28	0.1	5.1	0.67
Df(3R)Exel6142	82D2;82D6	3R:540172..632614	142	70	186	38	191	71	134	57	58	70	47	0.5	9.6	0.67
Df(3R)Exel7316	87B9;87B11	3R:8232007..8274849	178	56	215	39	264	64	116	42	115	60	40	3.8	1.4	0.67
Df(3R)Exel6191	94A9;94B2	3R:18184659..18347158	36	32	19	21	29	9	22	7	75	20	14	11.2	7.0	0.67
Df(3R)Exel6216	99F6;99F7	3R:26281120..26347656	30	36	22	33	52	64	22	35	23	50	34	13.6	1.0	0.67
Df(2L)Exel8028	34A1;34A2	2L:12821673..12885279	109	75	103	53	110	71	130	46	94	73	49	2.0	3.5	0.68
Df(3L)Exel6117	69D1;69E2	3L:12585381..12747632	205	61	235	41	252	55	154	37	180	58	39	3.2	1.8	0.68
Df(3R)Exel6259	98C4;98D6	3R:24141831..24416263	109	79	113	54	139	81	88	54	94	80	54	1.0	0.1	0.68
Df(2R)Exel7096	44C6;44D3	2R:3494419..3633520	72	43	74	27	64	36	74	28	76	40	27	3.4	0.5	0.68
Df(3R)Exel6151	85C3;85C11	3R:4878567..4983814	116	34	136	19	205	33	78	27	44	34	23	0.2	4.4	0.68
Df(3R)Exel6148	84F12;85A2	3R:4159516..4303326	159	45	229	34	193	46	162	28	50	45	31	0.6	2.8	0.68
Df(3R)Exel7329	89B14;89B19	3R:12067151..12184534	98	35	102	30	88	43	88	24	112	39	27	3.9	2.7	0.68

Df(3R)Exel6202	96D1;96E2	3R:21109291..21330985	47	73	55	41	49	76	34	61	49	75	51	1.9	10.2	0.68
Df(3R)Exel7320	87E8;87F2	3R:9207130..9369382	166	71	163	43	259	56	133	44	109	63	43	7.1	0.6	0.68
Df(3L)Exel6279	66A17;66B5	3L:7828548..8055183	173	63	141	41	228	71	106	50	218	67	46	3.8	4.6	0.68
Df(1)Exel9051	17D1;17D3	X:18423890..18472392	130	78	193	76	119	83	120	36	89	81	56	2.8	19.8	0.69
Df(3R)Exel8154	86E17;86F6	3R:7472871..7585229	112	56	90	35	116	57	129	42	113	56	39	0.5	3.6	0.69
Df(2R)Exel7138	52D1;52D12	2R:10982148..11071458	187	56	149	44	274	55	114	34	209	56	39	0.6	4.9	0.70
Df(3R)Exel6174	88F1;88F7	3R:11154373..11363206	59	43	65	43	54	48	40	21	78	45	32	2.2	11.0	0.70
Df(3L)Exel9002	73D1;73D1	3L:16755521..16793752	106	78	81	54	132	74	100	52	111	76	53	1.9	0.8	0.70
Df(3R)Exel6140	82A3;82A5	3R:107400..186685	117	36	81	27	84	35	126	22	175	35	25	0.4	2.5	0.70
Df(3R)Exel8158	87E3;87E7	3R:9067502..9190081	171	59	145	34	210	51	108	43	220	55	39	3.8	4.2	0.70
Df(3R)Exel8165	89E8;89E11	3R:12838705..12879728	107	49	105	34	178	35	51	25	93	42	30	6.6	4.8	0.70
Df(2R)Exel6068	56A1;56B5	2R:14011006..14205669	38	3	39	2	51	4	24	3	36	3	2	0.8	0.4	0.70
Df(3L)Exel6122	70D4;70D7	3L:14222043..14358721	205	69	312	47	172	83	214	60	121	76	54	7.0	6.6	0.70
Df(2L)Exel6049	40A5;40D3	2L:21661374..21852372	66	6	80	4	45	12	57	9	81	9	7	3.0	2.1	0.71
Df(1)Exel9054	17D1;17D3	X:18423890..18472392	128	83	174	78	103	95	126	49	107	89	63	6.0	14.5	0.71
Df(3R)Exel7312	87A4;87A7	3R:7803596..7905868	139	68	137	46	129	58	132	44	158	63	45	4.8	1.0	0.71
Df(3L)Exel6089	62D1;62D4	3L:2132373..2236727	64	90	59	55	85	90	49	73	62	90	64	0.0	9.0	0.71
Df(3R)Exel9025	99B10;99B10	3R:25559829..25575231	144	66	180	47	122	65	124	47	150	65	47	0.1	0.0	0.71
Df(3R)Exel7314	87B3;87B8	3R:8061009..8198770	113	58	126	43	103	65	110	45	114	61	44	3.3	1.0	0.71
Df(3L)Exel6083	61A6;61B2	3L:84980..160823	85	77	111	52	104	81	69	61	57	79	57	2.0	4.5	0.72
Df(3R)Exel9029	83A2;83A3	3R:1229848..1263156	124	94	112	58	149	86	116	71	118	90	64	3.8	6.7	0.72
Df(3R)Exel7306	86C7;86D7	3R:6696747..6982569	121	88	137	65	108	77	111	54	126	83	59	5.4	5.4	0.72
Df(3R)Exel9019	86F6;86F7	3R:7575337..7590141	137	78	156	49	192	75	80	61	119	76	55	1.3	5.8	0.72
Df(3L)Exel9065	78D5;78D5	3L:21434299..21440442	125	80	137	54	133	85	118	64	112	83	59	2.2	5.1	0.72
Df(3R)Exel7321	88A9;88B1	3R:9951230..10103945	142	51	260	43	102	63	104	38	102	57	41	5.9	2.5	0.72
Df(3R)Exel6187	93F1;93F8	3R:17536460..17691952	56	27	67	18	49	15	47	12	60	21	15	6.0	3.4	0.72
Df(3R)Exel6156	85F16;86B1	3R:6015388..6175954	26	20	30	19	31	31	13	17	29	25	18	5.4	1.1	0.72
Df(3L)Exel6105	64D1;64D6	3L:5325370..5567583	134	57	176	46	98	58	146	37	115	58	42	0.5	4.5	0.72
Df(3L)Exel6135	76B11;76C4	3L:19585788..19709627	171	33	230	24	168	30	140	21	147	31	23	1.3	1.7	0.73
Df(3R)Exel7318	87C7;87D5	3R:8549596..?	141	84	116	59	129	79	108	60	209	82	59	2.9	0.4	0.73
Df(3R)Exel6193	94D3;94E4	3R:18715609..18991826	47	38	32	36	33	19	37	5	84	28	21	9.3	15.8	0.73
Df(3R)Exel9056	96C4;96C5	3R:21013378..21025666	149	55	196	45	114	54	156	35	131	55	40	0.1	4.8	0.73
Df(2L)Exel6009	24C3;24C8	2L:3763937..3881546	111	46	112	31	108	50	103	39	119	48	35	2.0	4.5	0.74

Df(3L)Exel6121	70D3;70D4	3L:14139743..14222043	122	79	107	62	154	85	114	59	112	82	61	2.8	1.7	0.74
Df(3R)Exel6203	96E2;96E6	3R:21330985..21452963	30	56	16	45	33	61	36	41	34	59	43	2.4	2.1	0.74
Df(3R)Exel8160	88C10;88D6	3R:10475147..10701733	149	90	156	58	262	79	90	67	89	85	63	5.7	4.9	0.74
Df(3L)Exel6262	71B3;71C1	3L:15028352..15183406	139	56	78	52	97	68	114	40	267	62	46	5.6	5.7	0.74
Df(3L)Exel7210	65A1;65A5	3L:5885956..6024960	236	56	169	38	577	55	74	45	123	56	41	0.1	3.4	0.74
Df(3L)Exel9006	75A4;75A6	3L:17772738..17790327	64	89	27	62	106	81	68	64	56	85	63	4.0	1.0	0.75
Df(3R)Exel6147	84F6;84F13	3R:4076151..4166732	136	25	126	13	219	22	147	23	52	24	18	1.5	5.1	0.75
Df(3R)Exel9012	94E9;94E13	3R:19096137..19162766	82	59	102	30	86	54	46	55	95	57	42	2.2	12.3	0.75
Df(2L)Exel8040	37C1;37C5	2L:19088224..19139791	62	47	34	39	82	49	67	33	63	48	36	1.1	2.8	0.75
Df(3R)Exel8163	89D2;89D2	3R:12298786..12328350	103	57	108	42	98	66	122	51	84	62	47	4.5	4.7	0.75
Df(3L)Exel9057	61C1;61C1	3L:286798..300135	147	77	146	55	220	79	114	63	106	78	59	0.8	4.3	0.75
Df(3R)Exel6201	96C2;96C4	3R:20954218..21013378	128	70	148	49	126	66	157	53	79	68	51	1.7	2.0	0.75
Df(1)Exel9067	17D6;17E1	X:18520229..18543242	107	71	110	47	122	61	122	53	73	66	50	4.7	3.4	0.76
Df(3L)Exel6137	78F4;79A4	3L:21760860..21872368	148	32	159	16	132	28	116	29	184	30	23	2.2	6.7	0.76
Df(3R)Exel8194	100A4;100A7	3R:26571483..26703333	105	45	78	42	110	62	117	39	113	53	40	8.3	1.4	0.76
Df(3L)Exel7253	73D5;73E4	3L:16842928..16981186	122	68	157	57	104	71	123	49	104	69	53	1.6	3.8	0.77
Df(3R)Exel6190	94A2;94A9	3R:17950472..18184659	91	37	51	36	87	53	118	33	108	45	34	7.6	1.1	0.77
Df(2L)Exel9033	36E1;36E1	2L:18272815..18277277	117	71	112	67	106	78	128	48	120	74	57	3.8	9.7	0.77
Df(1)Exel6235	5A2;5A6	X:5257225..5334341	121	75	101	70	108	85	164	53	109	80	62	4.8	8.6	0.77
Df(3L)Exel9058	64B11;64B11	3L:4520046..4532356	119	68	121	51	115	65	117	52	124	66	52	1.4	0.6	0.78
Df(3L)Exel9066	78D5;78D6	3L:21457516..21472425	122	63	119	34	146	55	110	59	111	59	46	3.8	12.2	0.78
Df(3L)Exel6126	71A3;71B3	3L:14917337..15028545	136	33	230	27	145	39	59	30	111	36	28	3.0	1.4	0.79
Df(3L)Exel6127	72D1;72D8	3L:15995819..16078533	164	24	206	16	213	43	188	37	49	33	26	9.6	10.4	0.79
Df(2L)Exel7008	22B8;22D1	2L:?.2145025	47	67	24	48	106	63	35	54	24	65	51	1.9	3.0	0.79
Df(3L)Exel9004	73D1;73D5	3L:16775136..16844490	93	91	35	54	177	76	46	79	113	84	66	7.7	12.3	0.79
Df(3L)Exel9017	70B1;70B2	3L:13415642..13434817	74	81	86	60	167	96	23	81	21	89	71	7.1	10.2	0.80
Df(1)Exel6291	18A2;18A3	X:18759564..18884547	30	21	24	32	41	50	28	25	28	35	28	14.6	3.4	0.80
Df(3R)Exel9030	91B5;91B6	3R:14420735..14448184	139	67	124	63	96	83	218	57	117	75	60	7.8	2.6	0.80
Df(1)Exel6290	4F7;4F10	X:5105146..5169157	132	57	191	45	159	57	99	46	80	57	46	0.3	0.5	0.81
Df(2L)Exel7073	37B1;37B9	2L:18837269..19000178	45	32	44	14	44	9	35	19	57	20	16	11.6	2.8	0.82
Df(3L)Exel6131	74A1;74B2	3L:17187056..17370461	169	33	172	16	206	31	183	37	115	32	26	1.3	10.5	0.82
Df(3L)Exel7315	87B8;87B9	3L:8194850..8239875	53	41	17	49	63	65	40	38	93	53	43	11.9	5.8	0.82
Df(3R)Exel6158	86C2;86C3	3R:6399676..6464635	43	48	31	29	79	46	28	48	33	47	39	1.0	9.7	0.82

Df(1)Exel6248	12F4;13A1	X:14557007..14654681	140	58	186	50	137	54	102	42	135	56	46	2.1	3.7	0.82
Df(3R)Exel6189	93F14;94A2	3R:17859431..17950482	86	41	103.0	23	95.0	28	74.0	34	71.0	35	28	6.2	5.3	0.82
Df(3L)Exel8104	65F7;66A4	3L:7319515..7488792	138	56	129	44	190	63	119	54	115	59	49	3.6	4.9	0.83
Df(3L)Exel6138	79D3;79E3	3L:?.22325232	194	35	206	35	208	39	199	26	164	37	31	2.1	4.4	0.83
Df(3R)Exel8143	85A5;85B2	3R:4495318..?	132	35	159	31	128	42	104	33	135	38	32	3.9	0.7	0.83
Df(3R)Exel9018	86E2;86E4	3R:7103606..7178879	134	42	179	38	112	59	112	47	132	51	42	8.2	4.7	0.83
Df(3R)Exel6167	87D10;87E3	3R:8877198..9085120	47	37	46	36	66	47	30	34	44	42	35	4.9	1.1	0.84
Df(3R)Exel6168	87E3;87E8	3R:9105472..9205526	14	40	5	42	26	25	8	13	16	33	27	7.5	14.9	0.84
Df(2L)Exel8039	37B8;37B11	2L:18973867..19022529	126	42	96	38	161	39	102	31	143	40	34	1.2	3.6	0.85
Df(3R)Exel6145	83C1;83C4	3R:1542487..1638972	181	17	201	13	212	47	160	42	150	32	27	15.0	14.6	0.86
Df(3L)Exel6118	70A3;70A5	3L:13186195..?	144	52	219	39	155	57	158	55	44	54	47	2.7	7.9	0.86
Df(1)Exel6251	13F1;13F17	X:15535368..15598856	124	56	154	52	124	55	114	47	102	56	49	0.6	2.3	0.88
Df(3L)Exel9001	64B2;64B6	3L:4321864..4386729	112	75	110	68	128	79	108	68	103	77	68	2.1	0.0	0.89
Df(2L)Exel6031	33B3;33C2	2L:11959952..12055718	43	9	34	8	63	10	41	9	35	9	8	0.5	0.3	0.89
Df(3L)Exel6085	61C3;61C9	3L:529157..729932	54	76	58	63	71	86	32	84	56	81	74	5.0	10.5	0.91
Df(1)Exel9068	18B4;18B6	X:18972970..18990977	110	81	103	73	134	79	121	76	82	80	74	1.0	1.2	0.93
Df(1)Exel6244	11A11;11B1	X:12194245..12278611	107	64	106	52	107	56	89	61	124	60	57	4.0	4.5	0.94
Df(3R)Exel6205	97D12;97E1	3R:?.22885211	98	59	90	57	103	55	80	53	119	57	55	1.9	2.2	0.97
Df(3L)Exel6125	71A3;71B3	3L:14917302..15028545	173	29	229	32	133	45	161	43	168	37	38	8.0	5.3	1.01
Df(3L)Exel9048	67D1;67D2	3L:9860552..9921634	93	51	69	70	93	76	107	61	104	63	65	12.5	4.7	1.03
Df(3L)Exel9028	64B9;64B11	3L:4488223..4506042	112	59	147	44	94	52	104	73	104	56	58	3.6	14.7	1.05
Df(3R)Exel6195	95A4;95B1	3R:19457785..19540279	126	27	143	59	133	64	109	42	119	46	50	18.5	8.3	1.10
Df(3L)Exel6134	75C7;75D4	3L:18412069..18571335	170	23	198	45	139	36	166	19	175	29	32	6.4	12.9	1.11
Df(3R)Exel6141	82B3;82C4	3R:288184..425531	163	21	257	11	214	30	129	47	53	26	29	4.4	18.0	1.13
Df(2L)Exel6028	32D5;32E4	2L:11148234..11347474	25	13	23	0	37	0	21	18	17	7	9	6.5	8.8	1.35
Df(2R)Exel7163	57A2;57A6	2R:15487656..15646458	7	8	13	0	0	0	4	11	9	4	6	3.8	5.6	1.44
Df(2L)Exel6027	32D2;32D5	2L:11059438..11148234	8	15	13	0	7	18	11	50	2	17	25	1.4	25.0	1.49
Df(2L)Exel6030	33A2;33B3	2L:11796280..11959952	13	29	14	14	22	0	5	30	10	14	22	14.3	8.2	1.53
Df(2R)Exel7180	59E3;59F6	2R:18587644..18729914	24	3	30	0	24	0	25	7	15	2	3	1.7	3.3	2.00
Df(3L)Exel9000	64A10;64B1	3L:4207869..4264888	3	0	1	0	5	0	2	0	2	0	0	0.0	0.0	n.d
Df(2L)Exel6016	26C1;26D1	2L:6245225..6403707	13	0	13	0	18	0	5	0	14	0	0	0.0	0.0	n.d

Supplementary table 2:

All the abbreviations are like in supplementary table 1.

The average values of two sets of experiments (1 and 2) are shown.

Symbol	Estimated Cytology (R3)	Sequence Coordinates (R3)	1. Ø Egg number	1. Ø LHR 25°C (%)	1. Ø LHR 11°C (%)	1. σ LHR 25°C	1.σ LHR 11°C	2. Ø Egg number	2. Ø LHR 25°C (%)	2. Ø LHR 11°C (%)	2. σ LHR 25°C	2. σ LHR 11°C	CS ± σ
Df(3R)Exel9014	95B1;95D1	3R:19589500..19759383	221	52	15	4.0	3.8	92	56	8	14.3	3.8	0.22 ± 0.11
Df(3R)Exel6192	94B11;94D3	3R:18483028..18715579	133	78	12	1.4	1.1	56	78	7	0.9	0.5	0.13 ± 0.04
Df(3R)Exel6176	89E11;89F1	3R:12879395..12974859	154	50	30	6.8	9.7	127	50	21	10.4	7.2	0.51 ± 0.14
Df(2R)Exel7184	60B12;60C4	2R:19182947..19301415	53	6	7	0.7	0.3	24	4	4	1.2	0.4	1.10 ± 0.11
Df(2R)Exel7178	59D5;59D10	2R:18335053..18439482	175	43	16	1.0	10.5	99	49	20	5.2	18.7	0.38 ± 0.03
Df(2R)Exel7176	59B4;59C2	2R:17932540..18079391	185	51	29	2.5	1.5	117	51	20	11.5	3.1	0.48 ± 0.14
Df(2R)Exel7174	58E5;58F3	2R:17558161..17687264	129	56	34	0.3	18.6	125	51	14	0.5	6.4	0.44 ± 0.23
Df(2R)Exel6285	52A4;52B5	2R:10547243..10739931	157	37	11	3.3	7.9	112	31	8	1.7	4.6	0.27 ± 0.04
Df(2R)Exel9026	52A13;52A13	2R:10632353..10639555	148	42	19	5.0	0.5	55	48	7	16.4	2.0	0.30 ± 0.23
Df(2R)Exel7121	49B5;49C1	2R:7635400..7744466	64	18	6	4.0	0.5	31	26	5	7.5	3.7	0.29 ± 0.11
Df(2R)Exel8049	45F1;46A1	2R:4612208..?	148	49	10	5.3	2.5	81	51	18	0.7	8.3	0.28 ± 0.12
Df(2R)Exel6283	42E7;43A1	2R:2100923..2207951	114	35	17	1.5	0.1	70	52	16	1.4	5.6	0.40 ± 0.13
Df(2R)Exel9043	37E1;37E1	2R:19416148..19430995	85	38	8	3.3	6.2	42	48	11	7.8	0.9	0.22 ± 0.01
Df(2L)Exel7071	37A1;37A4	2L:18667136..18773903	148	47	19	8.0	3.3	50	24	17	13.7	7.7	0.56 ± 0.21
Df(2L)Exel9044	36C10;36C11	2L:17480597..17582843	156	59	16	0.1	2.2	48	60	11	22.6	8.3	0.23 ± 0.06
Df(2L)Exel8036	36B1;36C9	2L:16769571..17428338	83	28	7	1.2	7.5	47	32	7	9.8	9.8	0.24 ± 0.03
Df(2L)Exel7067	36A12;36B2	2L:16706459..16802992	139	33	7	6.2	1.5	80	29	6	3.0	3.7	0.21 ± 0.02
Df(2L)Exel7049	32B1;32C1	2L:10845856..10967695	131	37	18	1.0	2.7	143	46	11	1.0	3.4	0.37 ± 0.17
Df(2L)Exel8026	31F5;32B1	2L:10509084..10854392	194	43	11	0.4	8.2	116	49	8	1.9	7.9	0.21 ± 0.07
Df(2L)Exel7043	30D1;30F1	2L:9852245..9932618	178	70	37	1.1	2.7	123	61	35	7.1	13.3	0.55 ± 0.03
Df(2L)Exel6022	30B5;30B11	2L:9439878..9552718	84	19	6	4.5	2.5	76	28	7	7.0	3.5	0.29 ± 0.06
Df(2L)Exel8022	30B3;30B5	2L:9380364..?	75	53	9	8.6	1.3	32	43	15	14.3	12.6	0.26 ± 0.12
Df(2L)Exel7042	30B10;30C1	2L:9515175..9615216	58	15	4	0.6	0.8	35	10	25	7.0	20.8	1.34 ± 1.54
Df(2L)Exel7039	29D5;29F1	2L:8521355..8794191	165	34	13	0.9	4.4	101	39	11	0.5	9.1	0.34 ± 0.07
Df(2L)Exel7034	28E1;28F1	2L:8063541..8197397	110	37	29	5.3	2.3	57	44	17	6.7	11.3	0.57 ± 0.29
Df(2L)Exel8019	27E2;27E4	2L:7132386..7194548	147	46	17	13.4	10.4	48	51	27	11.3	3.1	0.45 ± 0.12
Df(2L)Exel7027	26F5;27B1	2L:6657034..6779122	28	26	8	7.5	7.5	18	56	9	22.2	5.2	0.23 ± 0.09
Df(2L)Exel7024	26A1;26A8	2L:5890506..5972368	136	46	8	5.1	5.8	53	56	12	5.2	5.7	0.20 ± 0.03
Df(2L)Exel6014	25F5;26A3	2L:5797539..5936895	89	58	16	2.4	2.2	62	57	22	5.5	19.9	0.33 ± 0.07
Df(2L)Exel8016	25E6;25F2	2L:5547264..5651500	195	42	9	8.8	4.0	141	40	14	0.3	3.4	0.29 ± 0.09
Df(2L)Exel8010	24C8;24D4	2L:3880550..4023894	85	39	9	11.0	9.3	29	61	8	7.4	7.6	0.18 ± 0.07
Df(2L)Exel7002	21B4;21B7	2L:203089..?	116	41	19	10.8	12.9	66	39	20	7.6	2.2	0.49 ± 0.04

Erklärung:

Hiermit versichere ich, die vorliegende Arbeit selbstständig verfasst und keine anderen als die von mir angegebenen Quellen und Hilfsmittel benutzt zu haben.

Ferner erkläre ich, dass ich weder an der Universität Bayreuth, noch an einer anderen Hochschule versucht habe, eine Dissertation einzureichen, oder mich einer Promotionsprüfung zu unterziehen.

Rahul Pandey

Bayreuth, November 2006